

V. STREAM DISCHARGE MEASUREMENTS

A. *Methods for Flow Measurement*

Determination of stream flow involves two steps: continuous measurement of stage (water level above a datum) at some cross-section and establishment of a mathematical relationship for converting that stage record to discharge. Ideally a structure with known hydraulic properties is constructed in the channel to standard specifications [e.g., Bos, 1985]. Structures such as weirs and flumes have advantages of a consistent, precalibrated stage-discharge relationship and accurate results [e.g. Herschy, 1985], but because of logistical considerations we chose to use dilution gaging techniques.

Water level of the lake at a point immediately above the outlet has been recorded by the U.S. Geological Survey (USGS) since October 1983. Water level in the stream a few meters below the outlet has been recorded by this project since August 1985. A second sensor, which was recorded independently, was installed in June 1986. Staff gages near both water level sensors were read manually and served as a permanent reference. The USGS sensor was a nitrogen-gas bubble gage with a precision of about 1 cm in stage. Because of the location of the USGS sensor in the lake, stage changes of a centimeter over the large surface area of the lake can mask considerable fluctuations in outflow discharge. This project's sensors were rugged pressure transducers (Montedero-Whitney Model 140 PC) of the differential type. The standard (1 psi) transducer is accurate to within 1.3 cm change in water level over the range of water temperatures occurring in the gaged streams (manufacturer's specifications). The transducers convert water pressure (which is a function of water depth) into voltage when an excitation voltage is applied. The transducers were mounted inside a short section of pipe to avoid influences of velocity on measured pressure [Herschy, 1985]. Transducer output was recorded by solid-state data loggers (Omni Data Easy Loggers). The loggers were programmed to record averages of 5 minute interval scans every 15 minutes.

Stream discharge (volume per unit time) was calculated from the stage records with an empirical stage-discharge relationship (rating curve). The development of a rating curve requires dozens of manual measurements of discharge over the complete range of expected stages. Conventional discharge measurement relies on measurement of mean velocity and the cross-sectional area of the channel. The product of velocity and area is discharge. Generally, velocity is measured at several points across a channel with a current meter and averaged to obtain a mean velocity for a measured cross-sectional area. Standard velocity measurements with a current meter tend to be unreliable in mountain streams. Velocity at a cross-section can fluctuate widely in turbulent high-gradient streams. At high flow, there may be air entrainment. At low flow, water depths can be so small that the size of even pygmy-type cup meters are on the order of the channel depth in many locations. Flow

velocities may be so low ($< 15 \text{ cm s}^{-1}$) that the frictional resistance of the meter is about the same as the force of the flowing water. In general, current meters have been found to overregister velocity in mountain streams [Jarrett, 1988].

An effective alternative to the velocity-area method is dilution gaging. "In rock-strewn shallow streams, the dilution method may provide the only effective means of estimating flow" [Hersch, 1985, p. 363]. Dilution gaging is thoroughly described by Church and Kellerhals [1970], Church [1975], and Hersch [1985]. The method was presented originally by Stromeyer [1905]. Though the tracer can take a variety of forms, such as a radio-isotope or fluorescent dye, neutral salts are the most common because they cause negligible environmental effects and can be measured using standard instrumentation. Of the chemical tracers, NaCl is the most practical. It is inexpensive, readily available and environmentally safe.

The dilution of the tracer in the stream is directly related to its discharge. The conductivity of the salt solution is linearly related to the concentration. Conductivity can be easily and accurately measured in the field, while concentration cannot.

There are two types of salt dilution methods. The first is the continuous injection method. This technique involves the continuous injection of a salt solution of known conductivity at a known rate into the stream. By measuring the conductivity of the stream before injection begins, and then again after an equilibrium conductivity has been reached, discharge can be calculated. The other technique is the slug injection method. This method involves the injection of a slug of known volume and conductivity into the stream. By measuring the background conductivity of the stream, and then the conductivity wave as it passes downstream, discharge can be calculated from

$$Q = C_s \frac{V_s}{\int_{t_i}^{t_f} (C_{ct} - Bk) dt} \quad (4)$$

where:

- V_s is volume of the salt solution slug (m^3),
- C_{ct} is channel conductivity at time t (μS),
- Bk is channel background conductivity (μS),
- C_s is conductivity of the salt solution slug (μS),
- t is time (s),
- t_i is initial time of conductivity wave passage,
- t_f is final time of conductivity wave passage.

This calculation is independent of the units of conductivity, which cancel, and gives discharge in $\text{m}^3 \text{s}^{-1}$. The dilution method assumes that the measurement site is sufficiently downstream from the slug injection site, that complete mixing of the slug has occurred, and that the measurement-time resolution is fine enough to account for variations in the conductivity wave as it passes. Bjerve and Groterud [1980] point out that the continuous injection method is inherently more accurate because it does not rely on these assumptions. Unfortunately, the logistical details associated with continuous injection are more involved than with the slug injection method.

The slug injection method of measuring stream discharge, when properly administered, should be almost as accurate and repeatable as the continuous injection method described by Bjerve and Groterud [1980]. The method is largely independent of channel geometry or discharge characteristics. The method used at Emerald Lake is an adaptation of the technique described by Østrem [1964]. Application of this technique to this study is described in detail in Dozier et al. [1987].

B. Discharge at Emerald Lake Outflow

Stream discharge measurements have been taken since the beginning of the project. In an effort to refine the stage-discharge relationship, we continued to gather stage and discharge measurements in the outflow and inflows during the 1988 water year. This effort was considered a priority because our previous results did not exhibit the precision we desired, and additional data could be used to verify and improve the rating curves being used in our water balance calculations. Discharge never reached the peak flows observed in 1986, so the uncertainty in the upper portions of the rating curves have not been improved. However, a number of measurements were gathered at low and medium flows by several techniques, giving us greater confidence in our results through this range.

1. Outflow Rating Curve

The outflow has been the subject of considerable attention in this project. It represents one of the few checks on other monitoring efforts and estimations within the watershed (e.g. snow accumulation and snowmelt).

The rating curve is based on 76 individual measurements of discharge, most of which were obtained by the slug injection method. The data were analyzed graphically to check for errors, determine distribution and select appropriate transforms. Coefficients for a rating curve were obtained from a regression of logged stage against logged discharge, using natural logs. This method is a widely used and accepted technique for constructing rating equations because it is derived from basic fluid dynamics principles [Chow, 1964; Herschy, 1985]. The stage-discharge relationship is described by:

$$\ln Q = \alpha + \beta \ln S \quad (5)$$

where:

- Q = discharge,
- α = intercept coefficient from the regression,
- β = slope coefficient from the regression,
- S = observed stage height.

The equation can be exponentiated to obtain discharge expressed in the common form:

$$Q = \alpha S^\beta \quad (6)$$

Examination of the log-log plot showed a minor change of slope at the 0.247m stage level. This shift indicates a change in the stage-discharge relationship above or below this flow level because of a change in channel geometry or some other complicating factor. This nonlinearity made it necessary to divide the stage-discharge relationship into two curves. The rating equations derived from the regression for the outflow follow:

$$Q_{low} = 1.42 S^{3.94} \quad \text{for } S < 0.2466 \text{ m} \quad (7)$$

$$Q_{high} = 2.46 S^{2.73} \quad \text{for } S \geq 0.2466 \text{ m} \quad (8)$$

The standard errors for the low-flow slope and intercept coefficients were 0.139 and 0.340, respectively, for the transformed data. The standard errors for the high-flow slope and intercept coefficients were 0.078 and 0.054, respectively, for the transformed data. The R^2 values were 0.97 for low flow and 0.96 for high flow, but the actual R^2 is slightly lower since these values are from the regression of the log transform.

Simulation of daily mean errors was carried out using discharge data and a modification of Herschy's [1985, p.501, Eqn. 14.50] formulation where adaptations were made for errors associated with our discharge measurement technique. The method is described for measurement structures and their errors, and we adapted it by estimating errors for the dilution measurements. Random errors in the dilution measurements were estimated to be $\pm 10\%$, based on the ability to measure the parameters used in the technique, primarily the shape and magnitude of the dilution wave. Errors in the transducer were ± 0.2 cm, and errors in reading the staff gage were ± 0.3 cm. A number of days were tested for both low flow and high flow situations, and daily mean error estimates are 10-15% for discharge below $5000 \text{ m}^3 \text{ day}^{-1}$ and 15-20% for greater discharges.

2. Transducer to Stream Stage Relationship

Voltage-stage relationships had to be established for both transducers from recorded voltage and observed stage. This relationship is linear since water in a stream can be considered an incompressible fluid, and a well defined correlation exists. In all cases the

relationship was of the form:

$$S = \alpha V + \beta \quad (9)$$

where:

- S = observed stream stage,
- α = slope coefficient from the regression,
- β = intercept coefficient from the regression,
- V = recorded voltage from pressure transducer.

It was necessary to separate the data set of voltage and stream stage and develop several relationships. The first relationship is described by:

$$S = 0.124 V - 0.093 \quad (10)$$

On October 31, 1985 an instrumental change was made in the system that altered the voltage output from the pressure transducer at the outflow. After that date and before 20 February, 1987 the appropriate equation is:

$$S = 0.200 V - 0.141 \quad (11)$$

On 20 February, 1987 the data logger was converted to read voltage and record stage directly, thus, there is no voltage-to-stage relationship during this period. The high resolution transducer was replaced on 19 November, 1987 and a new relationship had to be developed. The equation to be used from 19 November, 1987 until the project's end is:

$$S = 0.133 V - 0.118 \quad (12)$$

The equation for the lower resolution transducer holds true for the duration of the record and is:

$$S = 0.654 V - 0.628 \quad (13)$$

The R^2 values of 0.96, 0.99, 0.99 and 0.98 respectively, clearly indicate a strong linear relationship and a good fit.

C. Discharge from Emerald Lake Inflow Streams

Inflow streams were monitored to assist with the chemical balance and to provide a check on the outflow discharge. Water enters Emerald Lake in eight surface channels (5 major channels and 3 minor channels). Two of the major channels (inflows 1 and 2) drain about 60 percent of the basin. The stage in these two channels was automatically recorded. The three other major channels collectively drain about 25-30 percent of the basin. Staff gages in these three channels were observed periodically. The three remaining minor channels were not manually monitored in 1986. Two of these channels were manually

monitored in 1987 and 1988.

1. Main Inflows

Streamflow in the two main inflow channels was monitored more intensively than in the other channels. Each of these channels were equipped with a pressure transducer. Output from the transducers was recorded at 15-minute intervals. Primarily, the salt dilution technique was used to measure discharge in these channels. At low flows the streams were diverted into large containers, providing independent discharge measurements that agreed well with the slug injection measurements. Discharge was measured 76 times in inflow 1, and 56 measurements were obtained in inflow 2.

a. Inflow 1 and 2 Rating Curves The rating curves for both inflows 1 and 2 were constructed the same way as described for the outflow. Additional discharge data was gathered at both channels and added to the data set before analysis. The new rating curves are a significant improvement over the ones used in the past [Dozier et al., 1987], both because of an improvement in the fit of the rating curves to the observed data and because the new data supports previous observations.

The rating equation derived from the regression for inflow 1 is:

$$Q_{Inflow1} = 3.40 S^{5.17} \quad (14)$$

The R^2 was 0.96 and the standard errors of the slope and intercept coefficients were 0.121 and 0.133, respectively, for the transformed data.

The rating equation derived from the regression for inflow 2 is:

$$Q_{Inflow2} = 6.75 S^{5.88} \quad (15)$$

The R^2 was 0.97 and the standard errors of the slope and intercept coefficients were 0.141 and 0.127, respectively, for the transformed data. The relationships appear to do a reasonable job at higher flows based on the scant available data.

b. Transducer to Stream Stage for Inflows 1 and 2 A number of problems occurred with the inflow transducers over the study period. These included occasional transducer failure, lightning induced failure, and unexplained removal from the stream. These problems complicated matters and made it necessary to develop a number of voltage-to-stage relationships for both inflows 1 and 2. All regressions produced good linear relationships with high R^2 values. Conversion from voltage to stream stage should be done using the following relations for the specified time periods:

Inflow 1 - Transducer to Stream Stage

$$S = 0.235 V - 0.207 \quad \text{for period before 21 Dec 1986} \quad (16)$$

$S = 0.156V - 0.092$	after 21 Dec 1986 and before 25 May 1987	(17)
$S = 0.145V - 0.089$	after 25 May 1987 and before 12 July 1987	(18)
$S = 0.120V - 0.038$	after 12 July 1987 and before 28 March 1988	(19)
$S = 0.129V - 0.030$	after 28 March 1988	(20)

Inflow 2 - Transducer to Stream Stage

$S = 0.210V - 0.116$	for period before 26 Nov 1986	(21)
$S = 0.156V - 0.053$	after 26 Nov 1986 and before 25 May 1987	(22)
$S = 0.133V - 0.035$	after 25 May 1987 and before 3 June 1987	(23)
$S = 0.123V - 0.015$	after 3 June 1987 and before 21 March 1988	(24)
$S = 0.127V - 0.030$	after 21 March 1988	(25)

2. Minor Inflows

The smaller inflow channels to the lake were not equipped with automatic sensing and recording devices. Instead, manual observations of a staff gage are used to construct a record of daily flow volumes in these small channels. Staff gages were installed in inflow 4 in July 1985, the East Joint in April 1986 and the Southeast Gully in May 1986. Observations were obtained 2 to 5 times on most days during spring melt and at decreasing frequency as these streams receded. No attempt was made to excavate the staffs during winter. The staff gages were excavated as early as possible in spring.

The stage record from the staff gages was used to estimate an average stage for each day from the beginning of record through the drying or freezing of the channels. On days with several readings, an average stage was approximated by weighting the individual readings according to the time of observation in relation to an assumed snowmelt hydrograph. This estimation was by simple judgement. A more rigorous time-series approximation was not judged to be worthwhile because of the infrequent observations, low quality of the rating curves, and low magnitude of the flow volumes. On days with only one observation, the time of the observation relative to the typical daily snowmelt hydrograph was considered in estimating an average stage for the day. On days without any observations, values were interpolated between observations on the other days while considering changes in the gaged inflows and the outflow. The ungaged streams were assumed to respond in the same direction as the gaged streams.

Rating curves were developed from available measurements of discharge. Channel discharge was measured by the salt-dilution technique, a portable flume, and volumetrically with a bucket and stopwatch. Discharges were also calculated with the Chezy-Manning equation [e.g., Linsley et al., 1975] using measured channel geometry and a roughness factor calibrated from velocity measurements that were obtained from the dilution measurements.

Each estimate of discharge had its problems. The reaches available for salt dilution were generally too short for adequate mixing to occur. Assumptions regarding the precalibrated flume were usually violated because the sites lacked a straight approach to the flume and the slope was inadequate to avoid ponding below the throat. The flume was assumed to overestimate discharge at these sites, particularly at higher flows. Although volumetric measurement is the only absolute measure of discharge, the volumes measured were so small and the times were so short that errors were introduced at higher flows. Prior to directing the flow through pipes, the buckets usually captured only 80 to 95 percent of the total flow. This proportion collected was estimated and subject to error. The roughness coefficient in the Manning equation was calibrated at only a narrow range of flows. In these small channels, the banks may account for much of the overall hydraulic roughness. Thus, while the coefficient was assumed constant in the calculations, it was likely to have varied with stage.

Only about 30 discharge measurements of various types were available for each of these inflows. Although there were enough measurements to describe the general shape of the stage-discharge relationships, it did not allow identification of a well-defined curve. Thus, the discharge values estimated for a given stage can only be judged to be within ± 50 percent of their "true" value.

Daily stream flows were estimated from a single stage assumed to provide a flow rate equivalent to the integrated flows fluctuating over a 24 hour period. These flow rates were tabulated over the period of record and extended to include early spring of 1986. The foundations for the extrapolations were relatively weak relationships with other channels and assumptions about the pattern of early-spring snowmelt. These extrapolated periods include March 23 to April 19, 1986 in the East Joint inflow and April through June 17, 1986 for inflow 4. All estimates of daily stream flows in the channels without transducers must be regarded as approximations that can only provide an indication of the magnitude and timing of stream flow. Using an adaptation of Herschy's (1985) technique, uncertainties in the mean daily discharge were approximately 20, 30, and 60 percent for inflow 4, East Joint, and Southeast Gully, respectively.

One other inflow channel to the lake was not gaged at all. Inflow 3 enters the lake between inflows 2 and 4 and is essentially unchannelized. The flow occurs over bedrock in a shallow layer a few centimeters deep and up to 10m wide. Since the construction of diversion structures was not permitted, this inflow could not be monitored effectively. Based on contributing area and visual comparisons, the annual volume of inflow 3 is estimated to be about the same as the annual volume of inflow 4. However, inflow 3 rises more quickly during the spring, peaks earlier than inflow 4, and dries up by mid-summer.

D. Tracer Experiment

A tracer experiment utilizing lithium bromide (LiBr) was conducted between 4 and 8 June, 1987, to determine travel and residence time of snowmelt runoff in channels and subsurface reservoirs during snowmelt runoff. The experiment was carried out in cooperation with H. Taylor and J. Garbarino of the USGS, who also performed the laboratory analysis. The tracer was introduced to the saturated soil surface in the source area of inflow 4, in the well defined hole region above Emerald Lake, at an elevation of 2990 m. The hole region is characterized by large and extensive areas of talus and unconsolidated deposits, and has no surface runoff in its recharge area. Samples were collected at the gaging site in inflow 4, which is located close to the lake at an elevation of about 2815 m. The total relief between the application site and the collection site was about 175 m and the total linear distance was approximately 350 m, with an average slope of about 30°. The resulting response-time function derived from the stream samples provides information about the residence time of snowmelt runoff in the area of the hole and the travel time to the lake.

Water samples were collected before the tracer was introduced to determine background concentrations of Br^- and $^{6,7}\text{Li}^+$ at the application site and the collection site. Once the tracer was applied, stream water was sampled at the collection site at a decreasing rate: every 30 minutes for ten 30-minute intervals, every hour for ten 1 hour-intervals, every 1.5 hours for ten 1.5-hour intervals, then every 2 hours for ten 2-hour intervals, followed by every 3 hours for ten 3-hour intervals, and then at 0800, 1400 and 2000 hours for the next 3 days. Weather was variable during the experiment, with high winds and rapid snowmelt on 4 June, which produced discharge that approached the annual maximum in inflow 4. An estimated 11 mm of precipitation fell on 6 June between 0400 and 0700 PDT in an intense rain and hail shower. Clear mornings and cloudy afternoons on 7 and 8 June ended with approximately 13 mm of rain of 8 June. Maximum estimated discharge during the sampling period was about $0.031 \text{ m}^3 \text{ s}^{-1}$ occurring between 1800 and 1900 PDT, 4 June.

Every stream sample was analyzed for Br^- and $^{6,7}\text{Li}^+$ using ion chromatography and inductively coupled plasma-mass spectroscopy, respectively. The results for $^{6}\text{Li}^+$ ion intensity and $^{6}\text{Li}^+ / ^{7}\text{Li}^+$ ratio are not well-defined. The Li^+ response does exhibit a maximum, but decays slowly throughout the period of the experiment, never reaching background levels. This may indicate a less than conservative nature for Li^+ .

Br^- concentrations were below detection limit at the start and end of the experiment, and displayed a pronounced peak during the experiment (Figure 7). The Br^- results indicate conservation with a well defined temporal response curve. The response was characterized by a rapid increase in concentration followed by a slightly less rapid decrease to background levels. The first detection of the tracer was observed 9 hours after injection and

the last measurable amount was observed 10 hours later. The peak occurred 12 hours after injection and about 1 hour after discharge measured in inflow 4 reached its annual maximum. This result agrees with the modeling results from the Arizona groups conceptual model, which found that residence times were about 12 hours in the basin and could be ignored in modeling at daily or more lengthy time scales.

The tracer experiment indicates that residence time in subsurface storage areas of the hole during the peak of snowmelt runoff can be as low as 9 hours. The length of the Br^- pulse may be attributed to different paths taken as the Br^- percolated through the ground, as well as retention in eddies and pools found in the open channel. Chemical reactions between Br^- and soils, such as ion exchange reactions, may also contribute to the length of the Br^- signal.

This result is probably not representative of the basin as a whole, but it does provide insight into the residence time of solutes in this portion of the groundwater system and travel time in this channel during the period of maximum snowmelt runoff. It must be kept in mind that the result is specific to this location at this time, which is a combination of snowpack runoff, local infiltration rates, local hydraulic conductivity and prevalent weather conditions.

E. Streamflow and Runoff Summary

The voltage to stage relationships all exhibited well fitting linear relationships. These relationships exhibit a high degree of stability. The rating curves are not as well defined. They exhibit the errors associated with the different discharge measurement techniques, operator error in reading the staffs, and instrument errors in the transducers. Further error results from fitting a curve to the data. Both the data transforms and the regression techniques are approximations or "best fits" interpreted mathematically or by the analyst. It was necessary to transform all discharge data because it was lognormally distributed. The low to medium flows are probably approximated well by the rating curves. Flow estimates in the high regions are suspect. There are several techniques for extending rating curves to flows higher than those observed [Linsley et al., 1982]. None of the methods are completely adequate, and the assumptions they are based on, such as stable hydraulic geometry across the range of flows, certainly do not hold for the inflows and are dubious for the outflow. Only acquisition of more discharge measurements in the high flow regions will support these conjectures.

Two basic assumptions are made before establishing a stage-discharge relationship for a stream. The first is that a unique relationship exists. Such uniqueness is seldom true in nature, but a measure of the error associated with this assumption can be made and an operational relationship can usually be identified. Secondly, the assumption is made that

the relationship is invariant in time. Stable variance is also seldom true in nature, but can be used for long periods of time when a stable channel section is selected for the gaging site. The rating curve may vary through time because of instability in the channel or control, conditions altering the effect of the control, hysteresis effects on rising and falling stages, and hysteresis effects caused by changing channel characteristics.

The gaging site at the Emerald Lake outflow is located in a channel that is not affected by most of these factors. The channel bed itself is made up of rocks up to 20 cm radius with some exposed granite bedrock. The east bank is covered with vegetation and appears to have been stable over the four year study period. Maximum flows are rare and duration of bankfull discharge is short. The west bank is a steep wall of exposed granite bedrock and the major part of the flow in the gaging section is adjacent to this bank.

Conditions that radically alter the channel at the gaging site may exist through part of the year. In years when the snow cover is reduced the channel may freeze. Ice cover renders the gaging data useless because the channel geometry is changed markedly and ice cover effectively changes the flow from open to closed channel. However, there are two mitigating factors. Little flow occurs during these ice covered periods, thus the errors are insignificant in the annual water balance and in many years the streams may not become ice covered.

Rise and fall of the flood wave occurs rapidly because of the rapid response of the basin to rainfall and snowmelt events. Mountain streams often have a large bed slope relative to the changing water surface slope, which leads to reduced or negligible hysteresis effects in such channels (Dickinson, 1967). Hysteresis effects caused by changing channel geometry have also been found to be minor. They may be a serious problem in alluvial channels, but the bedrock and large grain size in the outflow appear to be unaffected by most observed flows. The closeness to the lake does not allow enough channel reach to generate a mobile sediment load capable of changing the frictional characteristics of the bed surface. In summary, most of the error in the stage-discharge relationship for the outflow can be attributed to error in individual measurements of stage and discharge.

There are more problems associated with the inflows. Inflow 1 has a stable bedrock channel bottom at the gaging site, but the banks are soil held in place by by vegetation with extensive rooting. Some change in channel geometry has been observed in the form of undercut banks. Inflow 2 has a stable cross section at the gaging site because of bedrock and boulders, but the banks suffer from erosion immediately above and below the site. Both inflows 1 and 2 have no interference on flow from vegetation and cascades are located immediately downstream, which removes ponding effects. Ice has proven to be a major problem in these smaller channels. They become ice covered and have even frozen to the

bed on years of minimal snow cover. A frozen channel renders the transducers at the gaging sites useless and forces runoff during the early part of the melt season to flow overland outside the channel. This problem has been minimized by early season excavation of the channel. The bed slopes are even steeper in the inflows than the outflow and hysteresis effects are thought to be negligible. A further problem exists in that peak flows exceed bankfull discharge considerably. No data exists for this situation, however it rarely occurs and is a condition of short duration.

In spite of the problems mentioned above, the rating curves for the inflows are reasonable and additional data collected during the recent field seasons fit the original relationship remarkably well, indicating a stable relationship through the study period. Again, the major source of error and uncertainty in the rating curves for the inflows can be attributed to individual errors in measurements of stage and discharge.

A rating equation and the stage record were used to calculate daily discharges in both principal inflows throughout the study period. Discharge at high flows has greater uncertainty than at low flows because of the relatively few measurements obtained at high flow. Stage at low flows under winter conditions may be artificially high because of constrictions in the channels from ice accumulations. Uncertainty in the mean daily discharges were estimated to be 10-15 percent at flows less than $1000\text{m}^3/\text{day}$ in inflow channel 1 and less than $2000\text{m}^3/\text{day}$ in inflow 2. At higher flows, uncertainties were estimated to be 15-20 percent.

In the Emerald Lake basin, most rainfall or snowmelt runoff enters the channel network as overland flow. Approximately 60 percent of the basin is bare rock surface [Huntington and Akeson, 1986]. This proportion of bare ground is much greater than in most basins that have been studied in relation to acid deposition. This extensive impermeable area allows rapid stream flow response to rainfall as detention storage is quickly filled and sheetflow soon concentrates in a network of small channels. Hydrologic pathways, and therefore travel and residence time, vary with precipitation intensity, duration, and areal distribution. Only 20% of the basin is composed of soils. Another 20% is talus and other colluvial deposits which may drain quickly. The scattered areas of soil and some of the colluvial deposits detain a portion of the water entering them, which increases residence time. Most of the surficial deposits are small in areal extent, isolated, and drain directly into a channel after water has percolated through them for only a short distance. Extensive deposits of unconsolidated materials occur in only six parts of the basin (east and west sections of the master joint, Aaron's bench, Danny's Hole and the slopes to the west, upper bench, and Alta cirque). These areas provide the greatest available storage in the basin and release most of the water contributing to summer stream flow.

In spring, after prolonged snowmelt, many of the soil pockets and colluvial deposits become saturated and allow relatively little water to infiltrate. Therefore, during much of the snowmelt period, most of the unconsolidated deposits are bypassed by melt waters. During the period of snow cover disappearance in June 1986, overland flow was observed immediately downslope of all snow patches except those overlying talus and the deep soils of the master joint. Although melt water often infiltrated the soil a few meters downslope of the edge of the snow, these observations suggest that overland flow was nearly universal, except for talus deposits, when snow cover was continuous. Formation of extensive basal ice at the snow/ground interface such as during winter of 1987 may also reduce infiltration of melt water into soils.

Streamflow out of the Emerald Lake basin is one of the most important and informative measurements of the hydrologic mass balance. Because losses and storage other than those related to the snow cover tend to be small, the basin outflow can provide an indication of the timing and quantity of rainfall and snowmelt. In combination with the knowledge of other components of the water balance, stream flow provides an excellent integration of the hydrology of the basin.

All known surface water outflow from the Emerald Lake basin passes through Emerald Lake and its single well-defined outlet at its northernmost point. There is no physical evidence of any groundwater seepage from the basin. The outflow channel is 2 to 4 meters wide in the first 10 meters below the lake. Its bed is composed of bedrock, boulders, cobbles, gravel, and sand and appears to be highly stable in all but catastrophic flows. Average water depth across the channel ranges up to about 60 cm, and peak discharge from snowmelt may approach $1 \text{ m}^3 \text{ s}^{-1}$.

The study period of July 1985 through June 1988 included two complete water years (October 1, 1985 to September 30, 1986 and October 1, 1986 to September 30, 1987). The water year is a fundamental concept in hydrologic studies of areas with highly seasonal precipitation regimes. The water year begins and ends when subsurface storage is at a minimum. This convention reduces problems of accounting for year-to-year carryover of stored moisture. The first water year studied (Oct. 1, 1985 - Sept. 30, 1986) was characterized by high precipitation throughout most of California. The second and third (incomplete) years were classified as dry by the California Department of Water Resources.

The total annual volume of water flowing out of the Emerald Lake basin over the complete period of record (Oct. 1983 - Sept. 1987) ranged from $670,000 \text{ m}^3$ to 2.6 million m^3 (Table 47). Thus, the maximum volume during water year 1986 was more than three times the minimum volume during water year 1985. For comparison, the total volume of Emerald Lake is about $180,000 \text{ m}^3$ [Melack et al., 1987]. The equivalent depths of water

averaged over the basin area of 1.2 km^2 were 94 cm in water year 1984, 56 cm in water year 1985, 214 cm in water year 1986, 68 cm in water year 1987, and 58 cm through mid-June 1988. Annual stream flow even during the low year was more than twice the national average of 23 cm [Leopold, 1974].

Hydrographs of the outflow and inflows 1 and 2 for water years 1986, 1987, and 1988 are plotted in Figures 8 - 16. The hydrograph (stream discharge plotted as a function of time) of water year 1986 (Figure 9) demonstrates the seasonal nature of surface water runoff production in the Emerald Lake basin. More than three-quarters of the annual runoff occurred in the months of April through July (Table 48). May and June were the two months of greatest flow, accounting for at least half of the water year volume in each of the five years. The months of September through March generally accounted for only a few percent of total annual flow and often accounted for less than one percent of the total.

The hydrographs and tabulation of monthly stream flow volumes clearly show that the majority of runoff occurred during the months of spring snowmelt. Streamflow declined through summer as snow cover receded and water slowly drained out of soils and other surficial deposits. Infrequent rainfall augmented stream flow by small amounts in summer and autumn. Some of the snowfall in autumn usually melted within a few days and accounted for increased flow in September, October, and November.

Streamflow generally receded through the winter months as groundwater outflow declined. Some of the stream flow out of the basin during winter resulted from the displacement of lake water by snowfall and avalanches on to the lake. This displacement flow provided an excellent record of the timing of winter snowfall. Analysis of the flow volumes may also provide an index of the quantity of snowfall. The volumes of water displaced from the lake by avalanches were substantial and resulted in the highest instantaneous flows observed in the outflow channel. Streamflow began to increase in April when snowmelt began in the small portion of the basin receiving early spring insolation. As more of the basin was exposed to greater energy input throughout spring, snowmelt and stream flow increased dramatically.

Tabulation of daily water volumes flowing out of the basin (Tables 49 - 51) illustrates the high variability of stream flow over short time periods. The highest daily volume of record was about $36,000 \text{ m}^3$ on May 30, 1986. Streamflow exceeded $20,000 \text{ m}^3 \text{ day}^{-1}$ (1.5 cm/day water depth averaged over the basin area) on 44 days during spring and summer snowmelt in water year 1986. Flows were above $10,000 \text{ m}^3 \text{ day}^{-1}$ (0.75 cm day^{-1}) on 71 days in water year 1986 versus 32 days in 1987, 26 in 1988, 24 in 1984, and 20 in 1985.

Instantaneous flows rarely exceeded $0.5 \text{ m}^3 \text{ s}^{-1}$ under snowmelt conditions. Under optimum combinations of conditions favoring high rates of snowmelt runoff, peak

discharges approached $1 \text{ m}^3 \text{ s}^{-1}$ during 3 days in 1986. The greatest instantaneous discharge during the study period occurred on February 15, 1986 when massive avalanches on to the ice cover of Emerald Lake displaced a substantial amount of the water in the lake. Peak flows between 10 and $20 \text{ m}^3 \text{ s}^{-1}$ were estimated from channel scour. The minimum flow in water year 1986 was about $180 \text{ m}^3 \text{ day}^{-1}$. The minima for the entire period of record were below $20 \text{ m}^3 \text{ day}^{-1}$ and occurred in mid-February to mid-March of 1985 and September and October of 1987.

Daily discharges in the inflow streams (Tables 52 - 60) followed a pattern similar to that of the outflow. In 1986 the outflow, inflow 1, and the combined minor inflows peaked within a few days of one another in early June, but peak discharge in inflow 2 did not occur until June 24. In 1987 and 1988 peak stream flows were not as well synchronized, perhaps because of the spring precipitation and rapid depletion of snow cover. In all three years the minor inflows receded much faster than inflow 1 and 2. This rapid recession was probably due to the smaller drainage areas and smaller proportion of area contributing groundwater to the minor inflows.

The ratio of the sum of all measured inflows to the outflow on an annual basis was 0.79 in 1986, 0.77 in 1987, and 0.68 in part of 1988 (Table 61). The low ratio in 1988 probably reflects the intermittent record of flow in the minor inflows that year. The monthly ratios were highly variable and apparently depended on snow and avalanche displacement of lake water in winter, lake evaporation in summer, and various measurement problems.

**TABLE 47. Total Monthly Water Flux from Emerald Lake
(October 1983 - June 1988)**

Month	Volume (m ³)				
	WY 1984	WY 1985	WY 1986	WY 1987	WY 1988
Oct	14,100	7,600	20,800	44,300	4,100
Nov	5,190	28,900	22,600	6,810	18,500
Dec	8,100	12,920	18,100	2,750	14,700
Jan	21,700	7,330	34,300	5,300	11,900
Feb	50,600	3,190	86,000	8,400	10,080
Mar	77,100	427	46,300	14,600	43,600
Apr	35,500	18,100	135,000	176,000	113,000
May	479,000	202,000	534,000	303,000	322,000
Jun	215,000	289,000	825,000	229,000	156,000+
Jul	149,000	68,380	612,000	24,500	
Aug	53,300	9,940	204,000	4,780	
Sep	17,800	20,500	36,400	1,630	
Total:	1,127,000	668,000	2,573,000	821,000	694,000+

TABLE 48. Measured Monthly Water Flux In- and Out- of Emerald Lake (m³)

1986 Water Year (Oct 1985 to Sept 1986)						
Month	Outflow	% annual	Inflow #1	% annual	Inflow #2	% annual
Oct	20,800	1	4,260	1	8,540	1
Nov	22,600	1	3,730	1	2,310	<1
Dec	18,100	1	5,220	1	2,390	<1
Jan	34,300	1	7,130	1	4,610	<1
Feb	86,000	3	4,770	1	2,200	<1
Mar	46,300	2	6,990	1	3,920	<1
Apr	135,000	5	31,500	6	58,200	5
May	534,000	21	110,100	21	230,000	19
Jun	825,000	32	195,800	37	451,000	37
Jul	612,000	24	129,600	24	331,000	27
Aug	204,000	8	26,400	5	99,200	8
Sep	36,400	1	6,340	1	14,240	1
Total	2,573,000	100	532,000	100	1,208,000	100

1987 Water Year (Oct 1986 to Sept 1987)						
Month	Outflow	% annual	Inflow #1	% annual	Inflow #2	% annual
Oct	44,300	5	8,180	4	11,600	4
Nov	6,810	<1	4,130	2	1,450	<1
Dec	2,750	<1	2,790	1	~500	<1
Jan	5,300	<1	1,100	<1	~500	<1
Feb	8,400	1	1,120	<1	~500	<1
Mar	14,600	2	4,530	2	~500	<1
Apr	176,000	21	46,200	25	45,500	16
May	303,000	37	38,900	21	117,900	42
Jun	229,000	28	53,300	28	92,100	33
Jul	24,500	3	16,830	9	8,150	3
Aug	4,780	<1	7,510	4	1,610	<1
Sep	1,630	<1	4,300	2	1,580	<1
Total	821,000	100	189,000	100	282,000	100

1988 partial Water Year (Oct. 1, 1987 to June 18, 1988)						
Month	Outflow	% annual	Inflow #1	% annual	Inflow #2	% annual
Oct	4,100	<1	2,730	1	1,710	<1
Nov	18,500	3	9,750	5	4,140	2
Dec	14,700	2	9,510	5	4,900	3
Jan	11,900	2	7,540	4	2,200	1
Feb	10,080	2	8,150	4	2,000	1
Mar	43,600	6	23,800	12	4,600	2
Apr	113,000	16	39,500	20	14,200	8
May	322,000	46	68,500	35	99,500	53
Jun	156,000+	22	26,100+	14	54,400+	29
Total	694,000	100	196,000	100	188,000	100

TABLE 49. Daily Discharge Volume (m³), Emerald Lake Outflow, 1986 Water Year

Day	Oct	Nov	Dec	Jan	Feb	Mar	Apr	May	Jun	Jul	Aug	Sep
1	280	550	670	490	1100	720	3000	14000	34000	28000	12000	2100
2	220	540	4000	440	950	780	2500	15000	32000	28000	12000	1900
3	220	490	1400	410	990	760	2400	15000	32000	32000	12000	1900
4	220	440	710	1500	940	740	2900	11000	32000	30000	11000	1900
5	220	400	680	7300	620	710	2900	7800	27000	25000	9800	1800
6	270	390	620	3200	520	690	2700	4300	26000	21000	10000	1800
7	560	350	510	2100	470	720	2200	3900	25000	20000	9400	1800
8	180	300	470	1500	430	3400	2000	3900	23000	19000	8500	1900
9	410	240	450	1100	400	2700	1700	3600	26000	21000	8200	1500
10	1200	980	470	750	370	2800	2200	4300	27000	22000	8700	1200
11	1200	2200	450	560	360	1700	2000	5600	28000	25000	8800	990
12	1100	980	400	490	4100	1500	1900	8100	28000	29000	9000	880
13	840	510	380	510	4100	1300	1700	11000	29000	28000	7900	800
14	670	360	360	570	2000	1200	1800	10000	29000	23000	7400	730
15	560	280	340	640	18000	1100	2100	11000	28000	21000	6700	650
16	470	260	330	670	18000	1100	2100	13000	28000	19000	6000	640
17	420	260	320	630	5800	940	1800	15000	27000	17000	5400	570
18	390	270	310	610	8400	820	1600	17000	26000	16000	4800	870
19	360	250	310	610	13000	750	1800	19000	25000	17000	3800	990
20	320	300	300	610	1100	760	3500	21000	24000	18000	4900	760
21	590	380	300	590	780	850	6800	22000	26000	18000	4600	610
22	700	330	310	570	590	1000	8600	24000	28000	20000	4600	520
23	810	360	310	560	510	1200	6700	25000	28000	16000	4100	530
24	1700	2000	310	530	460	1200	6600	27000	31000	14000	3600	1100
25	1700	2400	320	500	430	1300	8500	28000	30000	13000	3200	2100
26	1300	860	320	500	410	1600	8900	28000	29000	13000	3200	1200
27	1100	540	340	510	500	2100	9700	31000	28000	11000	3200	900
28	890	960	340	550	600	2800	11000	33000	23000	12000	3100	880
29	750	3000	580	740		3000	11000	32000	21000	12000	3000	1100
30	620	1400	840	3000		2800	12000	36000	25000	12000	2700	1800
31	550		610	1600		3300		34000		12000	2200	
Total	20800	22600	18100	34300	86000	46300	135000	534000	825000	612000	204000	36400

TABLE 50. Daily Discharge Volume (m³), Emerald Lake Outflow, 1987 Water Year

Day	Oct	Nov	Dec	Jan	Feb	Mar	Apr	May	Jun	Jul	Aug	Sep
1	2000	380	110	60	100	260	1700	6800	15000	2200	150	32
2	1700	290	100	60	89	260	2000	6400	15300	1800	190	60
3	1400	290	93	60	120	260	2700	9800	15000	1700	310	150
4	1500	270	88	60	110	260	1700	12000	14000	1500	320	140
5	2200	240	95	63	95	600	1400	12000	12000	1400	320	130
6	2800	220	160	1600	86	580	1400	12000	14000	1300	310	120
7	3000	200	190	310	78	300	1900	11000	9700	1300	300	100
8	3400	190	160	210	78	260	2500	13000	9800	1300	270	82
9	3300	180	140	150	96	260	3800	13000	10000	1200	260	75
10	2800	160	120	110	120	260	4700	12000	10000	1100	230	54
11	2600	160	110	90	140	260	4100	12000	10000	1100	220	49
12	2300	150	100	79	170	260	3900	14000	10000	1000	200	71
13	1900	140	94	69	2400	260	5400	15000	11000	1000	210	80
14	1600	130	87	74	960	370	6100	14000	9100	870	250	61
15	1500	130	78	93	540	830	6300	17000	6900	760	200	56
16	1200	130	74	150	350	460	7400	14000	5200	680	160	48
17	1000	130	75	230	240	340	6600	12000	4600	590	130	43
18	900	370	69	89	190	330	5400	12000	4000	470	100	39
19	760	480	71	88	170	380	5500	11000	4600	390	87	32
20	720	400	90	170	170	350	6400	8800	4400	310	86	28
21	620	350	78	98	180	630	7800	6000	4100	260	86	18
22	570	310	68	98	180	500	8500	5400	3500	240	76	18
23	560	280	68	140	350	440	8000	5200	3400	240	62	17
24	530	250	64	100	310	410	8500	5300	3900	250	51	18
25	520	230	59	80	260	350	9500	5300	4100	240	32	18
26	510	190	52	69	260	420	10000	3800	3800	220	30	18
27	500	160	50	87	260	530	10000	3400	2900	220	28	18
28	480	140	50	300	260	690	10000	4600	3100	220	34	18
29	490	140	45	200		910	13000	5100	2700	220	28	18
30	470	120	55	150		1200	9700	8200	2400	220	28	17
31	450		60	120		1400		13000		180	22	
Total	44300	6810	2750	5300	8400	14600	176000	303000	229000	24500	4780	1630

TABLE 51. Daily Discharge Volume (m³), Emerald Lake Outflow, 1988 Water Year

Day	Oct	Nov	Dec	Jan	Feb	Mar	Apr	May	Jun
1	18	1700	76	220	190	970	2600	3100	8200
2	18	2600	67	170	210	680	3300	2700	13000
3	18	1500	63	280	220	500	3500	3900	15000
4	18	1100	120	450	220	480	3700	4100	14000
5	18	1000	190	4800	230	460	5300	3200	9900
6	18	1100	920	660	180	440	5800	2400	5800
7	18	860	2800	220	150	440	5400	1900	4200
8	18	830	1100	140	150	580	4900	1700	4200
9	19	810	610	120	170	660	5600	2700	7500
10	18	690	460	95	180	590	6700	5700	9700
11	18	640	440	100	200	500	7000	12000	9500
12	18	630	540	130	220	430	6400	16000	9000
13	18	600	470	140	250	390	4900	16000	11000
14	18	600	260	130	270	390	4500	17000	12000
15	18	410	270	210	300	410	3000	19000	12000
16	18	340	550	240	340	410	2500	15000	11000
17	18	440	360	1100	330	430	2600	11000	
18	18	440	190	570	350	600	2700	12000	
19	18	330	180	290	340	1000	2300	14000	
20	18	250	160	210	330	1700	2600	15000	
21	18	310	150	180	380	1900	1800	16000	
22	16	250	200	150	430	1500	1500	15000	
23	14	200	260	140	480	2000	1300	15000	
24	45	150	210	140	470	2400	1100	17000	
25	120	160	180	140	500	2700	1800	16000	
26	120	120	140	140	550	4300	3300	15000	
27	190	120	130	140	620	4500	3600	13000	
28	620	160	270	140	830	3800	3500	12000	
29	1000	100	1400	150	990	3500	4900	12000	
30	910	74	1500	160		2900	5200	6700	
31	710		390	170		2000		6000	
Total	4100	18500	14700	11900	10080	43600	113000	322000	156000

TABLE 52. Daily Discharge Volume (m³), Emerald Lake Inflow #1, 1986 Water Year

Day	Oct	Nov	Dec	Jan	Feb	Mar	Apr	May	Jun	Jul	Aug	Sep
1	110	130	170	160	180	180	280	2600	7900	6800	2000	380
2	110	130	180	160	180	180	340	2800	8500	7100	1800	380
3	110	110	190	160	180	180	390	2600	8300	8600	1400	380
4	110	120	180	300	180	170	450	1400	7500	7900	1200	350
5	110	100	180	690	170	160	500	900	6200	6100	1400	340
6	110	100	180	410	170	160	550	580	6000	4800	1300	330
7	110	99	180	300	170	160	610	480	5700	4000	1000	340
8	110	81	180	270	170	340	660	500	5500	4200	860	320
9	120	65	180	250	160	510	710	460	6300	5100	890	250
10	130	67	180	240	160	360	760	470	6500	5600	1000	200
11	140	210	180	230	160	290	820	630	6600	7700	1200	210
12	130	100	170	230	170	250	870	1200	6600	7400	1200	200
13	110	120	170	220	190	240	920	2400	7100	6200	1100	200
14	110	120	170	220	170	220	970	2000	6800	4600	940	170
15	100	120	170	210	170	220	1000	2600	6400	4100	800	150
16	100	120	160	200	160	210	1100	3400	6600	3300	700	160
17	100	120	160	200	160	200	1100	4400	6100	3000	650	160
18	99	120	160	200	170	200	1200	4600	5900	2900	560	190
19	94	120	160	200	170	190	1200	4900	5600	3200	510	160
20	96	120	160	200	170	190	1300	5000	5500	3700	610	140
21	100	130	160	200	170	190	1300	4500	6200	3000	620	120
22	110	130	160	190	170	190	1300	3600	6600	4100	570	110
23	190	130	160	190	170	200	1400	3100	6500	2900	520	88
24	370	120	160	180	170	200	1400	3600	7800	2000	480	100
25	340	160	160	180	170	210	1500	5600	7200	1900	480	140
26	270	160	160	180	170	210	1500	6700	7200	1500	470	140
27	220	150	160	180	170	220	1600	7500	6600	1300	480	140
28	150	160	160	190	170	230	2000	8100	4800	1400	470	140
29	99	150	160	200		240	1700	7500	5100	1400	430	160
30	98	170	160	200		240	2100	8400	6200	1800	390	190
31	100		160	190		250		7600		2000	380	
Total	4260	3730	5220	7130	4770	6990	31500	40100	195800	129600	26400	6340

TABLE 53. Daily Discharge Volume (m³), Emerald Lake Inflow #1, 1987 Water Year

Day	Oct	Nov	Dec	Jan	Feb	Mar	Apr	May	Jun	Jul	Aug	Sep
1	140	170	110	52	9	60	480	620	3500	990	260	230
2	150	170	98	52	9	60	700	1100	3100	890	260	280
3	150	170	98	52	9	72	650	1800	2800	880	270	310
4	190	170	99	52	14	81	370	2100	2700	890	310	280
5	370	170	89	52	22	83	350	2200	2200	880	330	240
6	460	150	86	52	26	100	360	1600	2600	870	340	220
7	540	140	87	52	26	120	600	1800	1700	910	360	220
8	750	140	86	52	26	120	820	2200	1900	930	380	200
9	540	140	86	52	33	130	1500	1500	1900	930	390	160
10	440	130	98	52	35	130	1900	1400	2400	920	400	160
11	380	140	110	52	35	130	1400	1300	2000	870	380	150
12	280	130	110	52	35	140	1600	2000	2300	860	390	140
13	230	110	120	52	35	140	2700	1900	2200	700	350	180
14	210	100	130	52	40	140	3000	1600	2000	580	300	190
15	180	110	160	52	52	140	3200	1000	1400	430	260	150
16	160	120	110	48	52	150	3600	940	1300	390	220	140
17	120	120	110	43	52	150	2600	770	1200	320	190	130
18	160	150	200	39	52	150	1800	610	1400	250	170	120
19	220	150	140	35	52	150	1500	480	1300	230	170	110
20	250	150	91	35	52	150	1600	390	1400	210	150	97
21	220	130	51	25	52	150	1700	370	1300	200	150	90
22	210	200	52	17	52	150	1600	370	1200	220	140	86
23	200	130	52	9	52	150	1400	210	1300	250	130	84
24	210	130	52	9	59	150	1700	250	1300	260	140	82
25	210	150	52	9	60	160	1500	410	1300	260	200	80
26	210	120	52	9	60	160	1700	670	1100	270	160	73
27	200	110	52	9	60	160	1200	960	1200	280	140	62
28	200	120	52	9	60	170	1900	1200	1100	300	130	27
29	240	100	52	9		190	1800	1200	1100	310	130	8
30	200	110	52	9		280	950	2400	1100	280	140	0
31	160		52	9		410		3500		270	170	
Total	8180	4130	2790	1100	1120	4530	46200	38900	53300	16830	7510	4300

TABLE 54. Daily Discharge Volume (m³), Emerald Lake Inflow #1, 1988 Water Year

Day	Oct	Nov	Dec	Jan	Feb	Mar	Apr	May	Jun
1	0	530	220	240	240	320	1600	980	2100
2	0	530	220	240	240	310	1400	1100	2300
3	0	380	220	250	240	310	1400	1500	2300
4	0	380	230	250	240	320	1600	1300	1800
5	0	360	230	270	240	330	1900	950	1300
6	0	370	490	260	240	320	2000	780	1000
7	0	370	840	240	240	330	1800	670	800
8	0	410	480	240	250	380	1700	750	1300
9	0	390	400	240	250	410	2000	1300	1600
10	0	380	370	240	250	370	2200	2200	1700
11	0	400	350	240	250	350	2200	3100	1400
12	0	370	340	240	270	340	1800	3200	1600
13	0	350	320	240	280	330	1400	3400	1700
14	0	320	300	240	280	330	1100	3700	1700
15	0	300	290	240	290	340	980	3800	1900
16	0	290	290	240	290	330	940	2300	1600
17	0	300	280	250	290	330	1000	1900	
18	0	280	270	250	280	370	910	2800	
19	0	280	270	250	280	510	720	3300	
20	0	290	260	240	290	1100	590	3300	
21	0	270	260	240	300	1100	520	3300	
22	36	270	260	240	310	900	490	3000	
23	180	260	260	240	320	1100	460	3200	
24	190	250	260	240	320	1200	520	3200	
25	190	240	250	240	330	1400	860	2800	
26	190	240	250	240	340	1900	1400	2400	
27	330	230	250	240	340	1900	1300	2000	
28	470	240	250	240	330	1800	1500	1900	
29	420	230	250	240	330	1800	1800	1300	
30	370	240	300	240		1600	1400	1100	
31	350		250	240		1400		2000	
Total	2730	9750	9510	7540	8150	23800	39500	68500	26100

TABLE 55. Daily Discharge Volume (m³), Emerald Lake Inflow #2, 1986 Water Year

Day	Oct	Nov	Dec	Jan	Feb	Mar	Apr	May	Jun	Jul	Aug	Sep
1	380	73	78	69	78	84	270	5200	18000	16000	6300	870
2	380	64	100	70	78	86	370	5600	20000	17000	5900	820
3	380	78	92	78	78	80	470	5400	19000	22000	5200	820
4	380	110	82	180	78	73	580	3500	17000	19000	4900	860
5	380	99	79	860	78	69	680	2000	12000	14000	5200	850
6	380	89	83	500	77	69	790	960	12000	10000	5200	860
7	380	82	78	270	78	69	900	920	11000	8700	4700	870
8	380	72	78	200	78	200	1000	710	11000	8900	4400	860
9	460	59	78	160	78	350	1100	610	13000	11000	4500	640
10	460	46	78	150	78	220	1200	650	14000	12000	4800	470
11	430	74	78	140	75	160	1400	1000	15000	17000	4600	380
12	330	86	78	130	75	130	1500	2500	15000	19000	4100	320
13	190	79	78	120	130	110	1600	4500	16000	18000	3800	280
14	130	72	78	110	78	110	1700	4000	16000	13000	3600	240
15	100	74	78	110	75	100	1800	5000	15000	11000	3200	210
16	87	77	78	100	69	100	1900	6000	16000	9200	2800	180
17	78	78	78	100	69	99	2000	8400	14000	8200	2400	150
18	70	78	78	100	71	95	2100	9200	14000	8000	2000	420
19	61	72	78	95	77	90	2300	10000	13000	8600	1800	340
20	52	70	77	95	78	86	2400	10000	12000	9800	2500	200
21	66	70	77	95	78	89	2500	9700	14000	8300	2400	140
22	88	69	78	88	78	95	2600	7800	16000	10000	2200	110
23	500	69	76	86	77	100	2700	6200	17000	7700	1800	120
24	790	74	69	86	78	110	2800	7400	22000	5800	1500	250
25	530	91	69	86	77	120	2900	12000	20000	5900	1400	710
26	320	75	69	86	78	130	3000	13000	20000	5300	1400	270
27	230	73	69	86	78	140	3200	16000	16000	4800	1500	290
28	170	78	69	86	76	160	4100	17000	9600	5200	1500	350
29	140	87	69	92		180	3800	16000	9800	5200	1400	480
30	120	88	69	95		200	4500	21000	14000	5800	1200	880
31	93		69	86		220		18000		6300	970	
Total	8540	2310	2390	4610	2200	3920	58200	230000	451000	331000	99200	14240

TABLE 56. Daily Discharge Volume (m³), Emerald Lake Inflow #2, 1987 Water Year

Day	Oct	Nov	Dec	Jan	Feb	Mar	Apr	May	Jun	Jul	Aug	Sep
1	520	76	20	20	20	20	60	2100	6600	730	76	54
2	310	77	20	20	20	20	75	2400	8000	550	74	65
3	310	71	20	20	20	20	95	4400	7100	540	77	62
4	370	63	20	20	20	20	100	5000	6200	470	77	59
5	650	64	20	20	20	20	150	5400	4500	490	73	54
6	800	56	20	20	20	20	150	4700	5800	460	73	54
7	920	48	20	20	20	20	180	4600	3100	470	72	53
8	1200	50	20	20	20	20	210	5600	3800	460	73	52
9	930	49	20	20	20	20	220	4700	3100	420	73	50
10	770	48	20	20	20	20	290	4800	4300	370	71	46
11	660	44	20	20	20	20	290	4800	4000	330	73	48
12	510	45	20	20	20	20	310	7800	4200	290	70	60
13	440	42	20	20	20	20	410	7700	4500	230	73	55
14	390	39	20	20	20	20	410	7300	3800	200	68	54
15	350	42	20	20	20	20	460	5400	2300	190	62	53
16	310	44	20	20	20	20	700	4900	1800	200	59	51
17	240	42	20	20	20	20	760	4400	1400	150	55	51
18	230	76	20	20	20	20	820	4100	1500	170	50	58
19	190	62	20	20	20	20	2400	3700	1800	130	46	62
20	170	53	20	20	20	20	4700	3300	1700	150	44	62
21	150	52	20	20	20	20	3100	2900	1600	120	40	58
22	130	55	20	20	20	20	2800	2500	1300	130	28	54
23	130	55	20	20	20	20	2600	2100	1300	110	16	52
24	120	45	20	20	20	20	2900	1700	1500	100	23	60
25	120	26	20	20	20	20	3100	1400	1600	120	46	60
26	130	26	20	20	20	20	3600	980	1200	110	38	58
27	130	20	20	20	20	26	3300	600	1100	110	24	52
28	120	20	20	20	20	40	3800	460	1100	93	12	41
29	120	20	20	20		43	4600	600	990	89	9	30
30	110	20	20	20		43	2900	2700	940	84	9	14
31	94		20	20		53		4900		79	21	
Total	11600	1450	~500	~500	~500	~500	45500	117900	92100	8150	1610	1580

TABLE 57. Daily Discharge Volume (m³), Emerald Lake Inflow #2, 1988 Water Year

Day	Oct	Nov	Dec	Jan	Feb	Mar	Apr	May	Jun
1	7	350	86	78	69	69	320	230	2500
2	3	300	85	78	69	69	470	260	5100
3	2	250	81	78	69	69	450	410	6100
4	0	170	78	78	69	69	610	360	5000
5	0	160	85	78	69	69	920	230	2800
6	0	160	1200	78	69	69	930	180	1200
7	0	160	680	78	69	69	740	160	680
8	0	160	220	75	69	75	660	170	1200
9	0	170	170	69	69	78	1000	350	2700
10	0	140	160	69	69	78	1100	1500	3600
11	0	130	150	69	69	74	1200	3500	3000
12	34	140	140	69	69	69	860	4800	3200
13	33	130	130	69	69	69	480	5100	4000
14	33	120	120	69	69	69	300	6000	4400
15	35	120	110	69	69	69	210	7400	4800
16	33	110	110	69	69	69	180	4100	4100
17	26	110	100	69	69	69	200	2900	
18	21	110	95	69	69	72	200	3800	
19	15	110	95	69	69	87	180	4800	
20	10	110	95	69	69	130	160	5500	
21	16	100	87	69	69	140	140	6100	
22	64	100	86	69	69	110	140	5000	
23	66	95	86	69	70	160	130	5800	
24	79	95	86	69	69	170	130	6700	
25	72	95	86	69	69	260	200	6000	
26	73	94	85	69	71	520	330	5000	
27	170	88	78	69	76	500	310	3800	
28	250	86	78	69	72	390	390	3600	
29	260	91	78	69	69	370	660	2900	
30	210	86	78	69		-270	570	1600	
31	200		78	69		210		1200	
Total	1710	4140	4900	2200	2000	4600	14200	99500	54400

TABLE 58. Daily Discharge Volume (m³), Sum of Minor Inflows to Emerald Lake, 1986 Water Year

Day	Oct	Nov	Mar	Apr	May	Jun	Jul	Aug	Sep
1	90	5	na	1200	2000	6200	2000	160	50
2	70	5	na	1100	2300	7000	1800	160	40
3	70	2	na	1100	2300	7100	2800	130	30
4	60	2	na	1200	2200	5400	2100	100	30
5	60	2	na	1200	2000	4900	1700	100	30
6	50	2	na	1200	1900	4100	1600	110	30
7	50	1	na	1100	1800	3900	1500	100	40
8	100	1	na	1000	1600	3600	1400	100	40
9	100	0	na	900	1600	4500	1600	100	50
10	170	0	na	1100	1400	5000	1400	100	50
11	170	0	na	1000	1600	4100	1600	100	30
12	100	0	na	1100	1600	6500	1700	100	20
13	100	0	na	1000	2100	5400	1500	90	20
14	90	0	na	1000	2100	4500	1500	90	20
15	80	0	na	1100	2400	3300	1300	90	20
16	80	0	na	1200	3200	3100	1000	90	10
17	80	0	na	1100	3800	3200	1000	90	10
18	70	na	na	1000	4500	2800	800	90	20
19	70	na	na	1100	4300	2400	800	80	30
20	70	na	na	1200	3500	2600	600	90	20
21	60	na	na	1500	2700	2100	600	80	20
22	60	na	na	1500	2200	2100	700	80	10
23	50	na	400	1800	2300	2200	600	80	10
24	30	na	400	1800	2500	3300	400	80	20
25	20	na	400	1800	4400	2500	400	80	80
26	20	na	500	1800	4900	2800	300	80	50
27	10	na	1000	2000	5200	2700	200	80	40
28	10	na	1100	2000	5500	2200	200	80	40
29	5	na	1200	2000	5900	2000	200	70	30
30	5	na	1200	2000	6600	1900	200	70	30
31	5		1200		6300		200	60	
Total	2000	100+	7400+	40000+	97000	113000	34000	2900	900

TABLE 59. Daily Discharge Volume (m³), Sum of Minor Inflows to Emerald Lake, 1987 Water Year

Date	Oct	Nov	Apr	May	Jun	Jul	Aug	Sep
1	20	10	nr	1900	2800	300	60	10
2	70	10	nr	2500	2600	200	70	20
3	60	10	nr	2400	2700	200	70	20
4	60	20	nr	2900	2500	200	70	20
5	50	10	nr	3000	2200	200	70	20
6	50	10	nr	2200	2700	200	50	20
7	50	5	nr	2600	2200	200	30	20
8	50	5	nr	3100	2900	200	30	20
9	50	5	nr	2900	2000	200	30	20
10	40	5	nr	3000	1900	300	30	10
11	40	5	nr	3500	1700	300	30	10
12	40	5	nr	3700	1700	200	30	10
13	40	5	nr	3300	1400	200	20	10
14	40	5	nr	3400	1100	200	20	10
15	40	5	nr	4400	900	100	20	10
16	40	5	nr	3800	700	100	20	10
17	40	5	1800	3700	600	100	20	10
18	30	5	1600	3600	500	90	10	10
19	30	2	1800	3400	500	80	10	10
20	30	2	2100	2400	400	80	10	10
21	30	2	1900	1600	400	70	10	10
22	20	5	3200	1500	300	70	20	10
23	20	5	3300	1500	300	70	20	10
24	20	5	3500	1400	300	70	20	10
25	20	10	3400	1200	300	60	20	10
26	10	5	3000	1300	300	60	20	10
27	10	5	2500	1300	300	60	20	10
28	10	5	3300	1100	300	60	20	10
29	10	5	2800	1200	300	60	20	10
30	10	5	2600	1200	300	60	20	10
31	10			1400		60	20	
Total	1000	200	37000	76000	37000	4400	900	400

TABLE 60. Sum of Minor Inflows to Emerald Lake, 1988 Water Year

TABLE 61. Monthly Volume of Inflow and Outflow of Emerald Lake

Figure 7. Lithium Bromide Concentration Versus Time from Tracer Experiment in Inflow 4

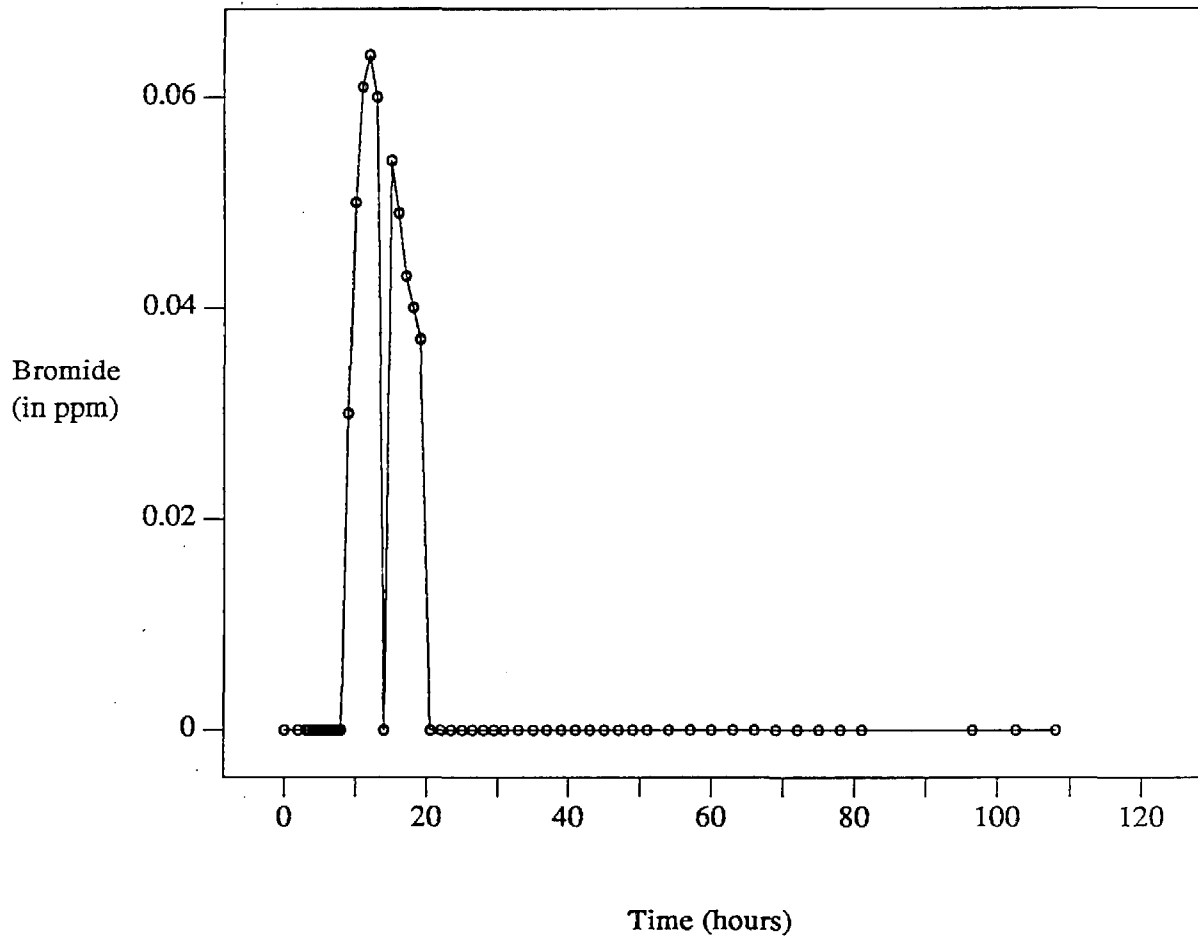


Figure 8. Hydrograph for Emerald Lake Outflow, 1986 Water Year

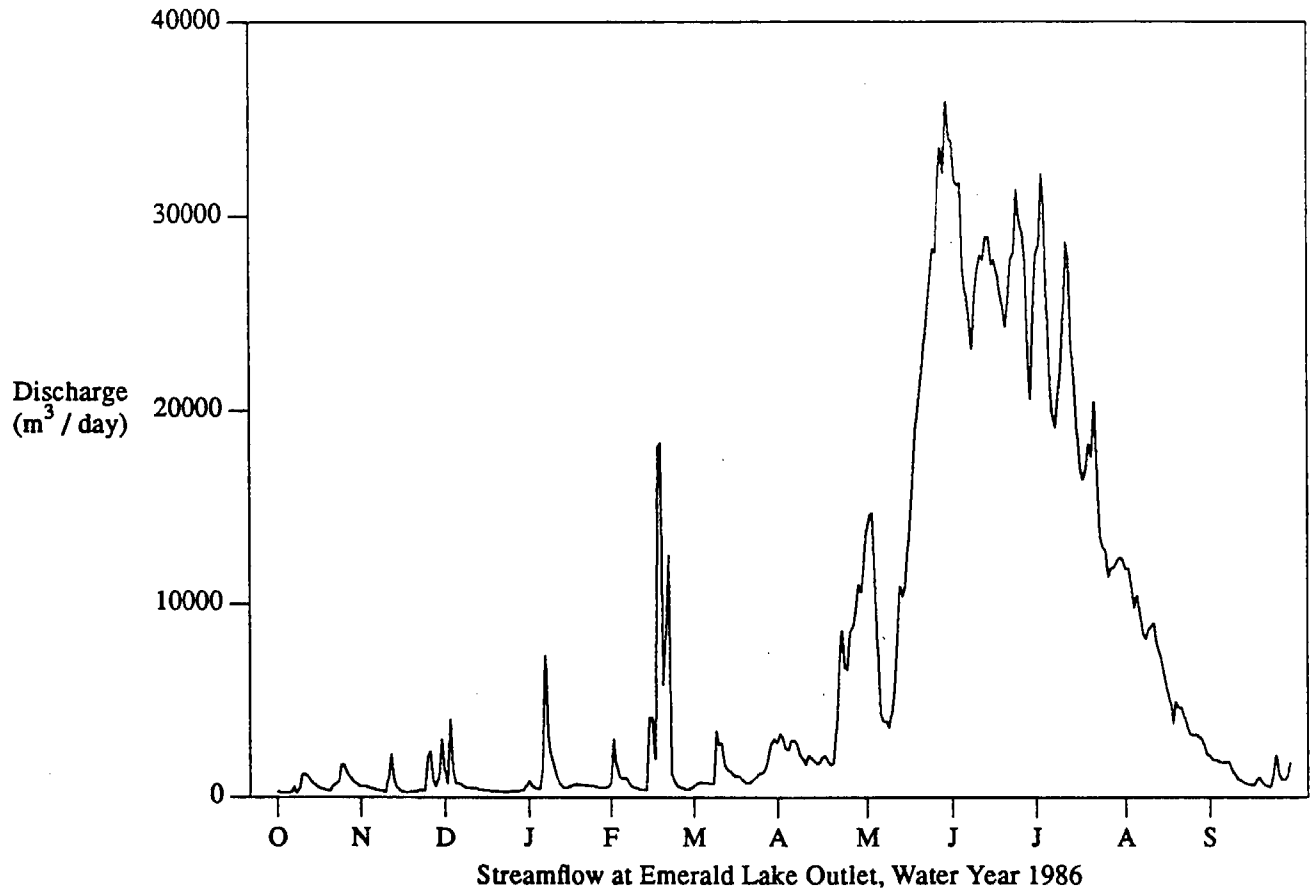


Figure 9. Hydrograph for Emerald Lake Outflow, 1987 Water Year

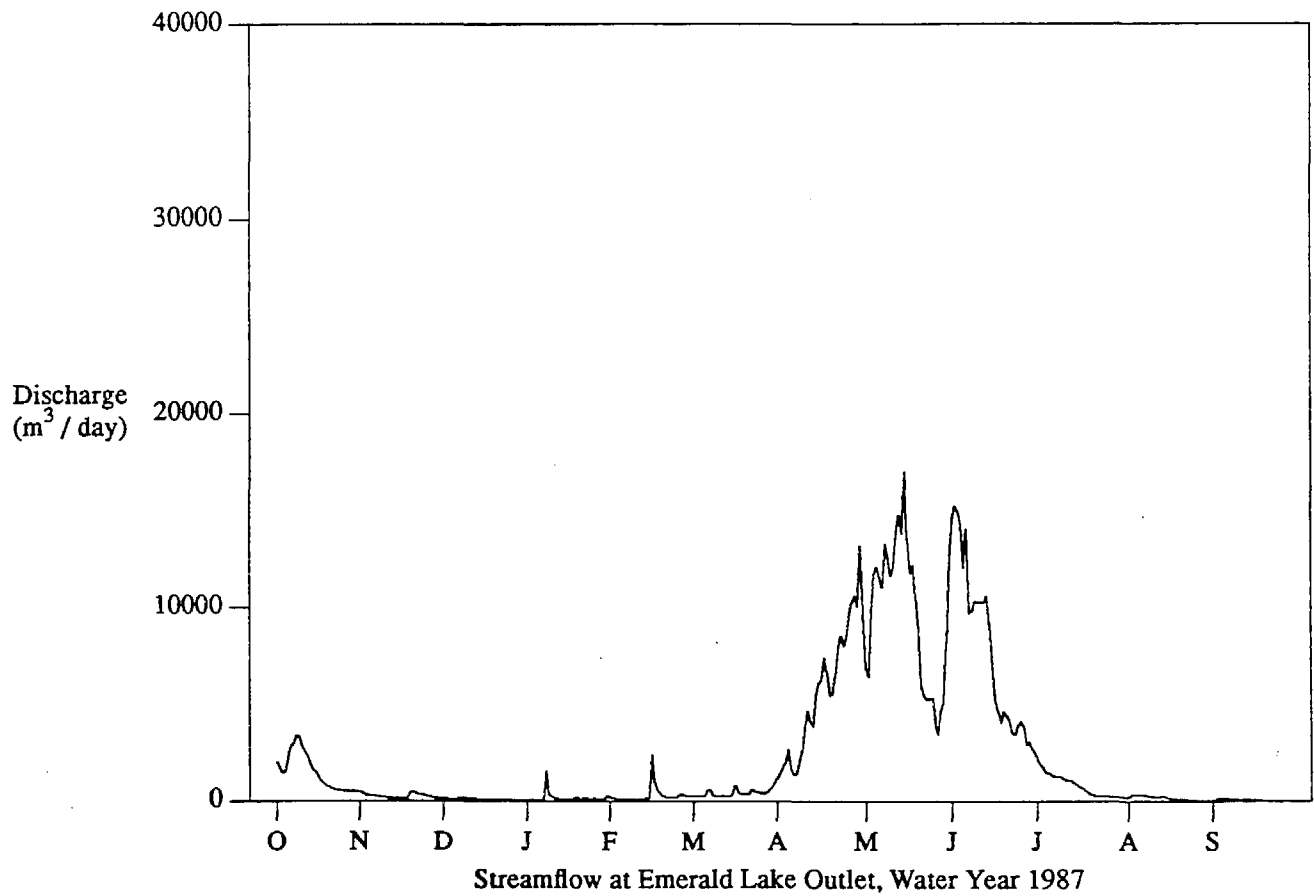


Figure 10. Hydrograph for Emerald Lake Outflow, 1988 Water Year

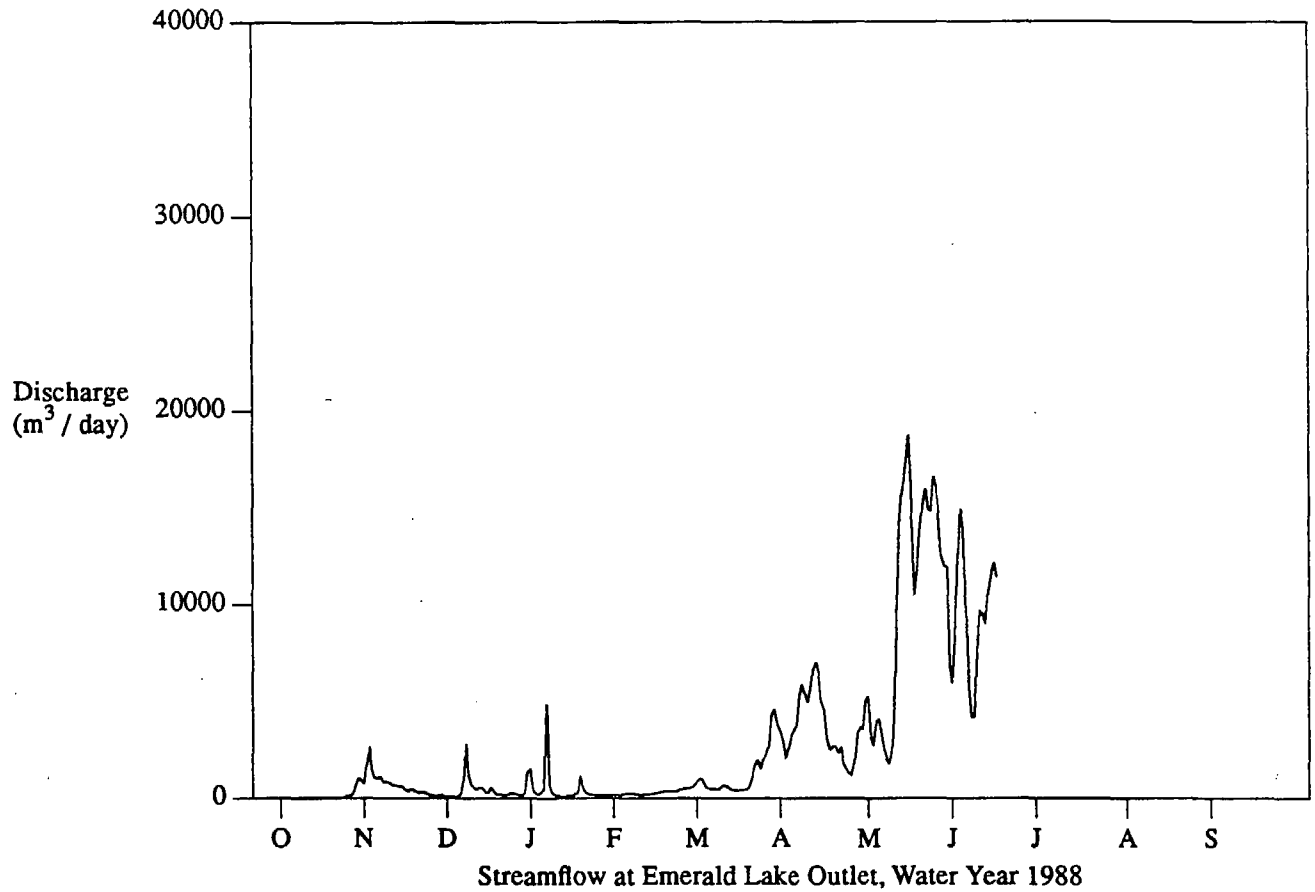


Figure 11. Hydrograph for Emerald Lake Inflow 1, 1986 Water Year

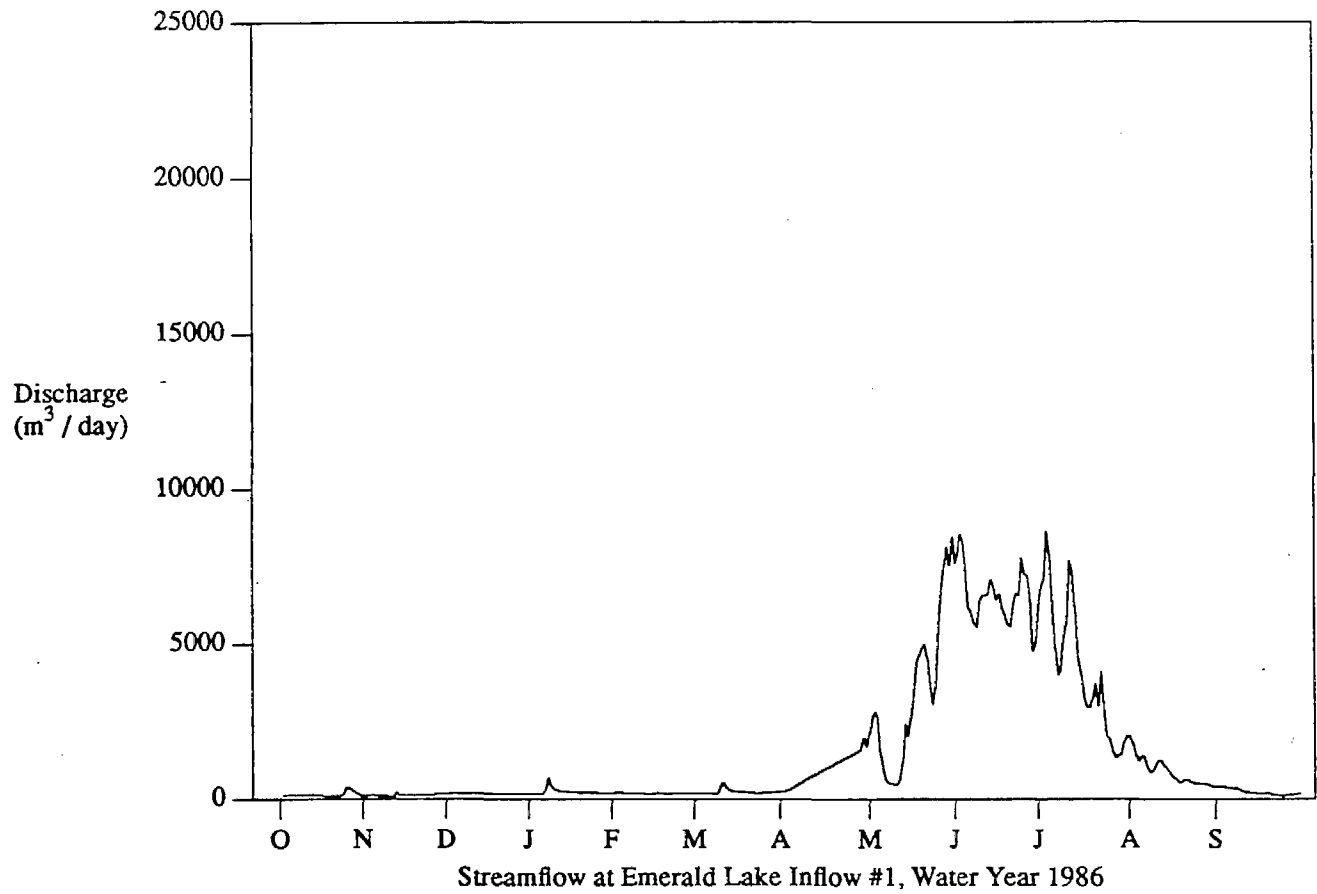


Figure 12. Hydrograph for Emerald Lake Inflow 1, 1987 Water Year

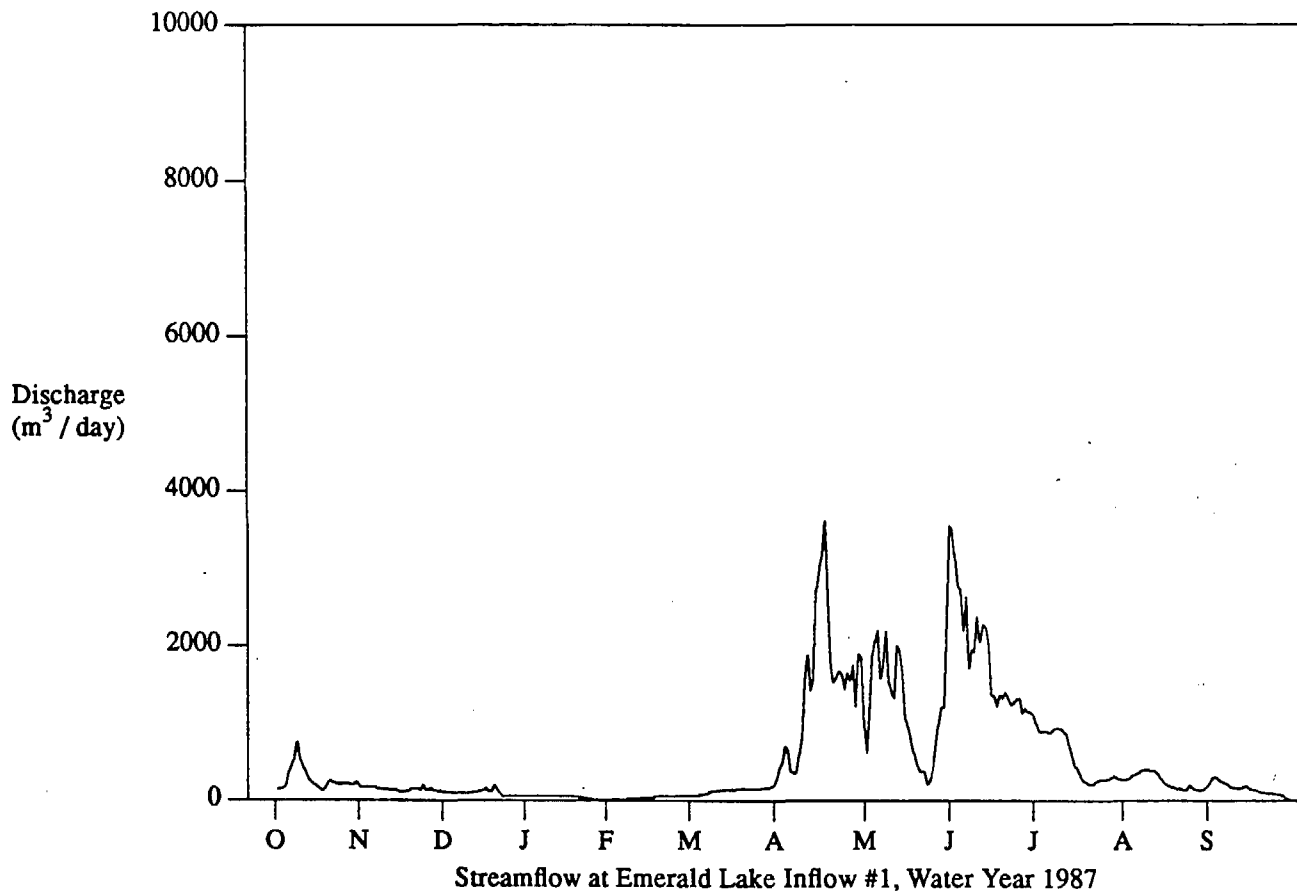


Figure 13. Hydrograph for Emerald Lake Inflow 1, 1988 Water Year

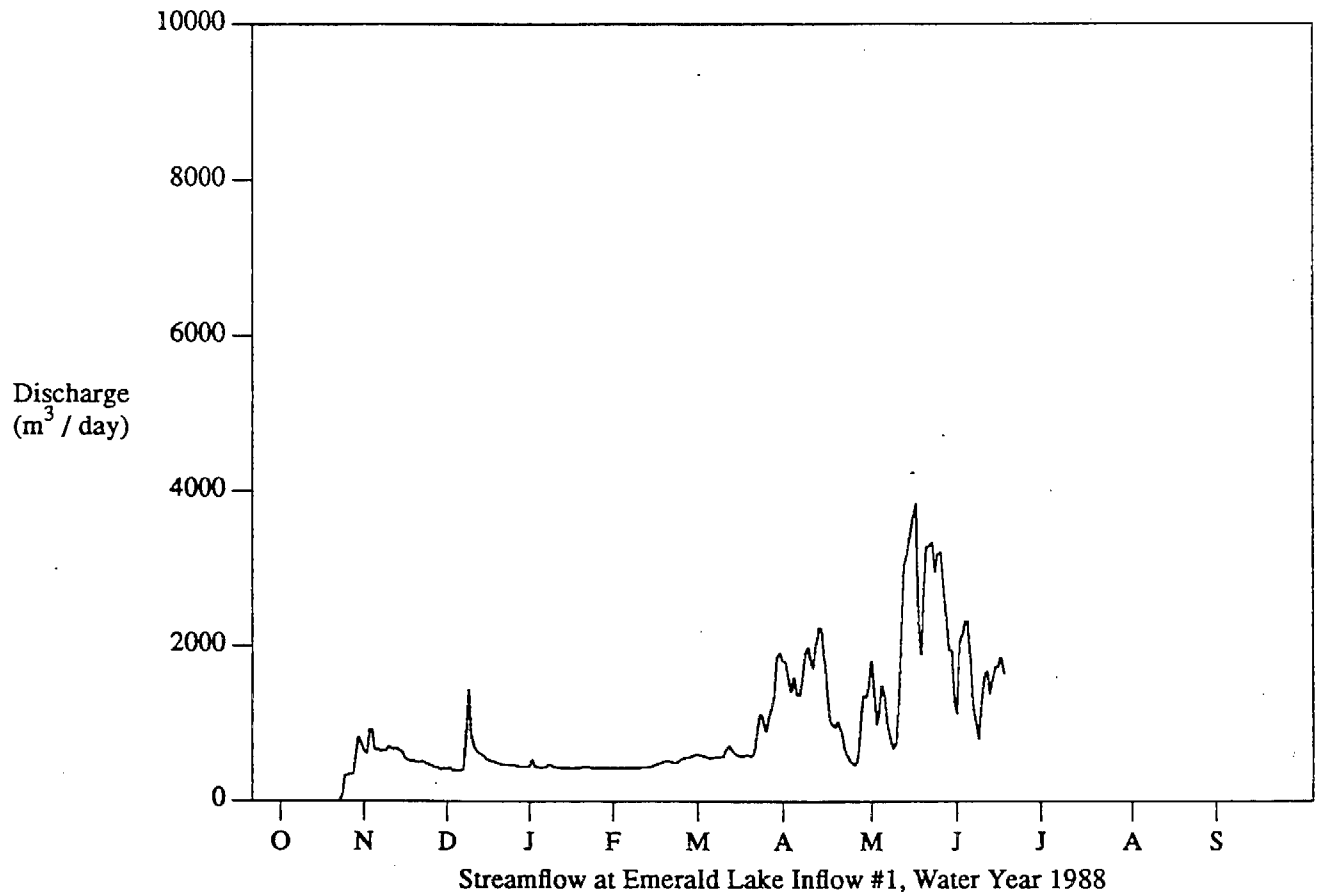


Figure 14. Hydrograph for Emerald Lake Inflow 2, 1986 Water Year

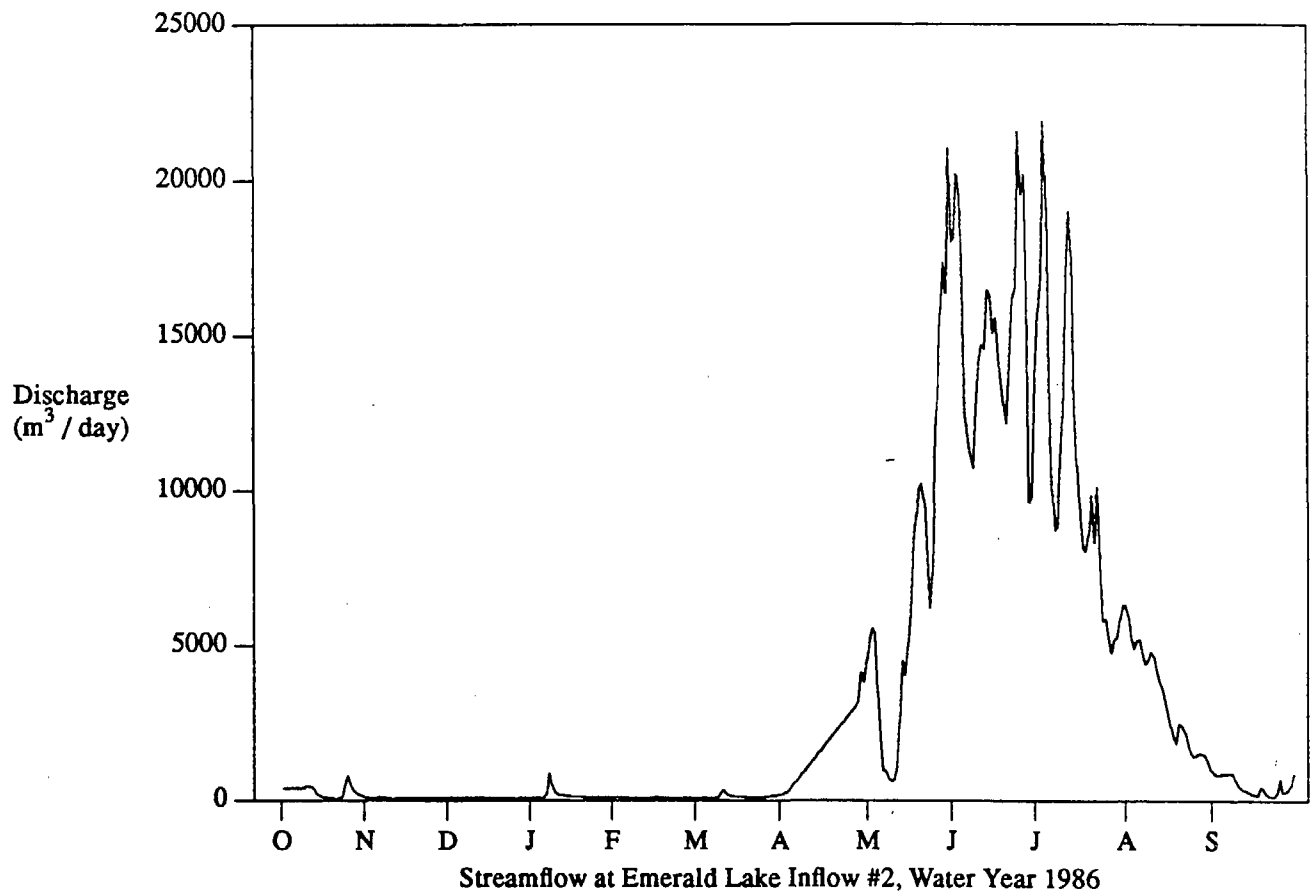


Figure 15. Hydrograph for Emerald Lake Inflow 2, 1987 Water Year

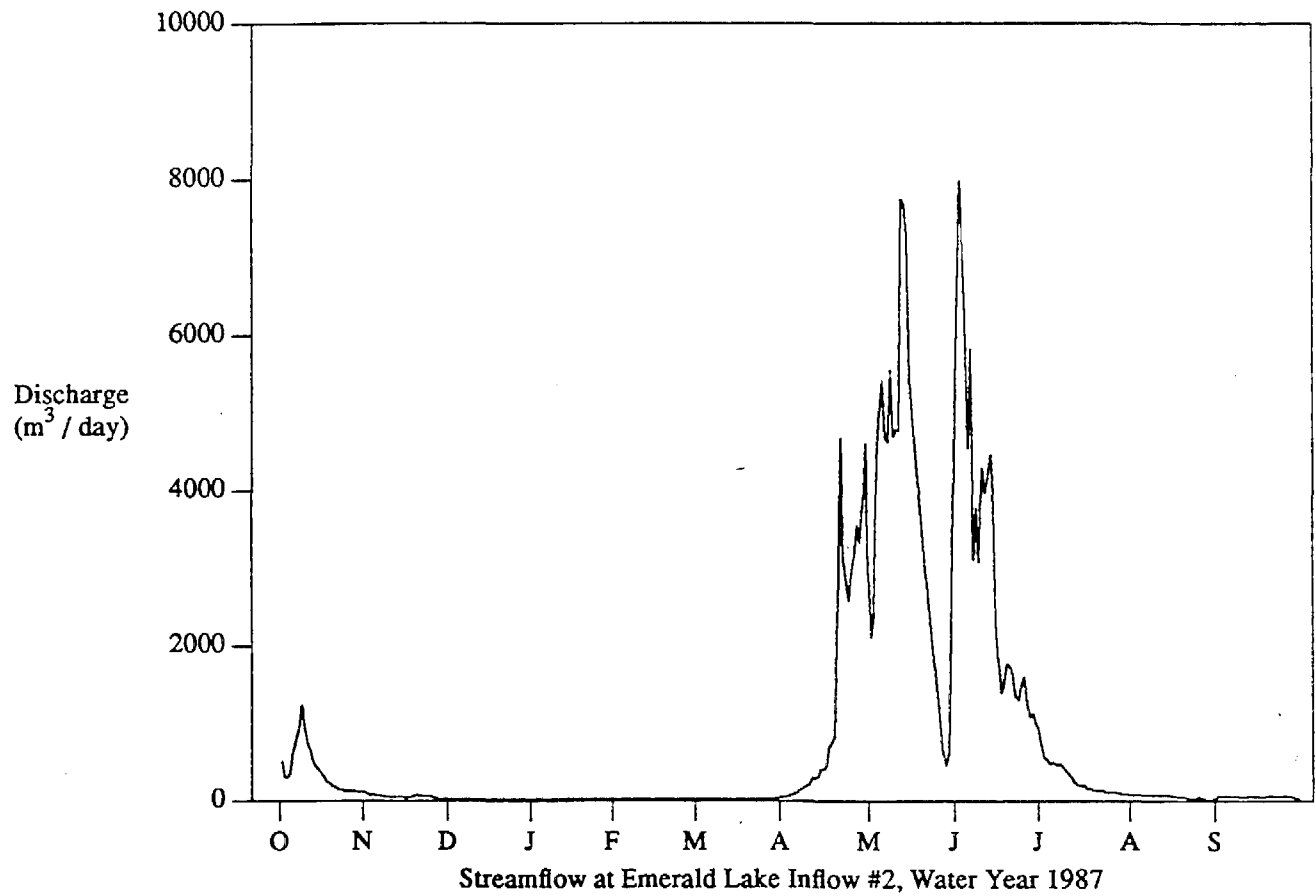
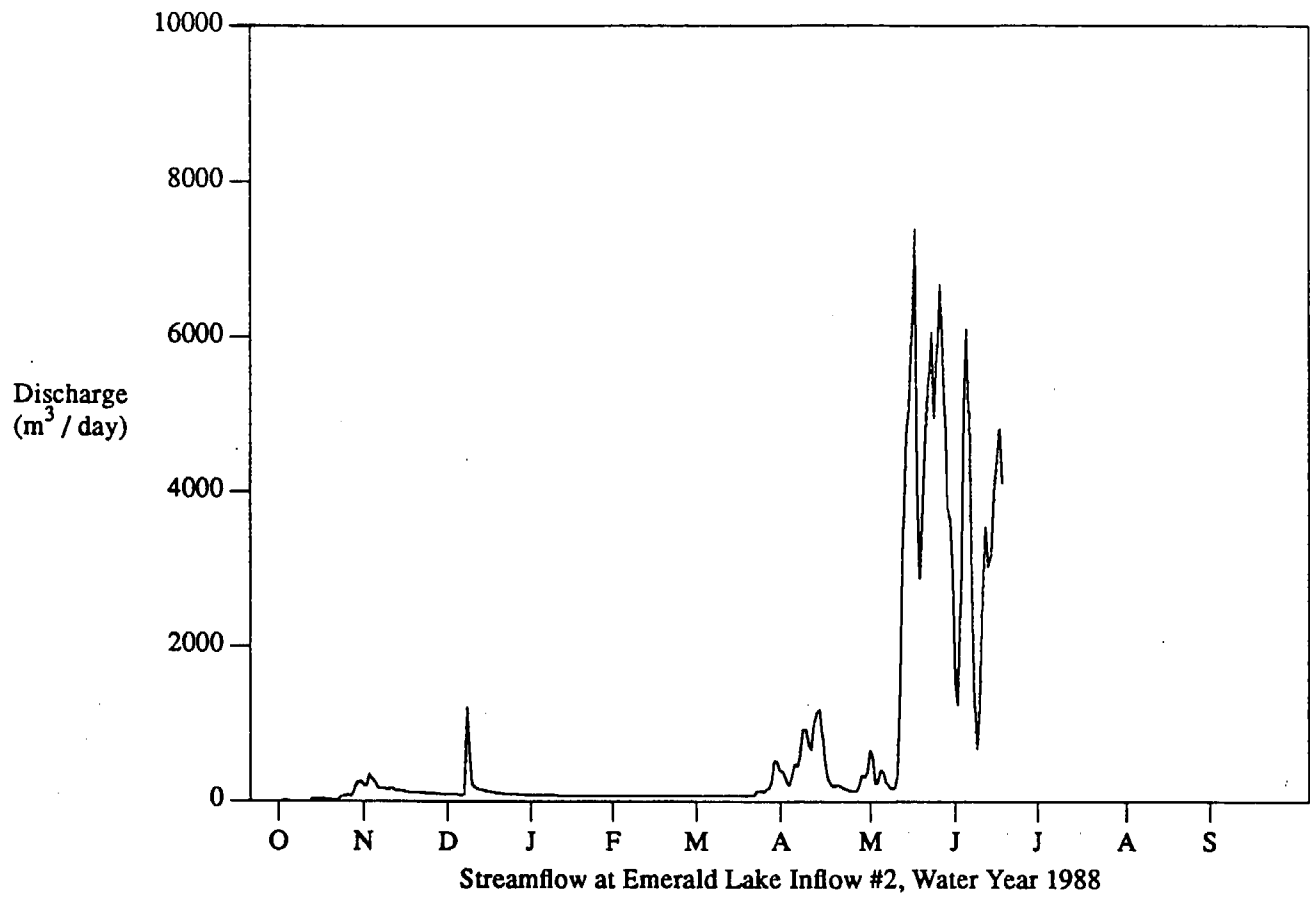


Figure 16. Hydrograph for Emerald Lake Inflow 2, 1988 Water Year



F. References

- Bjerve, L. and O. Groterud, Discharge measurements by a new-formed relative salt-dilution method in small turbulent streams, *Nordic Hydrol.*, 11, 121-132, 1980.
- Bos, M. G., *Long-throated Flumes and Broad-crested Weirs*, 141 pp., Martinus Nijhoff/Dr. W. Junk, Dordrecht, 1985.
- Chow, V. T., *Handbook of Applied Hydrology*, McGraw-Hill, New York, 1964.
- Church, M., Electrochemical and fluorometric tracer techniques for streamflow measurements, *Tech. Bulletin No. 12*, Published for the British Geomorphological Research Group by Geo Abstracts, Norwich, England, 1975.
- Church, M. and R. Kellerhals, Stream gauging techniques for remote areas using portable equipment, *Tech. Bulletin No. 25*, 89 pp., Inland Waters Branch, Department of Energy, Mines and Resources, Ottawa, 1970.
- Dickinson, W. T., *Accuracy of discharge determinations*, Hydrology Papers, Colorado State University, Fort Collins, Colo., 1967.
- Dozier, J., J. M. Melack, D. Marks, K. Elder, R. Kattelman, and M. Williams, Snow deposition, melt, runoff, and chemistry in a small alpine watershed, Emerald Lake Basin, Sequoia National Park, Final Rep., Contr. A3-106-32, Calif. Air Resour. Board, Sacramento, CA, 1987.
- Herschy, R. W., *Streamflow Measurement*, Elsevier, London, 1985.
- Huntington, G. L. and M. Akeson, Pedologic investigations in support of acid rain studies, Sequoia National Park, CA, (Tech. Rept.), Department of Land, Air and Water Resources, Univ. Calif., Davis, 1986.
- Jarrett, R. D., Hydraulic research of mountain rivers, *Eos, Trans. Amer. Geophys. Union*, 69, 1217, 1988.
- Linsley, R. K., M. A. Kohler, and J. Paulhus, *Hydrology for Engineers, Third Edition*, McGraw Hill, New York, 1982.
- Østrem, G., A method of measuring water discharge in turbulent streams, *Geographical Bulletin*, 6, 21-43, 1964.
- Stromeyer, C. E., The gauging of streams by chemical means, *Proceedings of the Institute of Civil Engineers*, 160, 349-363, 1905.

VI. CLIMATE

A. Introduction

Our measurements of several meteorological variables at Emerald Lake provide the first detailed description of the climate of an alpine site in the Sierra Nevada. Precipitation and temperature data exist for a few sites throughout the Sierra, and snowpack water equivalence has been measured at about 100 snow courses and snow sensors above 2500 m. However, comprehensive evaluation of the climate of an alpine catchment had not been attempted before the Integrated Watershed Study. Although the study did not last long enough to provide information on long-term variations of weather elements, the records from two to three years illustrate general conditions occurring in an alpine basin. The micro-meteorological data were essential in estimating various components of the hydrologic cycle. These data were used to calculate snowpack energy balance, snowmelt, snowpack sublimation, lake evaporation, and evapotranspiration. They also permit a general comparison of climatic conditions at Emerald Lake to other environments. This chapter covers air temperature, humidity, wind, and radiation. Precipitation is discussed in chapters 4 and 5.

B. Measurement Program

Instruments were located at four sites in the Emerald Lake basin: Tower (2802 m — #1 on topographic map [Figure 1]), Inlet (2813 m — #2 on map), Pond (2962 m — #4 on map), and Ridge (3085 m — #6 on map). Air temperature was monitored continuously at all four sites; humidity at the tower, inlet and ridge; wind speed at the inlet and ridge; and radiation at the tower and ridge.

Meteorological data were recorded with the EzLogger recording system manufactured by OmniData, Inc. This system was selected because it provided the flexibility to manage and process data from different types of instruments at multiple locations. The system was made up of modular, programmable field units that were light-weight ($\approx 1\text{kg}$), and easily transported to remote sites. Recording was on solid state EPROMs (erasable, programmable, read-only memory) that were stable during the variations of temperature and humidity found at an alpine site like Emerald Lake. The system had minimal power requirements, 8 D-Cell batteries for approximately 6 weeks of operation. The field units could be programmed to convert the raw voltage output to meteorological units so that field technicians could easily evaluate instrument performance. Recorded data could be transferred directly to a computer, reducing but not eliminating data processing time.

The EzLogger data recorder is a 12-bit system with 12 analog, 2 event counter, 1 frequency input channels, and 4 digital input/output channels. The analog channels could be assigned 5 V, 1 V, 100 mV, or 10 mV full-scale range, independent of sign. This capability allowed the recording of both negative and positive input voltages on the same channel, but reduced the sensitivity of these channels to 11-bits, or 0.05% of full-scale. This sensitivity was adequate for all meteorological instrumentation. One constant excitation voltage (5V) and one variable excitation voltage (0-10V) could be assigned to any of the analog input channels. Analog channels could be sampled at 1, 5, 15, 30 minute, and 1 hour intervals, with options of averaging, totalizing, or recording the maximum and

minimum readings. Sample time varied from 1 to 10 seconds, depending on how the channel was defined. Data could be recorded at the same intervals as sampling, but was usually done at a multiple of the sample intervals. The sampling interval selected was constant for the frequency and all analog channels. Up to five data-recording intervals could be selected for the 15 channels.

The number of channels used, sampling frequency, voltage excitation requirements, and data-recording frequency determined the rates of battery power and data storage consumption. The system performed well with one exception. Data loss occurred in the presence of a strong static charge that is common in high-elevation environments. During these conditions, several records could be lost. To combat this problem, all channels were set to a 5-minute sampling interval and a 15-minute recording interval. These intervals effectively solved the problem, but resulted in very large data rates and more frequent battery and EPROM changes, and complicated the data processing. The recorded data of all analog channels represent the average of three samples of over a 15-minute period. Data from the totalizing channel represent the total number of "events" (tips or revolutions of the anemometer) that occurred during the 15-minute period. Data from the frequency channel can represent the average frequency over the 15-minute period or the total number of revolutions during the recording period.

The data recorded at fifteen-minute intervals were integrated into hourly intervals by weighted averaging. The intervals were constructed so that all began at the same time in either location. The weighting was based on the proximity of each recorded time to the predetermined hourly endpoints. For example, if solar irradiance was measured 5 minutes from an hourly cutoff, that sample accounted for only 12.5 minutes of the hourly interval instead of a full 15 minutes.

Hourly averages were easily converted to daily means without having to weight any values, since each value spanned an equal amount of time. Monthly mean values are the average of the daily means. In the case of radiation, daily mean irradiance values are converted from Wm^{-2} to MJm^{-2} and summed for monthly totals of incident energy.

The quarter-hour data for the Emerald Lake watershed were not continuous at each site. Sensors sometimes yielded spurious values, or recording may have terminated for periods ranging from one half-hour to two weeks. Gaps in the dataset of more than one and up to three hours were filled by a combination of extrapolation from the alternate site and by interpolation between available times so that each hourly time step contained a value. Once these small gaps were filled, the data were converted to daily means.

If gaps were longer than three hours, they would usually be several days. Day-long gaps were filled in the same manner as the shorter ones: first by extrapolation from daily values at the alternate site, then by picking intervals near the period in question where both ridge and lake data exist, taking the mean of the residuals between sites, and adding that mean to the extrapolated values. If no record existed for either site, interpolation was done by substitution of the mean value for comparable intervals adjacent to the period in question, as was the case for twelve days in May of 1986. Data gaps longer than two days were filled before estimating monthly values, but finer temporal resolution was not attempted in these

cases.

Meteorological instrumentation had to be robust, have low power requirements, and be compatible with the data-recording system described above. All instrumentation was duplicated at least once in the watershed to insure data redundancy, and to improve our understanding of parameter uncertainty and spatial variance. A variety of instruments with different characteristics were used during the course of the project (Table 62). Estimates were made of the recorded data quality as affected by the data-recording system and the limitations of the type of instrument used. The "noise equivalent change" ($NE\Delta$) is the magnitude of parameter change required to cause a change in the recorded data. Linearity reflects instrument characteristics, and is based on the precision of the function used to convert instrument voltage to parameter units. Precision of the recorded data is estimated from the combined effects of $NE\Delta$, linearity, and instrument stability. In general, $NE\Delta$ should be substantially smaller than linearity, and estimated precision will be larger than linearity. $NE\Delta$ is computed from the full-scale range of the channel, converted to parameter units. Linearity and precision were computed for the mean parameter value during the snow season.

Air temperature probes were designed and constructed using thermistors manufactured by Yellow Springs Instruments, Inc. These thermistors were individually tested and calibrated to a temperature range expected at this site, improving both the linearity and the precision of temperature data from them. Temperature sensors manufactured by Vaisala and Physchem were also used. The broad calibration range of these sensors resulted in lower precision of the data recorded. A Weathertronics Hygro-Thermograph was used as a back-up for the digitally recorded air temperature and humidity instrumentation, but data from this instrument were not used in the analysis.

Most of the recorded air temperature data were of acceptable quality during windy or low sun periods. During calm conditions, however, radiation shielding was a problem for all instruments. A fabricated radiation shield made of four 10 cm square aluminum plates, painted with highly reflective white paint, proved to be inadequate in the thin atmosphere and high radiant intensities common in a high-altitude environment. Under calm conditions, radiant heating or cooling of the sensor would occur. A mechanically aspirated radiation shield would have solved the problem, but the required power could not have been supplied. A radiation shield manufactured by Met One (Model 071/5290) was self aspirating, and corrected the problem in all but the most calm conditions.

Humidity, or the water vapor content of the air, is another commonly measured meteorological parameter. This parameter is more difficult to monitor than air temperature, as it cannot be measured directly outside the laboratory. Many techniques are used to estimate humidity, but the most common are by changes in the flexibility of a hair, or filament, or changes in the electrical capacitance or conductance of a porous medium of a composition that has a known electrical response to changes in moisture content (e.g. lithium chloride). These methods usually estimate the relative humidity, or the ratio of the actual water vapor concentration to the saturation concentration at that temperature. A much more accurate method to measure humidity is to directly measure the dew point or

condensation temperature of the air by cooling or heating a surface until condensation occurs. Unfortunately, this requires more power than is likely to be available at a remote site, as both heating and cooling and mechanical aspiration of the sensor are required.

Humidity measurements were problematic during most of the 1986 snow season. The Physchem sensor estimated the relative humidity of the air by the change in resistance in a lithium chloride cell. This instrument was not designed for operation during the dry, cold conditions which are common in an alpine watershed. The precision of the instrument was poor at low humidity (<300 Pa) and once the lithium chloride cell was saturated with water or ice (common during blowing snow-deposition events), it could not be re-calibrated in the field. Very few data from this instrument were of useful quality. The Vaisala instrument was much more robust, was reliable across the full range of humidities, and did not suffer the calibration and hysteresis problems associated with the Physchem sensor. Data from this instrument were of acceptable quality, but were not available until mid-July, 1986.

In 1986, questionable results and missing data led to calculation of humidities during part of the year. Estimated humidities are calculated from thermal radiation, which is more easily measured than humidity. The calculation is based on the assumption that thermal radiation under clear skies is a function of the vapor pressure and air temperature [Brunt, 1932; Brutsaert, 1975]. The application to Emerald Lake is described by Marks [1988]. Assuming that measured air temperature was reliable, and that clear skies tended to persist during times when measured humidity were missing or unreliable, this approach was used to estimate vapor pressure. It gives some low vapor pressures at times, but in general produces a diurnal range and a daily mean which are consistent with measured dew point temperatures at similar sites in the Sierra Nevada. It will tend to over- or under-estimate vapor pressures during wind-free periods when the measured air temperature is incorrect, and will over-predict vapor pressure during cloudy periods. It is, however, the most reliable estimate of vapor pressure during much of the 1986 snow season at Emerald Lake.

Although air temperature does not directly affect the estimate of relative humidity by the instruments discussed above, the quality of the air temperature data are critical in the calculation of vapor pressure from relative humidity:

$$e_a = e_{a,sat} \times \frac{RH}{100} \quad (26)$$

where:

- e_a = vapor pressure of the air (Pa)
- $e_{a,sat}$ = saturation vapor pressure at T_a (Pa)
- RH = relative humidity

Over- or under-estimates of T_a will affect the calculation of e_a . Proper radiation shielding is essential for measuring both air temperature and humidity.

Wind speed was also routinely monitored at Emerald Lake. Wind direction was deemed so site-specific that we decided that the effort to adequately monitor this parameter was beyond the scope of this project. Wind is highly variable in both time and space and is difficult to characterize by sampling in either of these dimensions. Some averaging or

integration of the measurement is required in almost all cases. A totalizing anemometer, or a count of the number of turns of the anemometer during a specified time period, is a solution to the problem of temporal sampling that was initially applied at both sites with mixed results. Initially, at the ridge site, a recording interval of 1 hour was specified because of difficult access and limited recording capabilities. Wind speed was recorded as the average of four 15-minute totals utilizing an event-counter channel. Unfortunately, this channel was limited to a maximum recordable wind speed of 9 m s^{-1} during the 15-minute totalizing period, inadequate at either site. At the lake site, a 15-minute recording interval was used, because easier access would allow more frequent changing of the recording medium. At this site, wind speed was recorded as the average of three 5-minute totals, allowing a maximum recordable wind speed of 27 m s^{-1} during a 5-minute totalizing period. This proved adequate most of the time at the lake site.

The problem at the ridge site was realized in early December 1985, and the ridge data recorder was moved to a recording and sampling interval similar to that at the lake site. By mid-winter, however, the ridge site was regularly exceeding the maximum value of 27 m s^{-1} . Limits of both the recording and data storage media prohibited a more frequent recording or averaging intervals. The only solution to the problem was to abandon the totalizing anemometers, and replace them with current generators. This replacement allowed us to utilize frequency channels on the data recorder. The output from these channels was then sampled and averaged in a manner similar to the air temperature and humidity data. This change was implemented in early July at both sites.

Incident solar radiation was measured by Precision Spectral Pyranometers, and incident thermal radiation by Pyrgeometers manufactured by The Eppley Laboratory, Inc. These instruments were re-calibrated by the National Bureau of Standards just prior to the 1986 snow season. The pyranometers have a cosine response within $\pm 1\%$ from $0-70^\circ$ from nadir. The pyrgeometers have a perfect cosine response from a diffusing source like the atmosphere. The global solar pyranometers (285-2800nm) measured irradiance in excess of 1200 W m^{-2} at times. This produced an output voltage that exceeded 10 mV by 1 to 3 mV, forcing the use of the 100 mV range on the data recorder. The reduced sensitivity of the larger full-scale range resulted in the large $NE\Delta$ value for these data. Data linearity and precision were also affected, but not to such a great extent.

C. Results

1. Air Temperature

The most common meteorological data collected anywhere are of air temperature. Figure 17 shows daily mean air temperature from November 1985 through May 1988, at the ridge and lake sites. Ideally these measurements should be made at a specified height above the snow surface, shielded from the effects of radiation or conduction from sources other than the atmosphere. In practice, this is seldom the case. Some radiant heating or cooling of the instrument shelter is inevitable, but in most locations these influences produce only a minor effect. At an alpine site, such as Emerald Lake, the atmosphere is thin (70 kPa or less), with low turbidity, and solar insolation is very high. During the day, the temperature of the sensor can be higher than that of the air. On clear nights, incident thermal radiation

will be small, and radiant cooling can lower the temperature of the sensor below that of the air. The best passive radiation shields available will fail under these conditions. The problem is exacerbated during the day because of the high reflectivity of the snow and surrounding terrain, causing the air temperature sensor to receive solar energy from all sides. These effects are difficult to detect in the data, as they show up only as temperature extremes. This problem is maximized when wind speeds are low and mixing of the air is small. A solution would be to mechanically aspirate the temperature sensors, but this consumes power and is not possible at most remote sites. Careful evaluation of both wind and air temperature allows us to note those times when a problem may have occurred, but we cannot know the magnitude of the measurement error without another independent measurement at the same time.

There was a dramatic correspondence of extreme high and low temperatures with low wind speeds (Figure 18). Although isolation of the effects of radiation is difficult, this figure illustrates that both extreme high and low temperatures occurred during periods of light winds. Comparison of daily maxima and minima with data from other alpine sites in the Sierra Nevada and with spot measurements made in the watershed showed that the range of continuously measured daily air temperature was unrealistically large. Spot measurements of air temperature made during the snow season with a sling psychrometer never exceeded 15 °C.

Fortunately for energy exchange calculations, this problem does not cause significant errors, because at low wind speeds turbulent energy exchanges are also minimized. The success of temperature-index snowmelt models at forested or protected sites is due to both the correlation of measured air temperature and radiant energy flux, and the fact that most measurements of air temperature are affected by the intensity of radiant flux at low wind speeds.

Monthly air temperatures at the lake and ridge sites ranged from -4 to +12 °C (Table 63). Monthly average temperatures have little physical significance, but they allow us to evaluate longer-term variation of a parameter which is subject to so much stochastic short-term variation that it can be difficult to see differences between the sites. As indicated in Figure 17 and Table 63, the ridge is cooler than the lake site and has a larger range in temperature. The coldest months were December and February during our measurement period. At both sites, March or April were the months when the diurnal amplitude was maximized, which is expected as these are usually the months when net energy exchange begins the transition from negative to positive. Mean annual temperature from 1986 and 1987 is about 3 °C. Temperatures in January averaged about -1 °C, and temperatures in July averaged about 10 °C. These averages suggest that the Emerald Lake basin is both somewhat warmer in winter and cooler in summer than the few other alpine sites for which temperature data exists (Table 64). However, the short period of record prevents conclusive comparisons. Differences among the three years at Emerald Lake were not particularly dramatic. The monthly mean of daily averages ranged from -5 °C in the winter to 12 °C in the summer. The day-to-day means can change as much as 12 °C, but only change about 2 °C on the average. The mean monthly temperature for either site fell below 0 °C in November or December, and rose above 0 °C in any of three months from February to April.

The mean monthly temperature at the lake was greater than or equal to that of the ridge in 25 out of 32 months. The 285 m elevational difference between the ridge and lake sites is great enough to display a range of temperature gradients, but the gradients for some months are positive, suggesting that inversions may dominate during some months. Since the two meteorological stations lie within the territory of occasional inversions, the effects of topoclimate may blur any regional adiabatic lapse rate for the alpine area. Hansen-Bristow [1988] has reported the same phenomenon for several months of a 6-year study period in Colorado. The two sites at Emerald Lake differ by only 0.2 °C, and discussion of a local lapse rate is pointless. At lower elevations where several sites with longer records were available, a lapse rate of -5.6 °C km^{-1} for July and -4.7 °C km^{-1} for January in Sequoia National Park has been calculated [Stephenson 1988]. In the Yosemite area, lapse rates of -3.0 °C km^{-1} and -3.7 °C km^{-1} for July and January, respectively, have been calculated [Major, 1977].

2. Humidity

Summaries of atmospheric humidity demonstrate a general seasonal trend with higher values in spring and summer and minimum values in winter (Figure 19 and Table 65). Vapor pressure is the partial pressure of water vapor in the atmosphere, expressed here in Pascals. The lowest vapor pressure occurs during the winter as does the lowest mean monthly temperature. The humidity reaches a maximum in the summer, when the air is warmer and possesses a greater water vapor capacity. The day-to-day variation is about 80 Pa in the winter and 100 Pa during the summer. There was little difference between the atmospheric humidity values at the ridge and lake sites, except during summer when the lake was ice-free and relatively warm. At that time, humidity near the lake tended to be higher with a smaller diurnal variation than at the ridge. However, measurement or recording uncertainty is around 40 to 50 Pa, so these differences cannot be distinguished from measurement noise. These data suggest that there is no significant humidity difference between the sites, and that there was little spatial variation in vapor pressure over the watershed during most of the snow season. The relatively low values in late summer of 1986 are probably an attribute of the instrumentation. We believe that the peak values of 1987 and 1988 are more typical of the summer months. Similarly, the values in the early part of water year 1986 are probably excessively high.

The mean annual relative humidity for Emerald Lake is about 45%. Mean monthly relative humidity can range from 25% in the summer to 75% in the winter. In the winter, the temperature is low and the atmosphere has a small capacity for water vapor, but what little water vapor is present will be a large part of the atmosphere's water vapor capacity. Therefore, on a monthly basis the relative humidity is high during the winter although the absolute humidity is low.

3. Wind

Windspeed at the exposed ridge site tended to be at least 50 percent greater than that at the lake site (Table 66). In this case, longer term averages may be more meaningful than the shorter term data. Early season similarities between sites is an artifact of problems with the recording and averaging intervals discussed above. During the winter and spring, storms are usually part of a large low-pressure system that can affect a large fraction of the Sierra

Nevada. During the summer and fall, more localized, convective storms are most common [Major, 1977]. Although wind speed characteristics may differ between seasons, such a difference is not readily apparent at a monthly resolution. The usual daily mean for the ridge is about 6 ms^{-1} and 4 ms^{-1} for the lake. Such wind speeds are comparable to the speeds reported at the three lower-elevation sites in Colorado (Table 64).

4. Radiation

The radiant energy flux, or net all-wave radiation (S_{net}), at a point is the incident spectral irradiance ($S\downarrow$) less spectral exitance ($S\uparrow$) integrated over all wavelengths:

$$S_{net} = S\downarrow - S\uparrow \quad (27)$$

The irradiance term $S\downarrow$ includes direct and diffuse solar radiation and longwave radiation emitted from the atmosphere. Exitance $S\uparrow$ includes both reflected and emitted radiation from the surface.

Radiation is the only form of energy transfer that can be measured directly in the natural environment. Incident radiation can be reliably and accurately measured in broad wavelength band widths, using well established techniques and instrumentation [Monteith, 1973]. Under clear sky conditions, the distribution of incident radiation can be modeled over complex alpine terrain, for both solar [Dozier, 1980] and thermal [Marks and Dozier, 1979] wavelength ranges, but under cloudy conditions, measurements are necessary because the separate contributions of direct and diffuse solar and emitted thermal radiation from the atmosphere and clouds are not easily predicted or modeled. At some sites, irradiance includes significant contributions from reflection and emission from adjacent terrain. At Emerald Lake incident radiation is measured at two sites to calibrate the estimate of irradiance for terrain effects, atmospheric effects, and cloud cover. Parameters that cannot be reliably measured are modeled and net radiation is calculated from a combination of measured and modeled parameters. Net radiation at the earth's surface is separated into two solar and one thermal spectral bands.

Solar radiation (effectively wavelengths from 0.3 to $3.0 \mu\text{m}$) is absorbed and scattered by terrestrial materials, but not emitted. For snow, absorption and scattering are functions of wavelength, incidence angle, and the grain size and concentration of absorbing impurities in the surface layer [Bohren and Barkstrom, 1974; Warren, 1982].

Snow albedo varies spectrally, but detailed spectral measurements of radiation at the snow surface are difficult under controlled conditions and not possible at a remote site. A spectral approach to modeling solar radiation [e.g. Dozier, 1980] will give an accurate result under clear skies, but it is complicated computationally and requires detailed information about the atmosphere and the snow surface that cannot be known when monitoring a remote site. Other investigators have taken a single-band, global approach to modeling solar radiation over remote alpine areas [Davies and Idso, 1979; Munroe and Young, 1982; Olyphant, 1984]. This simplifies the calculation of net radiation so that it can be done at a remote site, but it ignores the distinct differences in the absorption and scattering properties of the snow surface in the visible and near-infrared wavelengths.

Marshall and Warren [1987] point out that most general circulation models (GCMs) parameterize solar radiation into two wavelength bands, and suggest that snow albedo can also be parameterized to reduce computational difficulties while retaining the important spectral features affecting net solar radiation at the snow surface. We use their approach to examine net solar radiation at the snow surface. Incident and reflected solar radiation are measured in two wavelength bands: visible (0.3–0.7 μm) and near-infrared (0.7–2.8 μm). The net solar radiation at a point is calculated by:

$$S_{net,solar} = S_{vis} (1.0 - R_{vis}) + S_{nir} (1.0 - R_{nir}) \quad (28)$$

where

S_{vis}	= incident solar radiation in the visible band
R_{vis}	= reflected solar radiation in the visible band
S_{nir}	= incident solar radiation in the near-infrared band
R_{nir}	= reflected solar radiation in the near-infrared band

The albedos are calculated from a model presented by Marks [1988] which is based on effective snow grain radius and solar zenith angle as detailed by Marshall and Warren [1987]. Net solar radiation was computed from the modeled albedos and measured irradiances for two sites in the Emerald Lake watershed. Near-infrared irradiance represents 53% of the total solar irradiance at the ridge site and 60% of the total at the lake site, but it represents 85% of the net solar input at the ridge and 89% at the lake site (Tables 67 and 68). In early winter, the ridge site receives more solar irradiance than the lake site, but by early spring they receive the same amount, and by late spring the lake site receives significantly more solar radiation than the ridge. Large solar zenith angles during winter cause the lake site to be shadowed for a significant part of the day, but in spring the sun is higher in the sky, and this shadowing is reduced. Moreover, in the spring reflected radiation from near by terrain adds to the radiation received at the lake site.

Solar irradiance is at a maximum during June and July (Figure 20). Thermal irradiance is greatest during the summer and fall. Solar irradiance is of greater magnitude than thermal irradiance during the summer and fall, and they are of comparable magnitude during the April - May and August - September periods. Solar radiation accounts for 45% of the total irradiance on a yearly basis. During the spring, when the snowmelt season begins, solar radiation accounts for 50% of the total irradiance. The near-infrared portion of solar irradiance usually exceeds the visible portion, and is greater at the lake than at the ridge.

Monthly totals of irradiance for the period of April through June are comparable between years to within 10%. The total monthly solar and all-wave irradiance for the 1986 snowmelt season (May through July) is greater than that of the 1987 and 1988 snowmelt seasons (April through June) by about 15%, partially due to the snowmelt season beginning a month later in 1986.

Thermal radiation (effectively 3.5 to 50 μm) is absorbed and emitted by the atmosphere without appreciable scattering [Paltridge and Platt, 1976]. Because the emissivity of snow is spectrally rather flat [Dozier and Warren, 1982], spectral variability in incoming thermal radiation can be ignored. Integrated thermal irradiance can be measured and broad band

emissivities can be used for the snow surface and surrounding terrain. The thermal irradiance in an alpine region is a function of the atmospheric conditions and the temperature and configuration of the surrounding terrain [Marks and Dozier, 1979]. Net thermal radiation is:

$$S_{net, lw} = S\downarrow_{lw} - (\epsilon_s \sigma T_s^4) \quad (29)$$

where

$S\downarrow_{lw}$ = incoming thermal longwave radiation

ϵ_s = emissivity of snow

σ = Stefan-Boltzmann constant

T_s = temperature of snow in Kelvins

Considerable effort has gone into development of simple models of thermal irradiance from the atmosphere, but most of these are applicable only to clear-sky conditions. Cloud cover increases thermal irradiance at the surface, and, as for solar radiation, this effect is not easily modeled. The atmospheric contribution to thermal radiation generally does not vary much over an area the size of the Emerald Lake watershed, and measured values at a few points effectively characterize it, incorporating the effect of cloud cover.

Thermal exitance is a function of the snow surface temperature and emissivity. The emissivity of snow is 0.988-0.990 for all grain sizes above $r = 75\mu\text{m}$; for fine-grained snow, $r = 50\mu\text{m}$, the emissivity drops slightly to 0.985 [Dozier and Warren, 1982].

TABLE 62. Recorded Parameters and Instrumentation

Radiation: I_{sol}, I_{nir}, I_{lw} Measured at Tower, Ridge					
Wavelength Range	Instrument	Model & Filter	Recorded Data		
			$NE\Delta$	Linearity (Wm^{-2})	Precision (Wm^{-2})
285-2800 nm	Pyranometer	Eppley PSP, WG7	5.0	± 7	± 10
700-2800 nm	Pyranometer	Eppley PSP, RG8	0.5	± 3.5	± 5
4-50 μm	Pyrgeometer	Eppley PIR, Silicon	0.5	± 5	± 10
Air Temperature: T_a Measured at Tower, Inlet, Pond, Ridge					
Effective Range	Instrument	Model	Recorded Data		
			$NE\Delta$ ($^{\circ}C$)	Linearity ($^{\circ}C$)	Precision ($^{\circ}C$)
-25 to 25 $^{\circ}C$	Thermistor	YSI 44104	0.04	± 0.12	± 0.25
-40 to 80 $^{\circ}C$	Thermistor	Physchem TH15	0.04	± 0.25	± 0.5
-40 to 60 $^{\circ}C$	Thermistor	Vaisala HMP113Y	0.04	± 0.3	± 0.5
-20 to 40 $^{\circ}C$	Thermograph	Weathertronics	0.5	± 1.0	± 2.0
Humidity: RH, e_a Measured at Tower, Inlet, Ridge					
Range	Instrument	Model	Recorded Data		
			$NE\Delta$	Linearity	Precision
0 to 101324 Pa	Condensation Mirror	General Eastern 1200 DPS	0.25Pa	$\pm 1.0Pa$	$\pm 5.0Pa$
20 to 90 % 12 to 4115 Pa	<i>licl</i> Resistance	Physchem TH15	0.05% 0.3Pa	$\pm 5%$ $\pm 30Pa$	$\pm 10%$ $\pm 60Pa$
0 to 100 0 to 4242 Pa	% Electrical Capacitance	Vaisala HMP113Y	0.05% 0.3Pa	$\pm 2%$ $\pm 12Pa$	$\pm 4%$ $\pm 25Pa$
0 to 90 % 0 to 4115 Pa	Hygrograph	Weathertronics	0.5% 3Pa	$\pm 5%$ $\pm 30Pa$	$\pm 15%$ $\pm 100Pa$
Snow & Soil Temperature: $T_s, T_g, 0, T_g$ Measured at Inlet, Pond, Ridge					
Effective Range	Instrument	Model	Recorded Data		
			$NE\Delta$ ($^{\circ}C$)	Linearity ($^{\circ}C$)	Precision ($^{\circ}C$)
-25 to 10 $^{\circ}C$	Thermistor	YSI 44104	0.04	± 0.12	± 0.25
Wind Speed: u Measured at Inlet, Ridge					
Effective Range	Instrument	Model	Recorded Data		
			$NE\Delta$ (ms^{-1})	Linearity (ms^{-1})	Precision (ms^{-1})
0.5 to 27.2 ms^{-1}	Cup Anemometer	Met One 014L	± 0.25	± 0.5	± 1.0
0.4 to 50 ms^{-1}	Cup Anemometer	RM Young 12005	± 0.02	± 0.5	± 0.6

TABLE 63. Monthly Air Temperatures at the Lake and Ridge, 1986-1988

Month	Lake Site				Ridge Site			
	T_a	T_{max}	T_{min}	Range	T_a	T_{max}	T_{min}	Range
1986								
Nov	-1	3	-4	7	-2	2	-5	7
Dec	0	3	-3	6	-5	-4	-7	2
Jan	1	4	-2	6	-1	5	-4	10
Feb	-2	3	-4	7	-2	2	-5	7
Mar	1	6	-3	9	-1	2	-3	5
Apr	1	8	-3	11	1	10	-5	14
May	5	10	1	9	6	12	1	11
Jun	8	12	5	7	9	13	6	7
Jul	9	12	6	6	9	12	6	5
Aug	10	13	8	5	10	13	8	5
Sep	4	7	2	6	4	8	1	7
1987								
Oct	3	7	1	6	3	8	0	8
Nov	2	5	0	5	3	8	-1	9
Dec	-1	3	-3	6	-1	6	-4	11
Jan	-2	2	-6	7	-3	2	-7	9
Feb	-3	2	-6	9	-4	3	-8	11
Mar	-1	5	-5	10	-2	5	-7	12
Apr	4	9	0	9	4	11	0	11
May	4	7	2	6	4	9	0	8
Jun	9	12	7	5	10	14	7	7
Jul	9	12	7	5	11	15	7	7
Aug	11	13	9	5	12	16	9	7
Sep	9	12	7	5	10	14	6	7
1988								
Oct	7	12	4	8	6	5	-5	10
Nov	1	6	-3	9	1	8	-4	14
Dec	-4	-1	-8	7	-4	9	-4	13
Jan	-1	4	-5	8	-1	9	-3	12
Feb	1	8	-3	11	1	10	-1	11
Mar	2	10	-3	13	1	11	1	12
Apr	4	13	-2	15	2	10	-3	13
May	5	13	0	13	5	6	0	6
Jun	7	12	3	8	6			

TABLE 64. Comparison of ELW Climate to other Alpine Climates

Site	Elev. (m)	Annual Precip. (mm)	Mean Temperatures			Windspeed (m s ⁻¹)	Period of Record	Source
			Annual (°C)	January (°C)	July (°C)			
Emerald Lake	2940	1600	3	-1	10	5	1986-1988	
California								
Caples Lake	2480		4	-4	13		?	Major, 1977
Kaiser Pass	2803		3	-6	12		1947-1959	Longacre and Blaney, 1962
Ellery Lake	2890	640	3	-5	13		1931-1950	Klikoff, 1965
Southern Sierra	3000			-5	13			Baker, 1944
Piute Pass	3540	780			10		1968	Chabot and Billings, 1972
Colorado								
Como	3050	770	+1	-7	12	3(annual)	1952-1970	Barry, 1973
Red Mtn Pass	3400			-10		6(winter)	1972-1975	Armstrong and Ives, 1976
Berthoud Pass	3500		-2	-12	17	7(winter)	1963-1975	Judson, 1977
Niwot Ridge	3750	1020	-4	-13	8	10(annual)	1952-1970	Barry, 1973

TABLE 65. Air and Snow Surface Vapor Pressure, Water Year 1986

Month	Ridge Site					Lake Site				
	e_a	$e_{a_max}^\dagger$	$e_{a_min}^\dagger$	Range	e_s	Month	e_a	e_{a_max}	e_{a_min}	Range
Water Year 1986										
Nov	320	384	249	134	497	340	397	285	111	522
Dec	292	354	236	118	391	292	354	237	116	543
Jan	331	380	268	112	524	322	390	254	135	591
Feb	314	380	260	119	481	304	388	228	159	495
Mar	365	416	320	96	528	330	394	276	118	553
Apr	351	412	302	109	557	343	406	293	112	569
May	361	419	324	94	588	371	424	334	90	599
Jun	361	415	326	88	610	355	402	323	79	610
Jul	379	430	341	88	610	371	417	338	78	610
Aug	303	387	240	146	610	378	414	353	60	610
Sep	273	352	214	138	591	366	416	328	87	597
Year	332	394	280	113	544	343	400	295	104	573
Water Year 1987										
Oct	376	579	175	404	595	429	577	282	295	602
Nov	177	284	86	198	591	243	347	164	183	600
Dec	153	245	86	159	536	214	291	150	141	548
Jan	128	205	57	148	470	192	271	119	152	490
Feb	208	373	104	269	442	222	350	136	214	475
Mar	307	558	134	424	483	289	467	168	299	512
Apr	419	709	211	498	594	372	544	217	327	600
May	572	832	381	450	590	525	686	371	315	597
Jun	604	919	334	585	611	439	685	214	471	611
Jul	631	987	300	687	610	468	774	209	565	610
Aug	633	867	401	465	611	370	581	199	382	611
Sep	555	792	364	428	611	446	627	290	337	611
Year	397	613	220	393	562	351	516	210	307	572
Water Year 1988										
Oct	507	---	---	---	---	592	791	401	389	611
Nov	377	---	---	---	---	362	575	229	347	569
Dec	289	---	---	---	---	293	414	179	236	424
Jan	195	---	---	---	---	274	431	149	282	507
Feb	218	---	---	---	---	275	470	155	315	566
Mar	339	---	---	---	---	410	844	189	655	563
Apr	409	---	---	---	---	539	1024	254	770	578
May	506	---	---	---	---	617	1005	328	677	573
Jun	576	---	---	---	---	660	949	386	563	593
Year	380	---	---	---	---	447	722	252	470	554

† e_{a_max} and e_{a_min} are the monthly or yearly average of the daily maximum and minimum vapor pressure.

TABLE 66. Wind Speed, Water Year 1986

Month	Ridge Site				Lake Site			
	μ	μ_{\max}^\dagger	μ_{\min}^\dagger	Range	μ	μ_{\max}	μ_{\min}	Range
Water Year 1986								
Nov	7	9	4	5	4	7	2	5
Dec	6	12	2	10	7	9	4	5
Jan	7	14	3	11	5	9	3	6
Feb	7	14	3	11	4	9	1	8
Mar	9	17	3	14	4	8	2	6
Apr	9	17	3	14	5	8	1	7
May	7	14	2	12	5	7	2	5
Jun	6	14	1	13	5	8	2	6
Jul	6	12	1	11	4	6	1	5
Aug	6	14	1	13	3	6	1	5
Sep	7	14	1	12	3	7	1	6
Year	7	14	2	12	5	8	2	6
Water Year 1987								
Oct	5	10	2	8	4	6	2	4
Nov	6	11	2	9	5	8	3	5
Dec	5	11	2	9	5	7	3	4
Jan	7	13	3	10	6	10	3	7
Feb	7	16	2	15	5	10	2	8
Mar	9	17	3	15	4	8	1	6
Apr	8	16	3	13	5	7	2	5
May	6	13	2	11	4	6	2	5
Jun	8	16	2	15	4	7	1	6
Jul	8	16	3	13	3	7	1	6
Aug	9	18	3	16	3	7	1	6
Sep	8	16	2	14	4	6	1	5
Year	7	14	2	12	4	7	2	6
Oct								
Nov	3	---	---	---	2	3	1	2
Dec	3	---	---	---	2	5	1	4
Jan	3	---	---	---	2	4	1	3
Feb	3	---	---	---	3	5	2	4
Mar	3	---	---	---	2	4	1	3
Apr	3	---	---	---	2	4	1	3
May	3	---	---	---	2	3	1	3
Jun	3	---	---	---	2	3	0	3
Year	3	---	---	---	2	4	1	3

$\dagger \mu_{\max}$ and μ_{\min} are the monthly or yearly average of the daily maximum and minimum wind speed.

TABLE 67. Measurement of Radiation Parameters at the Lake, 1986-1988

Monthly totals (MJm^{-2}) of daily mean solar (iradsol), visible (iradvis), near-infrared (iradir) and thermal-infrared (iradth) irradiance at the Emerald Lake watershed lake site, water years 1986 - 1988. Values marked with an asterisk include an estimation during that month.

Month	iradsol (.28-2.8 μm)	iradvis (.28-.7 μm)	% of iradsol	iradir (.7-2.8 μm)	% of iradsol	iradth (3.5-50 μm)
Water Year 1986						
Oct	385	151	39	234	61	678
Nov	210	88	42	122	58	585
Dec	191	82	43	109	57	502
Jan	217	92	42	125	58	568
Feb	254	105	41	149	59	478
Mar	450	181	40	269	60	587
Apr	628	254	40	374	60	600
May	789*	319*	40	470*	60	653*
Jun	874	338	39	536	61	666
Jul	798	310	39	488	61	730
Aug	752	293	39	459	61	764
Sep	499	195	39	304	61	660
Water Year 1987						
Oct	395	154	39	241	61	600
Nov	256	103	40	153	60	561*
Dec	187	77	41	110	59	553*
Jan	213	87	41	126	59	549*
Feb	282	111	39	171	61	542*
Mar	426	166	39	260	61	632
Apr	637	254	40	383	60	619
May	543	212	39	331	61	711
Jun	819	309	38	510	62	710
Jul	824	307	37	517	63	762
Aug	722	271	38	451	62	816
Sep	565*	209*	37	356*	63	753
Water Year 1988						
Oct	392	148	38	244	62	757
Nov	213	83	39	130	61	NA
Dec	158	64	41	94	59	NA
Jan	211*	89*	42	122	58	NA
Feb	350*	138*	39	212	61	533
Mar	548	212	39	336	61	601
Apr	527	195	37	332	63	669
May	745	274	37	471	63	714
Jun	796*	300*	38	496*	62	706*

TABLE 68. Measurement of Radiation Parameters at the Ridge, 1986-1988

Monthly totals (MJm^{-2}) of daily mean solar (iradsol), visible (iradvis), near-infrared (iradir) and thermal-infrared (iradth) irradiance at the Emerald Lake watershed lake site, water years 1986 - 1988. Values marked with an asterisk include an estimation during that month.

Month	iradsol (.28-2.8 μm)	iradvis (.28-.7 μm)	% of iradsol	iradir (.7-2.8 μm)	% of iradsol	iradth (3.5-50 μm)
Water Year 1986						
Oct	404	185	46	219	54	621
Nov	250	119	48	131	52	531
Dec	218	103	47	115	53	488
Jan	245	115	47	130	53	568
Feb	252	126	50	126	50	480
Mar	351	180	51	171	49	643
Apr	573	276	48	297	52	611
May	733*	346*	47	387*	53	672*
Jun	891	407	46	484	54	675
Jul	786	363	46	423	54	742
Aug	721	335	46	386	54	716
Sep	486	227	47	259	53	577
Water Year 1987						
Oct	398	182	46	216	54	936
Nov	319	140	44	179	56	772
Dec	214	94	44	120	56	561
Jan	260	114	44	146	56	557
Feb	295	138	47	157	53	545
Mar	464	223	48	241	52	639
Apr	627	293	47	334	53	637
May	585	279	48	306	52	724
Jun	780	361	46	419	54	749
Jul	830	382	46	448	54	783
Aug	737	337	46	400	54	801
Sep	577	257	45	320	55	731
Water Year 1988						
Oct	394	175	44	219	56	740
Nov	240*	109*	45	131*	55	686*
Dec	162*	78*	48	84*	52	789*
Jan	218*	94*	43	124*	57	698*
Feb	339	148	44	191	56	580*
Mar	536	241	45	295	55	612*
Apr	549	260	47	289	53	678*
May	756	349	46	407	54	724
Jun	809*	367*	45	442*	55	710*

Figure 17. Daily Mean Air Temperatures at the Lake and Ridge, 1986-1988

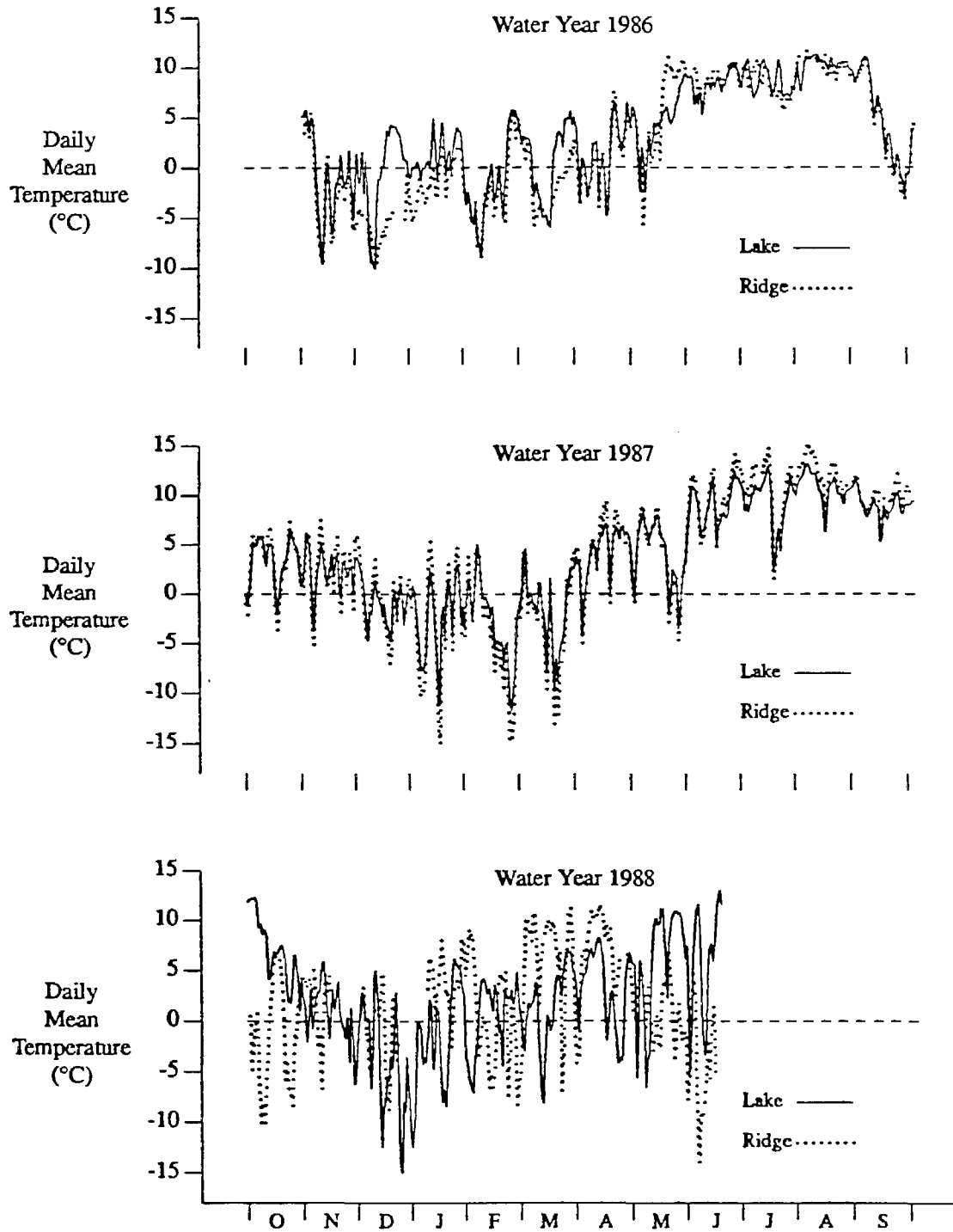


Figure 18. Wind Speed Versus Air Temperature at the Ridge and Lake, 1986

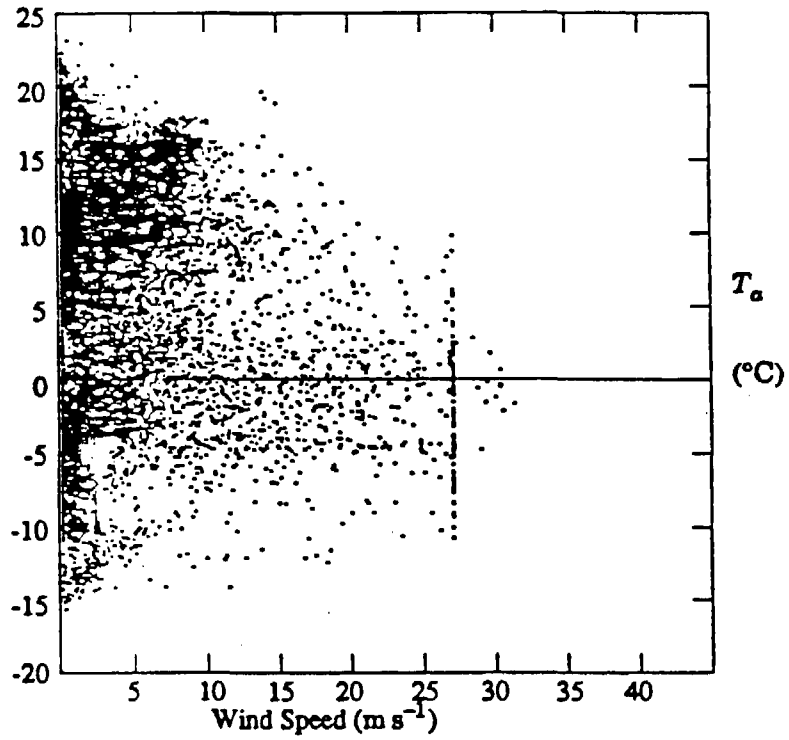


Figure 19. Monthly Mean Vapor Pressure at the Lake and Ridge, 1986-1988

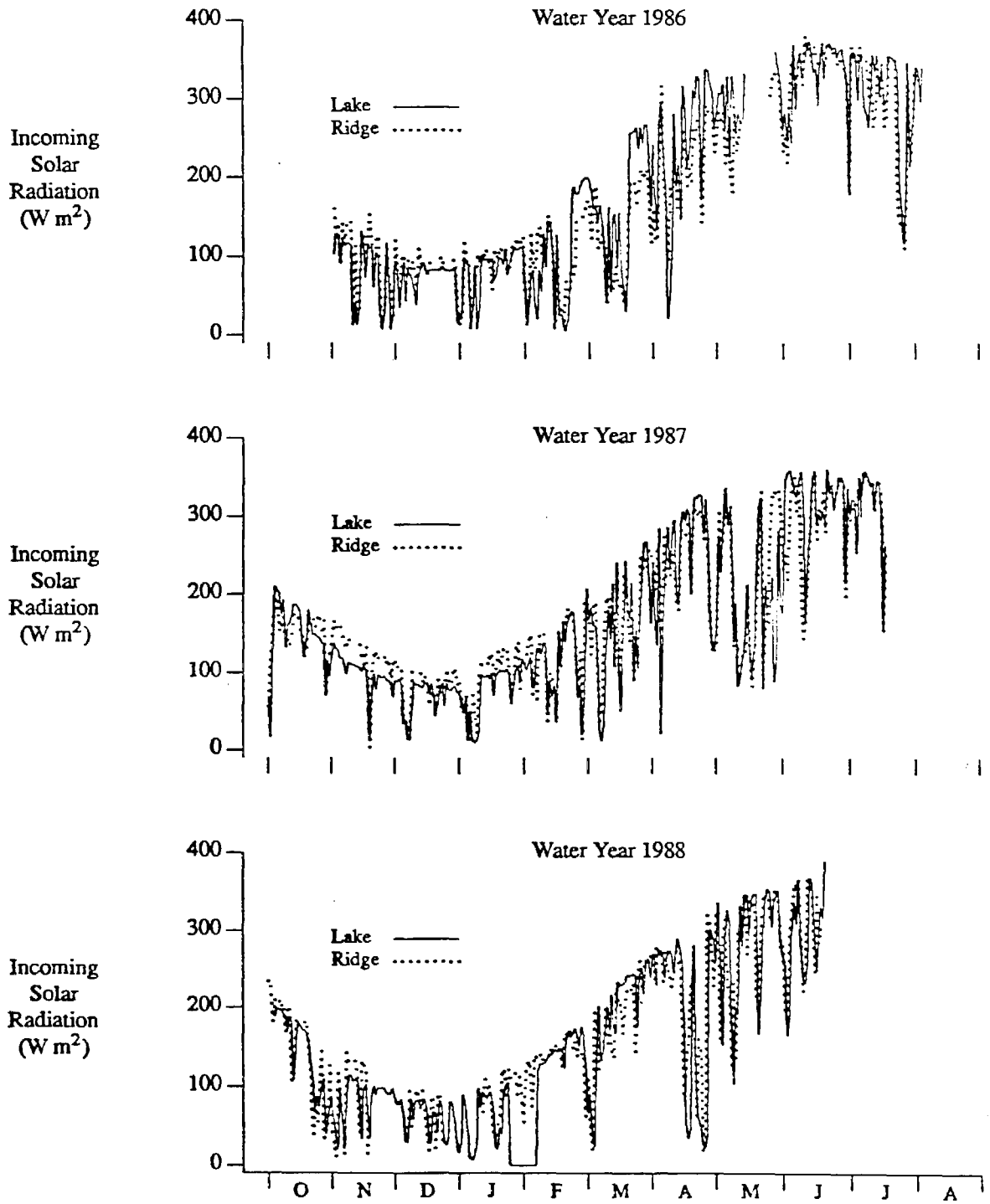
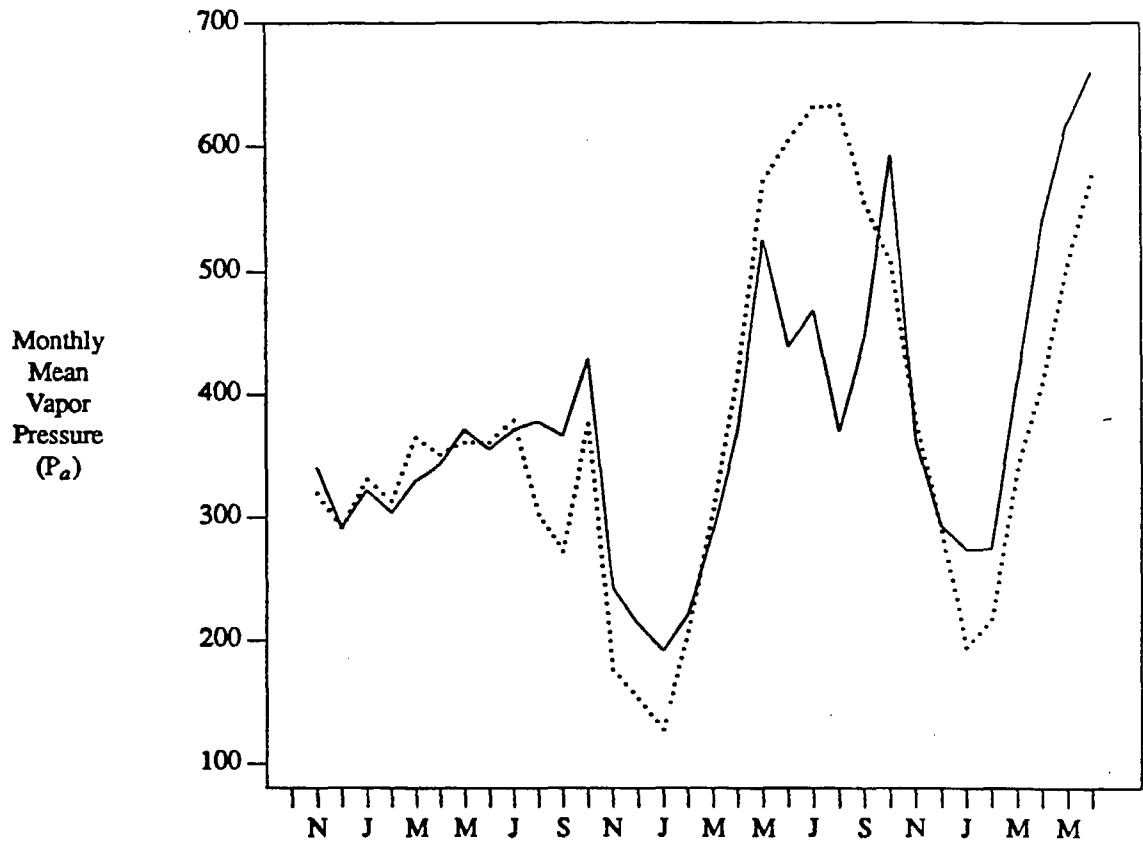


Figure 20. Daily Mean Incoming Solar Radiation at the Lake and Ridge, 1986-1988



D. References

- Armstrong, R. L. and J. D. Ives, eds., Avalanche release and snow characteristics, *Occasional Pap. No. 19*, Institute of Arctic and Alpine Research, Boulder, 1976.
- Baker, F. S., Mountain climates of the western United States, *Ecological Monographs*, 14, 223-254, 1944.
- Barry, R. G., A climatological transect on the east slope of the Front Range, Colorado, *Arctic Alpine Res.*, 5, 89-110, 1973.
- Bohren, C. F. and B. R. Barkstrom, Theory of the optical properties of snow, *J. Geophys. Res.*, 79, 4527-4535, 1974.
- Brunt, D., Notes on radiation in the atmosphere, *Journal of the Royal Meteorological Society*, 58, 389-420, 1932.
- Brutsaert, W., On a derivable formula for long-wave radiation from clear skies, *Water Resour. Res.*, 11, 742-744, 1975.
- Chabot, B. F. and W. D. Billings, Origins and ecology of the Sierran alpine flora and vegetation, *Ecological Monographs*, 42, 163-199, 1972.
- Davies, J. A. and S. B. Idso, Estimating the surface radiation balance and its components, in *Modification of the Aerial Environments of Plants*, edited by J. F. Gerber and B. J. Barfield, ASAE Monograph 2, pp. 183-210, American Society of Agricultural Engineers, St. Joseph, Mich., 1979.
- Dozier, J., A clear-sky spectral solar radiation model for snow-covered mountainous terrain, *Water Resour. Res.*, 16, 709-718, 1980.
- Dozier, J. and S. G. Warren, Effect of viewing angle on the infrared brightness temperature of snow, *Water Resour. Res.*, 18, 1424-1434, 1982.
- Judson, A., Climatological data from the Berthoud Pass area of Colorado, *General Tech. Rep. RM-42*, 94 pp., USDA-Forest Service, Fort Collins, 1977.
- Klikoff, L. G., Microenvironmental influence on vegetational pattern near timberline in the central Sierra Nevada, *Ecological Monographs*, 35, 188-211, 1965.
- Longacre, L. L. and H. F. Blaney, Evaporation at high elevations in California, *Journal of the Irrigation and Drainage Division, American Society of Civil Engineers*, 88, 33-54, 1962.
- Major, J., California climate in relation to vegetation, in *Terrestrial Vegetation of California*, edited by M. B. Barbour and J. Major, pp. 11-74, Wiley-Interscience, New York, 1977.
- Marks, D., Climate and energy exchange at the snow surface in Emerald Lake Basin, Sierra Nevada, Ph.D. Thesis, 159 pp., Dept. Geogr., Univ. Calif., Santa Barbara, 1988.

- Marks, D. and J. Dozier, A clear-sky longwave radiation model for remote alpine areas, *Arch. Meteorol. Geophys. Bioklim.*, B-27, 159-187, 1979.
- Marshall, S. E. and S. G. Warren, Parameterization of snow albedo for climate models, in *Large Scale Effects of Seasonal Snow Cover*, edited by B. E. Goodison, R. G. Barry, and J. Dozier, IAHS Publ. No. 166, pp. 43-50, Intl. Assoc. Hydrol. Sci., Wallingford, UK, 1987.
- Monteith, J. L., *Principles of Environmental Physics*, Edward Arnold Press, London, 1973.
- Munroe, D. S., G. J. Young, and S. Mustafa, Comment on 'On the statistical characteristics of drought events' and 'On the definition of droughts' by John A. Dracup et. al., *Water Resour. Res.*, 17, 441, 1981.
- Olyphant, G. A., Insolation topoclimates and potential ablation in alpine snow accumulation basins: Front Range, Colorado, *Water Resour. Res.*, 20, 491-498, 1984.
- Paltridge, G. W. and C. M. R. Platt, *Radiative Processes in Meteorology and Climatology*, Elsevier, Amsterdam, 1976.
- Stephenson, N., Climate and the water balance in Sequoia National Park, California, (unpublished manuscript on file Sequoia National Park headquarters), 1988.
- Warren, S. G., Optical properties of snow, *Rev. Geophys. Space Phys.*, 20, 67-89, 1982.

VII. TOPOGRAPHIC DISTRIBUTION OF SOLAR RADIATION

A. Introduction

Variability in solar radiation is responsible for the largest topographically caused variations in surface climate in alpine terrain, and it contributes most to widely different rates of snow metamorphism and melt found throughout a drainage basin. In trying to measure such snow processes, it is normally impossible to adequately sample the variability caused by the terrain. Therefore the normal approach is to measure energy exchange at a few well-instrumented sites, and to use these measurements to evaluate the spatial variation of energy flux to the snowpack over a drainage basin. Only in this way can we estimate the location and size of source areas and forecast the timing and magnitude of generation of melt water. The objective in this section, therefore, is to calculate topographic distribution of solar radiation, based on measurements at a small number of sites, from which atmospheric properties are inferred, and to combine the resulting atmospheric radiation model with a digital elevation grid to estimate solar radiation at every grid point.

B. Solar Radiation in the Snow Pack Energy Balance

1. Energy Exchange at the Snow Surface

Snow metamorphism and melt and transport of chemical species in the snowpack are driven by energy exchange at the snow surface. By calculating or measuring energy fluxes to a snowpack, one can estimate the temperature profile of the pack and account for loss of snow water equivalence through sublimation and melting [Anderson, 1976]. This requires that we monitor surface energy exchange for the study of snow properties and processes in alpine drainage basins. The sources for heat transfer to the snowpack are direct and diffuse solar radiation, thermal radiation emitted by the atmosphere and by adjacent terrain, sensible and latent heat flux, heat conducted from the soil, and advected heat from rain. A detailed description of the principles and an extensive review of previous work are found in Male and Granger [1981], and recent work is summarized by Dozier [1987].

In many mountainous environments, solar radiation is an important source of energy for snow metamorphism and snowmelt. Figure 21 shows daily average values of the components of the surface energy exchange for an exposed, level site in the Emerald Lake drainage basin, in the Sierra Nevada, over the 1987 snow season. While the magnitudes of sensible and latent heat exchange are as large as net solar radiation, they are usually of opposite signs. Thus the net solar radiation is the important component that causes the daily-average, net, all-wave radiation to change from negative to positive in the spring. Moreover, solar radiation has the largest topographically caused variation and therefore contributes most to the widely different rates of metamorphism and melt found throughout a drainage basin. For investigation of some processes in alpine watersheds, for example the effect of an acid pulse from a melting snow cover on streams and lakes, we require not only a detailed understanding of energy exchange at a few well-instrumented sites, but knowledge of the time of initiation of melt throughout the drainage basin. Therefore evaluation of the spatial variation of energy flux to the snowpack over a basin is necessary for the development of an energy balance model that will provide information about the location and size of the source areas and the timing and magnitude of generation of melt

water. A key component in such a model must be the topographic distribution of net solar radiation.

2. Net Solar Radiation at the Snow Surface

The solar radiation absorbed by the snowpack is determined by the integral of the spectral distribution of the incoming solar direct and diffuse fluxes and the spectral reflectance (albedo):

$$F_{\text{net}} = \int_{\lambda_1}^{\lambda_2} \left\{ \mu_s [1 - R_s(\mu_s; \lambda)] S_0(\lambda) e^{-\tau_0(\lambda)/\mu_0} + [1 - R_d(\lambda)] F_{\downarrow}(\lambda) \right\} d\lambda \quad (30)$$

S_0 is the exoatmospheric spectral solar flux at wavelength λ on a plane normal to the solar beam, which is incident at angle $\arccos \mu_0$. μ_s is the cosine of the local illumination angle on a slope. τ_0 is the spectral optical depth of the atmosphere. F_{\downarrow} is the spectral diffuse flux, whose source is radiation scattered from the atmosphere and from nearby terrain. R_s and R_d are the spectral reflectances to direct and diffuse illumination. The limits of integration $[\lambda_1, \lambda_2]$ include essentially all of the incoming solar flux when they are set at $[0.3, 3.0 \mu\text{m}]$.

In extensive calculations of the surface energy balance over points throughout a drainage basin, the detailed spectral integration in (30) will be too time-consuming. However, using a single spectrally integrated albedo for the snow surface will also be inaccurate, because the albedo varies in the visible and in the near-infrared regions owing to different physical properties [Warren, 1982]. In the visible wavelengths, the albedo of snow is insensitive to grain size, but is affected by two variables, finite depth and the presence of absorbing impurities, such as dust and soot. In the near-infrared wavelengths, albedo is sensitive to grain size. For rapid calculation, therefore, Marshall and Warren [1987] divide the solar spectrum into two broad wavelength regions, visible ($0.35 - 0.8 \mu\text{m}$) and near-infrared ($0.8 - 2.8 \mu\text{m}$), and calculate a spectrally integrated albedo for each region.

C. Scattering and Absorption of Light by the Atmosphere

The scattering and absorption of light by the clear atmosphere and by clouds are analyzed with a multiple-scattering model, a two-stream approximation to the radiative transfer equation. The fundamental scattering properties of the water droplets or ice crystals in clouds and the aerosols in the atmosphere are calculated by the complex angular momentum approximation to the Mie equations [Nussenzveig and Wiscombe, 1980]. The LOWTRAN model [Kneizys et al., 1988] is used to obtain values for molecular absorption in the atmosphere at the desired wavelengths.

The radiative transfer equation [Chandrasekhar, 1960] is used to calculate the multiple scattering and absorption of the incident radiation. It is computationally time-consuming to calculate the angular distribution of the radiation that is transmitted or reflected by the atmosphere, but it is comparatively simple to examine the radiation integrated over all upward or downward angles. That is, we restrict the calculations to the upward and downward fluxes:

$$F_{\downarrow} = \int_0^1 \int_0^{2\pi} \mu L(\mu, \phi) d\mu d\phi \quad (31a)$$

$$F_{\uparrow} = \int_0^1 \int_0^{2\pi} \mu L(\mu, \phi) d\mu d\phi \quad (31b)$$

$L(\mu, \phi)$ is the radiance at the direction-angle $\arccos \mu$ and azimuth ϕ . Positive values of μ are downward.

1. Two-Stream Solution to the Radiative Transfer Equation

We can solve this kind of problem analytically with the two-stream approximation to the radiative transfer equation for a homogeneous medium [Meador and Weaver, 1980]:

$$\frac{dF_{\uparrow}(\tau)}{d\tau} = \gamma_1 F_{\uparrow}(\tau) - \gamma_2 F_{\downarrow}(\tau) - \gamma_3 \omega_0 S_0 e^{-\tau/\mu_0} \quad (32a)$$

$$\frac{dF_{\downarrow}(\tau)}{d\tau} = \gamma_2 F_{\uparrow}(\tau) - \gamma_1 F_{\downarrow}(\tau) + \gamma_4 \omega_0 S_0 e^{-\tau/\mu_0} \quad (32b)$$

F_{\uparrow} and F_{\downarrow} are upward and downward fluxes, ω_0 is the single-scattering albedo (i.e. the ratio of extinction by scattering to total extinction), and the γ -values parameterize the scattering phase function. The Mie equations are used to calculate the single-scattering albedo ω_0 and the scattering asymmetry parameter g , and the γ -values are functions of ω_0 , g , and μ_0 . To estimate the optical depth coordinate τ as a function of physical properties, we also need the extinction efficiency Q_{ext} and the number density of the scatterers.

Top and bottom boundary conditions are needed for the solution of (32a, 32b). At the top of the medium there is no downward diffuse flux. At the bottom, optical depth τ_0 , the upward diffuse flux is the reflected diffuse and direct radiation from a horizontal surface, whose reflectance is R_0 . Thus the boundary conditions for a level surface are

$$F_{\downarrow}(0) = 0 \quad (33a)$$

$$F_{\uparrow}(\tau_0) = R_0 \left[F_{\downarrow}(\tau_0) + \mu_0 S_0 e^{-\tau_0/\mu_0} \right] \quad (33b)$$

With these boundary conditions, the two-stream equations can be solved, and the values of F_{\downarrow} or F_{\uparrow} can be calculated for any level within the atmosphere. A later section considers the topographic problem.

The directional-hemispherical transmittance T_s through the atmosphere, equivalent to what is measured with a level pyranometer, is

$$T_s \equiv \frac{F \downarrow(\tau_0) + \mu_0 S_0 e^{-\tau_0/\mu_0}}{\mu_0 S_0} \quad (34)$$

$$= \frac{2q\xi\gamma_2(\mu_0\alpha_1 + \gamma_4) + e^{-\tau_0/\mu_0}(P^+U^- - P^-U^+)}{P^+V^- - P^-V^+}$$

where

$$P^\pm = (\gamma_1 \pm \xi) e^{\pm \xi \tau_0}$$

$$q = \frac{\omega_0}{1 - \xi^2 \mu_0^2}$$

$$Q^\pm = \frac{V^\mp e^{\pm \xi \tau_0} (\alpha_2 \pm \xi \gamma_3)}{1 \pm \xi \mu_0}$$

$$U^\pm = \gamma_2 - \frac{\omega_0 (\alpha_2 \pm \xi \gamma_3)}{1 \pm \xi \mu_0}$$

$$V^\pm = \gamma_2 - R_0 (\gamma_1 \pm \xi)$$

$$\xi^2 = \gamma_1^2 - \gamma_2^2$$

$$\alpha_1 = \gamma_1 \gamma_4 + \gamma_2 \gamma_3$$

$$\alpha_2 = \gamma_2 \gamma_4 + \gamma_1 \gamma_3$$

2. Parameters in the Two-stream Equations

To evaluate (34) we need values for the atmospheric extinction parameters τ_0 , ω_0 , and γ_1 through γ_4 . Meador and Weaver [1980, Table 1] give γ expressions for seven different two-stream approximations; one of which is the Meador-Weaver hybrid method:

$$\gamma_1 = \frac{7 - 3g^2 + \omega_0(4 + 3g) + \omega_0 g^2(4\beta_0 + 3g)}{4[1 - g^2(1 - \mu_0)]} \quad (35a)$$

$$\gamma_2 = -\frac{1 - g^2 - \omega_0(4 - 3g) - \omega_0 g^2(4\beta_0 + 3g - 4)}{4[1 - g^2(1 - \mu_0)]} \quad (35b)$$

$$\gamma_3 = \beta_0 = 1 - \frac{1}{2\omega_0} \int_0^1 p(\mu_0, \mu') d\mu' \quad (35c)$$

$$\gamma_4 = 1 - \gamma_3 \quad (35d)$$

g is the scattering asymmetry parameter, and β_0 is the integral of the azimuthally integrated scattering function p from the incidence angle over all upward directions. The Henyey-Greenstein scattering function for p is expanded in Legendre polynomials P_n [van de Hulst,

1980, pp. 331-332].

$$p(\mu_0, \mu') = \omega_0 \sum_{n=0}^{\infty} (2n+1) g^n P_n(\mu_0) P_n(\mu') \quad (36)$$

In integrating this to solve (35c), the even-valued terms in the series vanish and the series coefficients can be computed recursively [Davis, 1965; Hochstrasser, 1965].

$$\beta_0 = \frac{1}{2} \left[1 - \sum_{n=0}^{\infty} C_n P_{2n+1}(\mu_0) \right] \quad (37)$$

where

$$C_0 = \frac{3g}{2} \quad \text{and} \quad \frac{C_{n+1}}{C_n} = - \frac{g^2 (4n+7)(2n+1)}{2(4n+3)(n+2)}$$

The quantities that are not known, and thus must be determined from measurements of incoming solar radiation, are τ_0 , ω_0 , and g . Strictly speaking, these are all spectral quantities, and the proper way to employ (34) is to break the problem into narrow wavelength intervals and sum over these. For clear skies we perhaps could use approximate values for τ_0 , ω_0 , and g , based on standard atmospheric profiles, but we would prefer to use values based on measurements made in the drainage basin during the period for which the distribution of solar radiation is needed. Because the instruments that measure incoming radiation must operate unattended for long periods in harsh, remote locations, it is unlikely that they will have the necessary spectral resolution to determine wavelength-dependent atmospheric properties.

Instead we assume that wavelength-averaged values, over broad portions of the solar spectrum, for τ_0 , ω_0 , and g can be used, and subdivide the solar spectrum into two broad bands: visible (0.3–0.8 μm) and near-infrared (0.8–2.8 μm). Measurements at the surface with pyranometers that have filters corresponding to these wavelength bands are analyzed to estimate the atmospheric parameters.

From (34) we can calculate atmospheric transmittance, and from pyranometers we can measure it in the two broad wavelength bands, at several different times during the day as the solar zenith angle changes. If we assume that the atmospheric parameters do not change over the same period, we can find a least-squares solution to their values. Specifically, we find the triplet $[\tau_0, \omega_0, g]$ that minimizes $\sum (T_{\text{calc}} - T_{\text{meas}})^2$, and solve with the nonlinear least-squares routine NL2SOL [Dennis et al., 1981].

D. Use of Digital Elevation Models in Radiation Calculations

In all but very gentle terrain, significant variation in the surface climate results from local topographic effects. The major contributors to this variation are solar and longwave (thermal) radiation, although there are also important topographic variations in wind speed and soil moisture. The topographic effects on solar irradiance are mainly variation in illumination angle and shadowing from local horizons [Williams et al., 1972; Dozier and Outcalt, 1979; Dozier et al., 1981; Olyphant, 1984]. In the thermal part of the electromagnetic spectrum, the emission from surrounding slopes usually causes valley

bottoms to receive more thermal irradiance than unobstructed areas [Marks and Dozier, 1979; Olyphant, 1986].

Most radiation calculations over terrain are made with the aid of digital elevation grids, whereby elevation data are represented by a matrix. In the U.S., these are available as Digital Elevation Models (DEMs) from the U.S. Geological Survey [Elassal and Caruso, 1983]. The 1:250,000 quadrangles for the entire U.S. are available at a grid resolution of 63.5 m (0.01 inch at map scale), and the 1:24,000 quadrangles are available at 30 m resolution. Several commercial firms sell software that will derive digital elevation models from digital stereophotography from aircraft or satellite, and one current research emphasis in remote sensing is the determination of surface topography from radar altimeters.

1. Direct and Diffuse Irradiance in Alpine Terrain

In the solar spectrum, irradiance in alpine terrain has three sources: (1) $S_0 e^{-\tau_0/\mu_0}$, direct irradiance from the sun; (2) $F_{\downarrow}^{(d)}$, diffuse irradiance from the sky, where a portion of the overlying hemisphere is obscured by terrain; and (3) $F_{\downarrow}^{(t)}$, direct and diffuse irradiance, on nearby terrain, that is reflected toward the point whose radiation flux we want to calculate.

The direct irradiance on a slope is $\mu_s S_0 e^{-\tau_0/\mu_0}$, where μ_0 is the cosine of the solar illumination angle, θ_0 , on a horizontal surface and μ_s is the cosine of the solar illumination angle on the slope, given by:

$$\begin{aligned} \mu_s &= \cos\theta_0 \cos S + \sin\theta_0 \sin S \cos(\phi_0 - A) \\ &= \mu_0 \cos S + (1 - \mu_0^2)^{1/2} \sin S \cos(\phi_0 - A) \end{aligned} \quad (38)$$

S is the slope angle; A is the slope's azimuth; and ϕ_0 is the solar azimuth. Azimuths are usually measured from south, with positive angles east of south (counter-clockwise). The effect of earth and atmosphere curvature on the path length is less than 1% for $\theta_0 \leq 72^\circ$; for larger solar zenith angles Kasten's [1966] empirical equations for the optical path length can be used.

Scattered diffuse irradiance from the sky is

$$F_{\downarrow}^{(d)} = V_d \overline{F_{\downarrow}}(\tau_0) \quad (39)$$

$\overline{F_{\downarrow}}$ is the downward irradiance on an unobstructed horizontal surface. The sky-view factor, V_d , is the ratio of the diffuse sky irradiance at a point to that on an unobstructed horizontal surface, i.e. $0 < V_d \leq 1$. It accounts for the slope and orientation of the point and the portion of the overlying hemisphere visible to the point. It can also be adapted to account for anisotropy in the diffuse irradiance, but the two-stream equations assume that diffuse irradiance is isotropic. V_d on slope S with azimuth A is found by projecting each element of the sky onto the slope and integrating over the unobstructed hemisphere, i.e. from the zenith downward to the local horizon, through angle H_ϕ , for each direction ϕ . For an unobstructed horizontal surface $H_\phi = \pi/2$ (Figure 22). The horizon can result either from "self-shadowing" by the slope itself or from adjacent ridges.

$$V_d = \frac{1}{2\pi} \int_0^{2\pi} [\cos S \sin^2 H_\phi + \sin S \cos(\phi - A) (H_\phi - \sin H_\phi \cos H_\phi)] d\phi \quad (39)$$

Contribution from the surrounding terrain is

$$F_{\downarrow}^{(t)} = C_t \overline{F_{\uparrow}}(\tau_0) \quad (40)$$

The average irradiance reflected from the surrounding terrain is $\overline{F_{\uparrow}}$. The terrain configuration factor, C_t , includes both the anisotropy of the radiation and the geometric effects between that point and each point in the surrounding terrain with which it is mutually visible. The contribution of each of these terrain elements to the configuration factor could be computed [Siegel and Howell, 1981], but this is a formidable computational problem. Rigorous calculation is difficult because it is necessary to consider every terrain facet visible from a point. In contrast to the sky radiation, the isotropic assumption is unrealistic because considerable anisotropy results from geometric effects even if the surrounding terrain is a Lambertian reflector. We, therefore, note that V_d for an infinitely long slope is $(1 + \cos S)/2$, and approximate C_t by

$$C_t \approx \frac{1 + \cos S}{2} - V_d \quad (41)$$

2. Calculation of Topographic Parameters from the Elevation Grid

The elevation grid is oriented as shown in Figure 23. Spacing between grid points is ΔH in both the x and y directions. The grid is oriented with the rows from west to east and the columns from north to south, so that x increases southward and y increases eastward.

The equations for slope S and azimuth A are given below. The signs of the numerator and denominator allow A to be uniquely specified over $[-\pi, \pi]$.

$$\tan S \equiv |\nabla z| = \left[(\partial z / \partial x)^2 + (\partial z / \partial y)^2 \right]^{1/2} \quad (42a)$$

$$\tan A = \frac{-\partial z / \partial y}{-\partial z / \partial x} \quad (42b)$$

$\partial z / \partial x$ and $\partial z / \partial y$ are calculated by finite differences. At point i, j

$$\frac{\partial z}{\partial x} = \frac{z_{i+1, j} - z_{i-1, j}}{2\Delta h} \quad (43a)$$

$$\frac{\partial z}{\partial y} = \frac{z_{i, j+1} - z_{i, j-1}}{2\Delta h} \quad (43b)$$

Figure 24 shows a slope and azimuth image of the Emerald Lake watershed, and Figure 25 shows a shaded relief image for a mid-morning, mid-February sun position. The effect of local horizons in mountainous terrain is shown in Figures 26 and 27.

E. Incoming Solar Radiation in the Emerald Lake Watershed

The methods described in the previous section are used to analyze solar radiation data collected at the unobstructed site on the ridge separating the Emerald Lake drainage from that of Pear Lake.

The spatial and temporal distribution of solar radiation is characterized by low spatial variance at low magnitudes in the winter, higher spatial variance in the early spring, and low variance at high magnitudes in the late spring and early summer. Figure 28 shows the average daily values of solar radiation for clear-sky conditions in each winter and spring month, and Figure 29 shows the corresponding histograms.

F. Conclusion

Among the energy fluxes controlling snow metamorphism and snowmelt in mountainous drainage basins, solar radiation has the largest topographically caused variation and is responsible for the major spatial variations in snowmelt, metamorphism, and ion elution. A two-stream atmospheric radiation model calculates solar radiation over alpine terrain in two broad wavelength bands — visible and near-infrared — and a spectral model for the albedo of snow is parameterized to the same wavelength bands to estimate net solar radiation. A least-squares fit to surface measurements finds the necessary atmospheric attenuation parameters, and the topographic variables are calculated from digital elevation data.

The spatial and temporal distribution of solar radiation is characterized by low spatial variance at low magnitudes in the winter, higher spatial variance in the early spring, and low variance at high magnitudes in the late spring and early summer.

G. Notation

A	Slope azimuth, from south
C_n	Coefficients in Legendre expansion of β_0
g	Scattering asymmetry parameter
p	Azimuthally integrated scattering function
P_n	n -th order Legendre polynomial
$F_{\uparrow}, F_{\downarrow}$	Upward and downward diffuse fluxes
$F_{\downarrow}^{(d)}$	Diffuse flux on slope from sky
$F_{\downarrow}^{(t)}$	Diffuse flux on slope from reflection off nearby terrain
R_s	Direct reflectance
R_d	Diffuse reflectance
R_0	Surface reflectance (general)
S	Slope angle, from horizontal
S_0	Direct exoatmospheric flux (normal to beam)
T_a	Atmospheric transmittance
β_0	Integrated scattering function for beam radiation into upward hemisphere
λ	Wavelength (μm)
μ_s	Cosine of local illumination angle on slope
μ_0	Cosine of illumination angle on horizontal surface
τ	Optical depth coordinate
τ_0	Optical depth of atmosphere

ϕ_0	Azimuth of sun, from south
ω_0	Single scattering albedo
$\gamma_1, \gamma_2, \gamma_3, \gamma_4$	Parameters to approximate scattering function

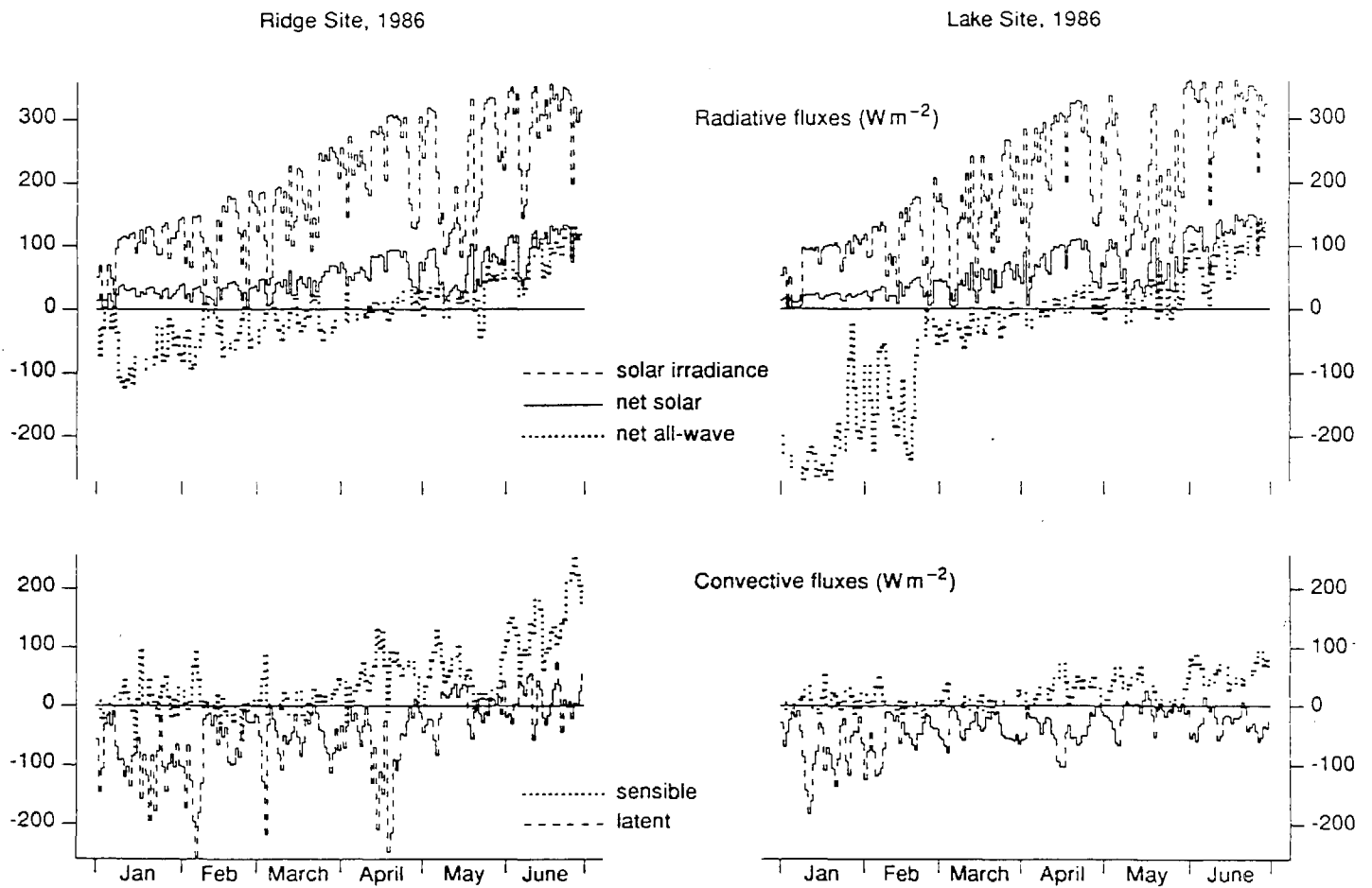


Figure 21. Daily Average Values of Components of Snow-Surface Energy Exchange

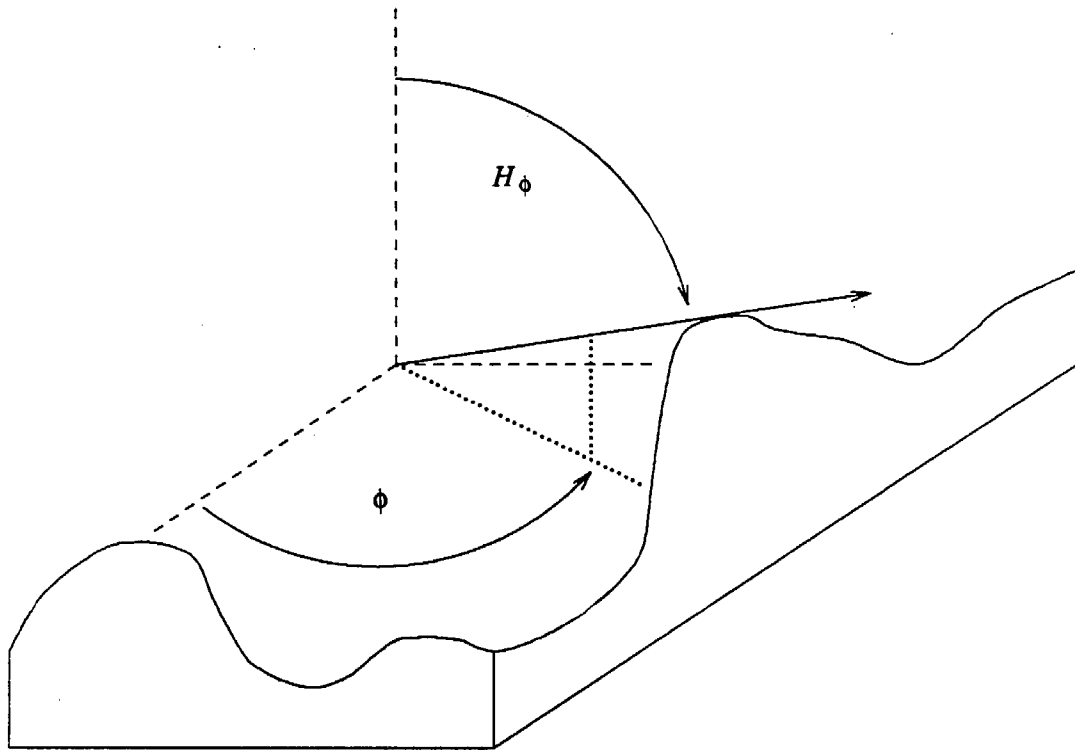


Figure 22. Horizon Angle H_ϕ for Direction ϕ

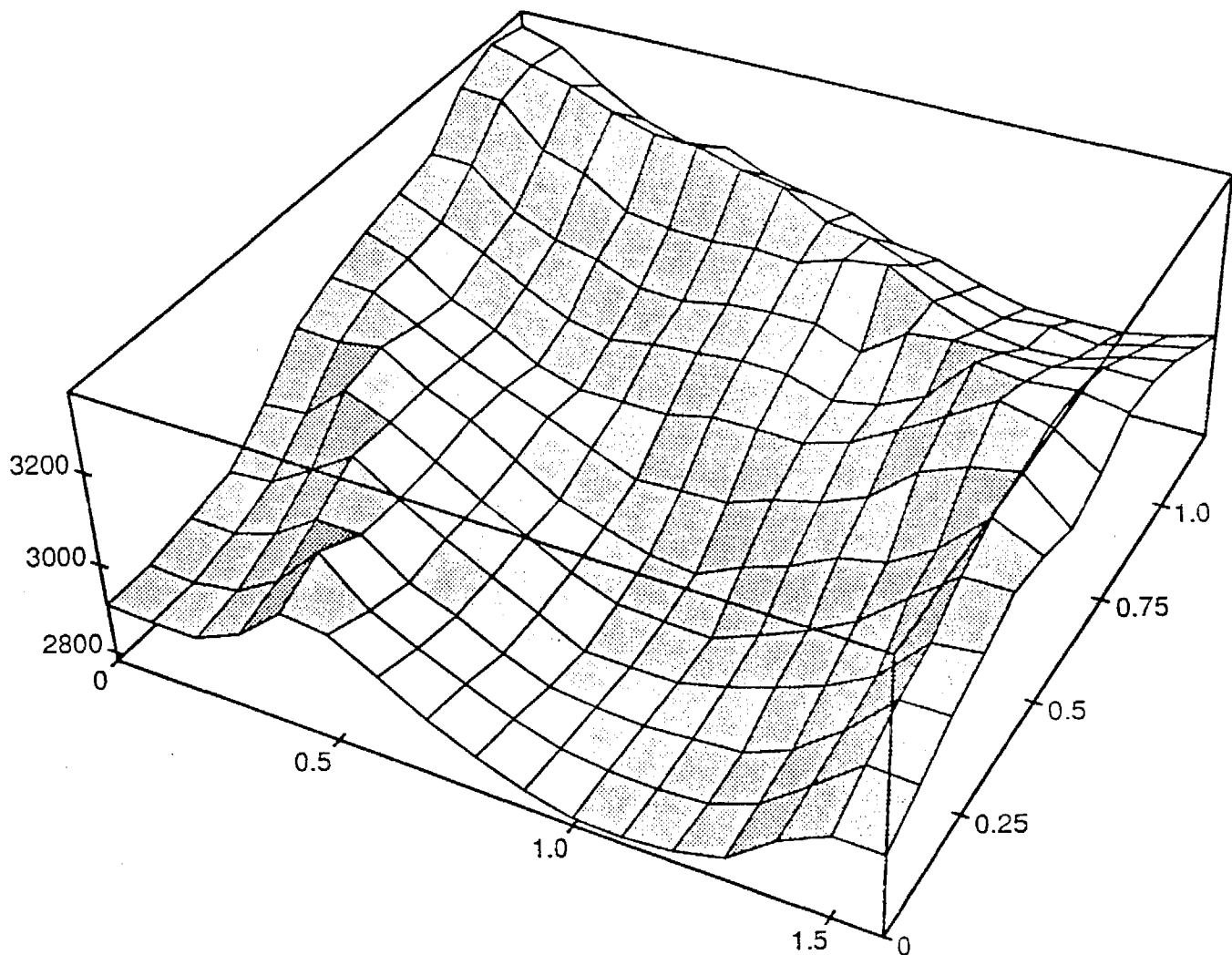


Figure 23. Coarse Digital Elevation Perspective of Emerald Lake Basin

The elevation model, made by stereo-photogrammetry from low altitude aerial photographs, covers 1.45×2.40 km at a grid spacing of 5 m. This view of the digital elevation model from the northwest shows the grid re-sampled at a spacing of about 100 m. Elevations along the vertical axis are in meters; distances along the horizontal axes are in kilometers.

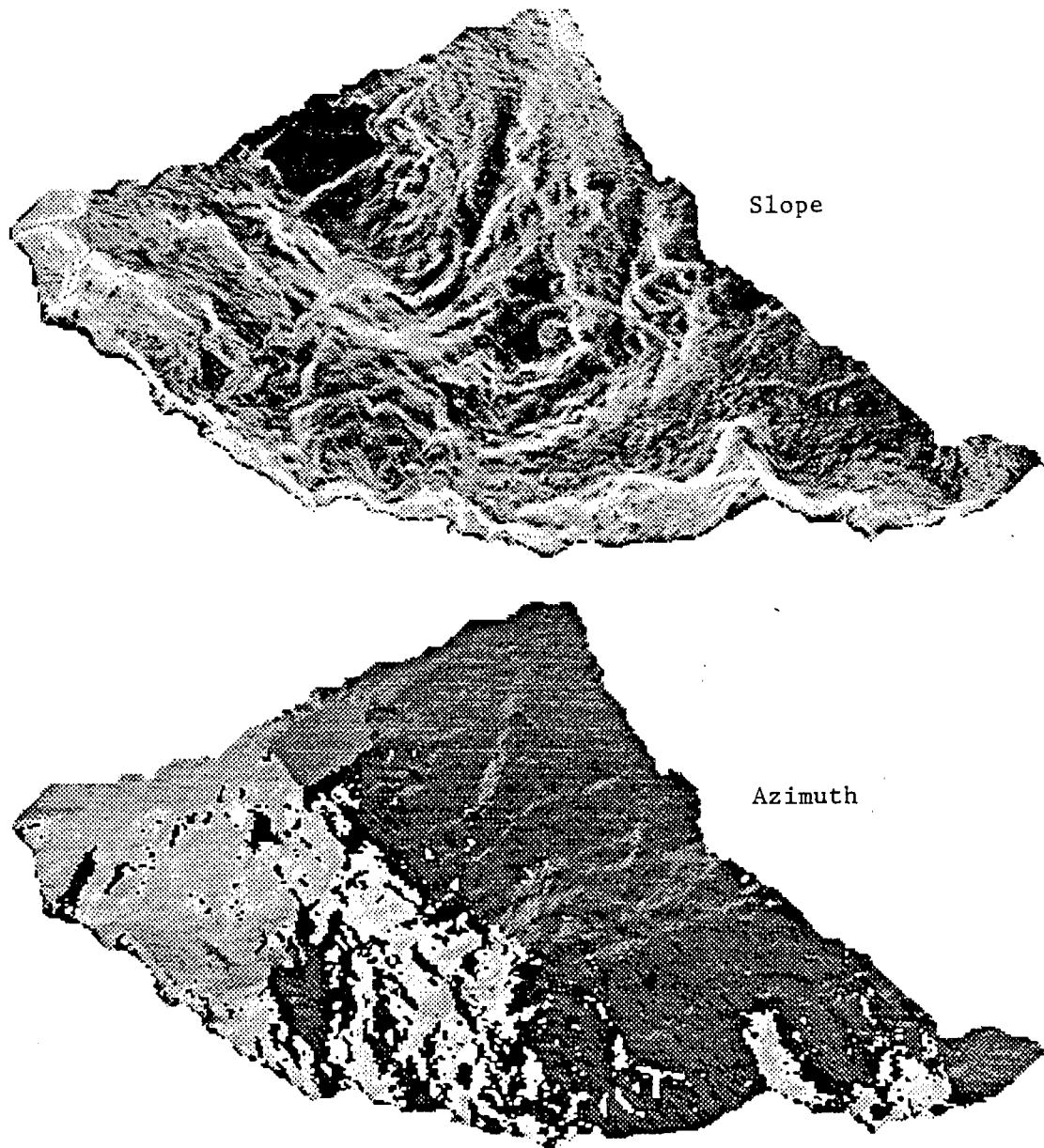


Figure 24. Slope and Azimuth Images of Emerald Lake Elevation Grid

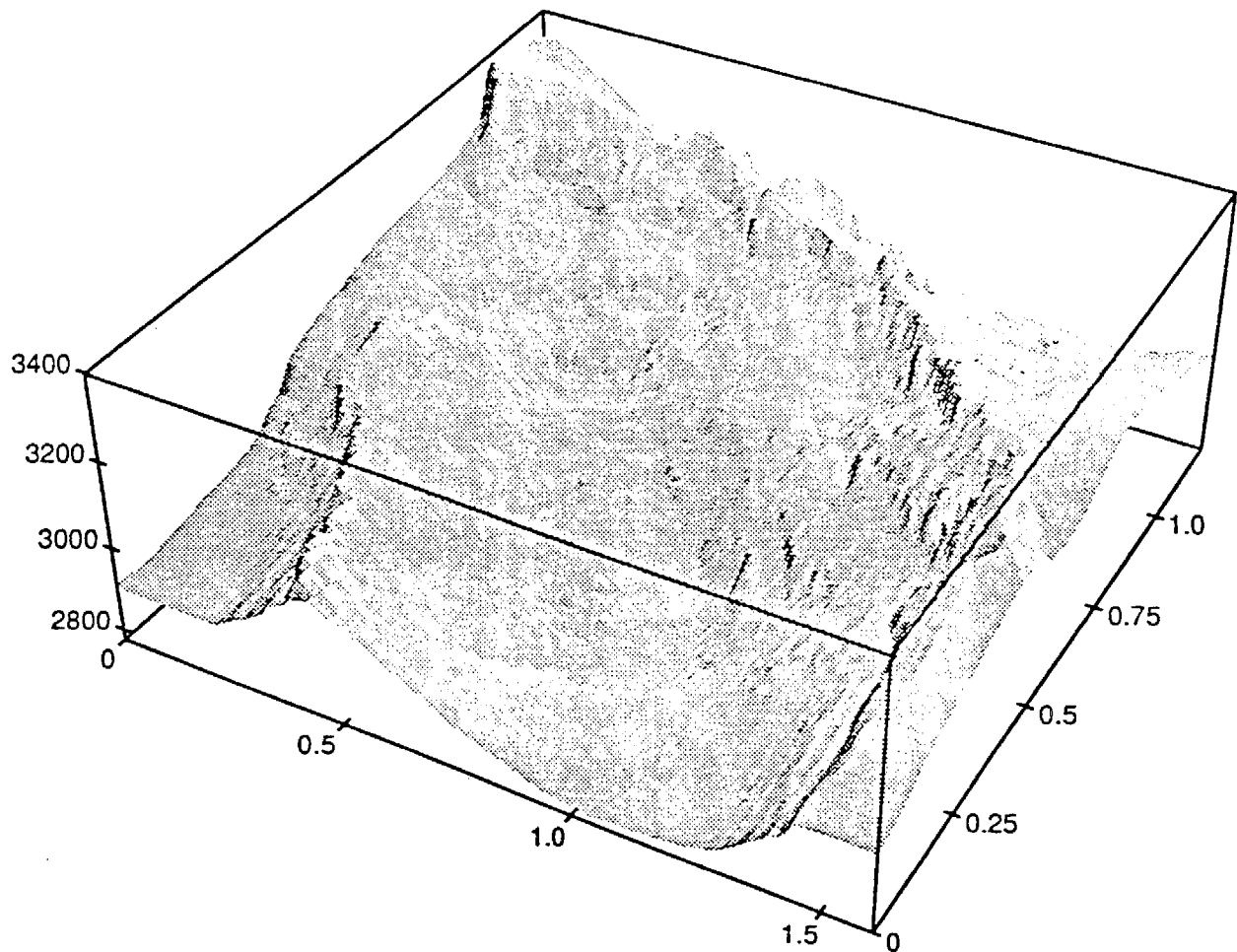


Figure 25. Shaded Relief Perspective of the Emerald Lake Drainage Basin

Elevations along the vertical axis are in meters; distances along the horizontal axes are in kilometers.

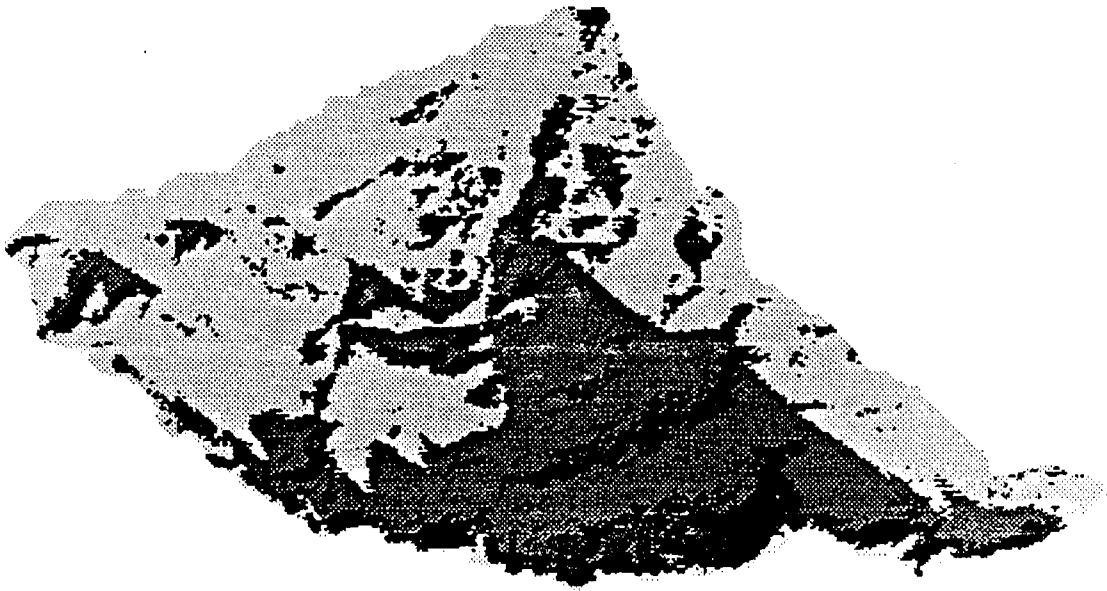


Figure 26. Shadowed Portions of the Emerald Lake Drainage Basin

Solar zenith angle is 60° and solar azimuth is 42° east of south, corresponding to the solar position at the time of a mid-February Landsat overpass; black areas are "self-shadowed," i.e. the orientation of the slope is such that it is hidden from the sun; grey areas are shadowed by local horizons.

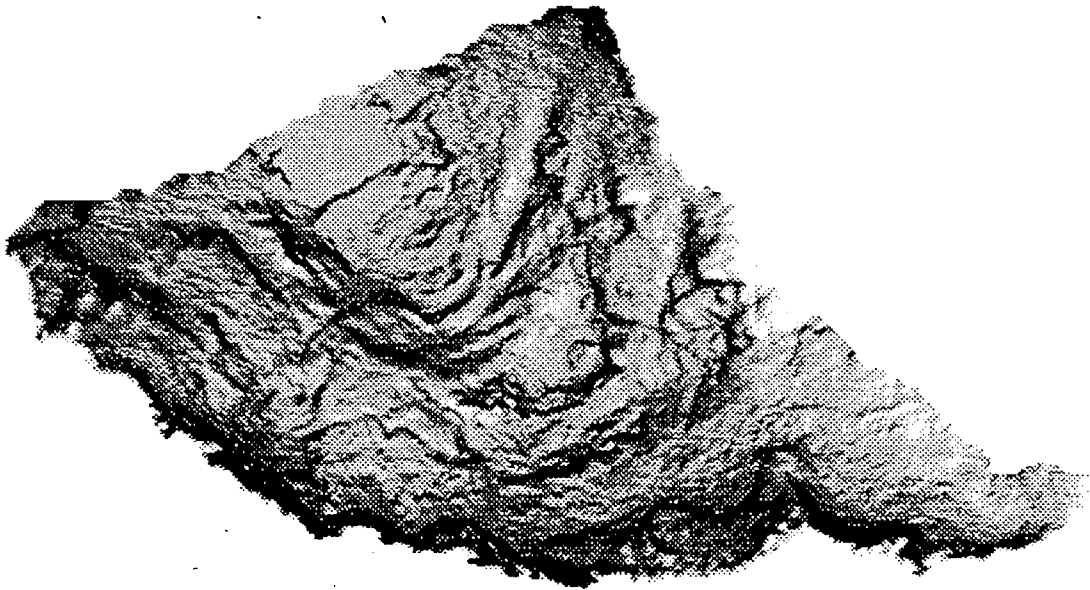


Figure 27. View Factors for Sky Radiation

Bright areas see a large portion of the 2π sky hemisphere; dark areas have much of the overlying hemisphere obscured by adjacent terrain.

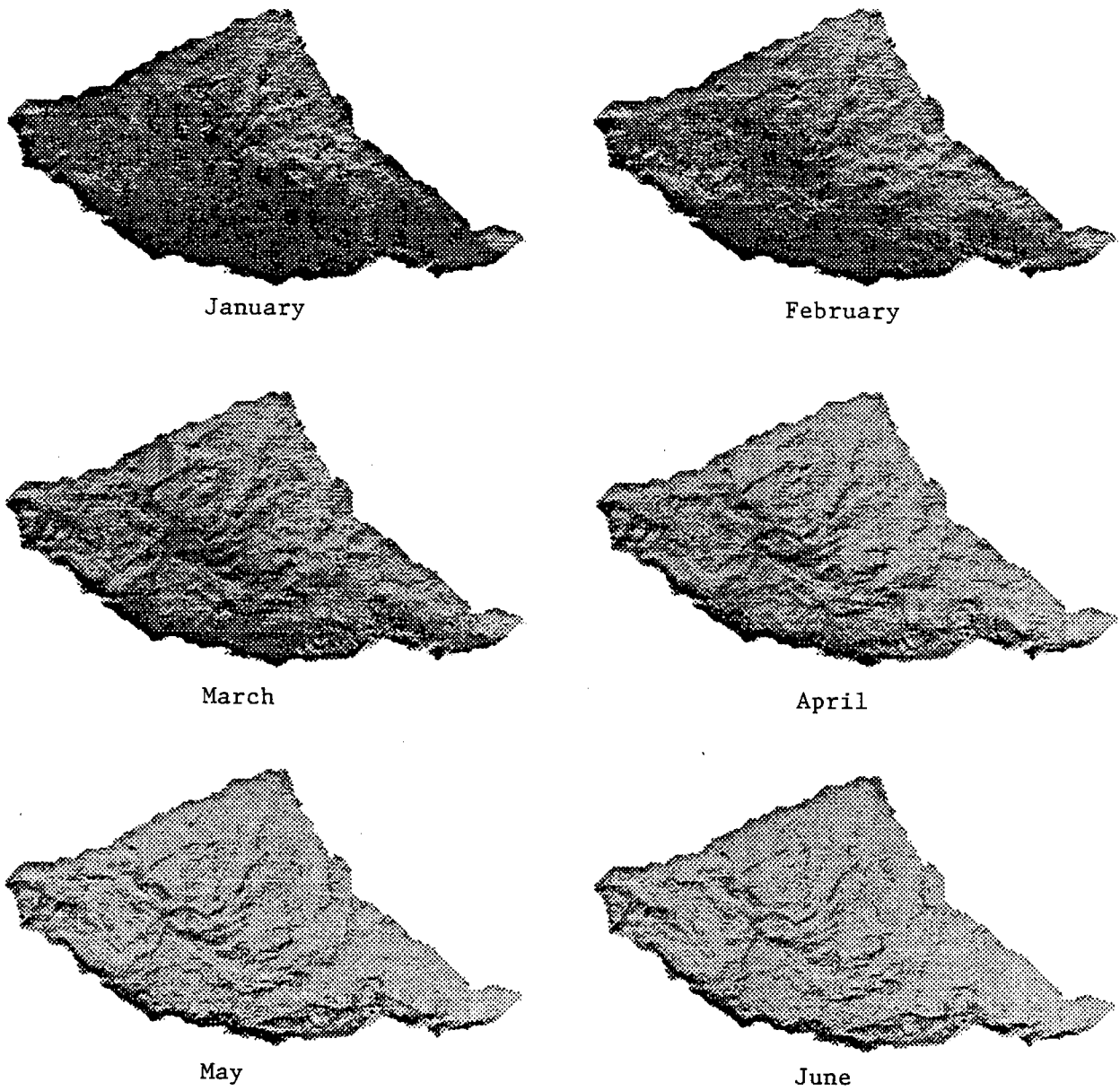


Figure 28. Mean Daily Solar Radiation Images, January through June

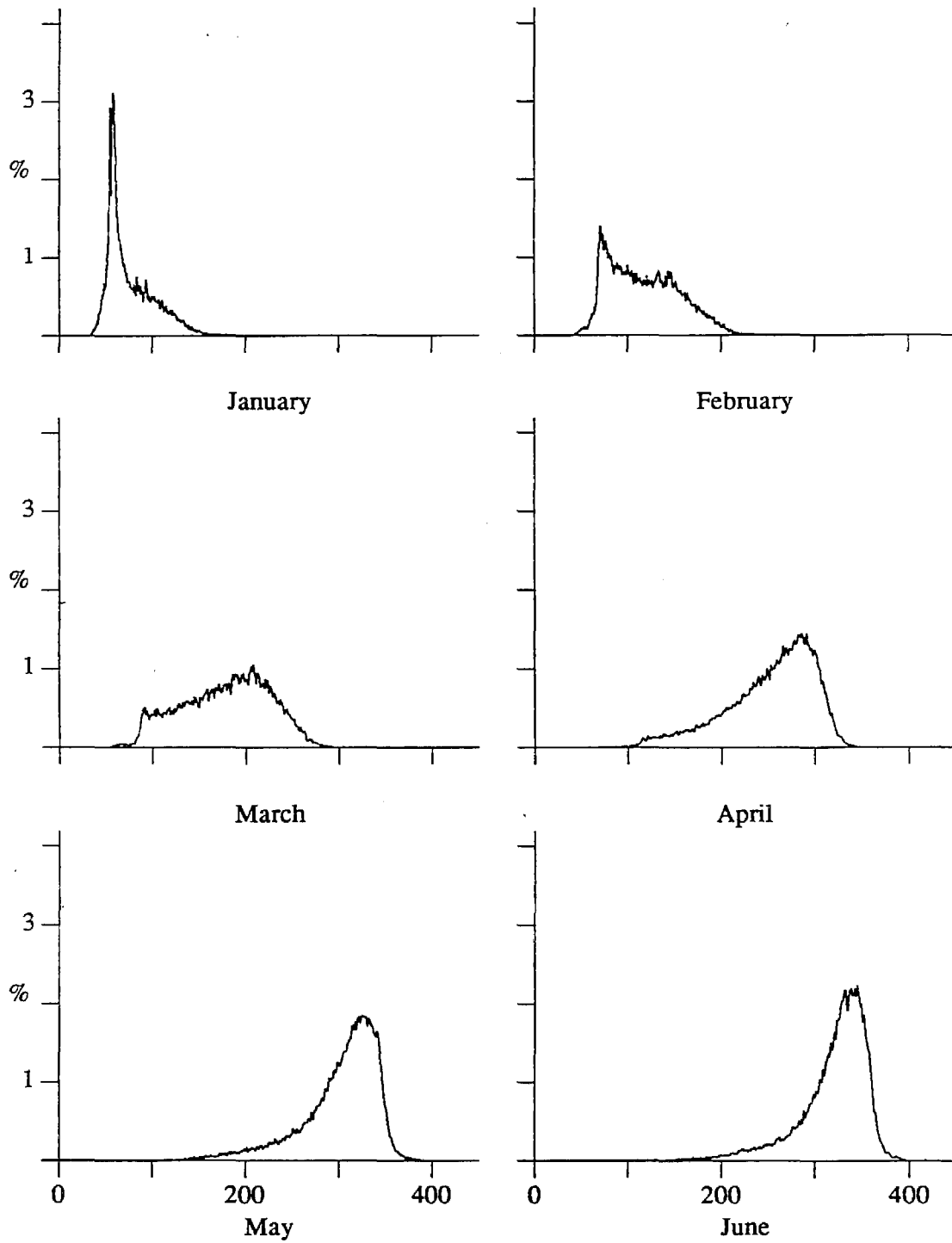


Figure 29. Histograms of Daily Radiation ($W m^{-2}$), January through June

H. References

- Anderson, E. A., A point energy and mass balance model of a snow cover, *Tech. Rep. NWS 19*, NOAA, Washington, DC, 1976.
- Chandrasekhar, S., *Radiative Transfer*, Dover Publications, New York, 1960.
- Davis, P. J., Gamma function and related functions, in *Handbook of Mathematical Functions*, edited by M. Abramowitz and I. A. Stegun, pp. 253-293, Dover, New York, 1965.
- Dennis, J. E., D. M. Gay, and R. E. Welsch, An adaptive nonlinear least-squares algorithm, *ACM Trans. Math. Software*, 7, 753, 1981.
- Dozier, J., A clear-sky spectral solar radiation model for snow-covered mountainous terrain, *Water Resour. Res.*, 16, 709-718, 1980.
- Dozier, J., Recent research in snow hydrology, *Rev. Geophys.*, 25, 153-161, 1987.
- Dozier, J., J. Bruno, and P. Downey, A faster solution to the horizon problem, *Comput. Geosci.*, 7, 145-151, 1981.
- Dozier, J. and S. I. Outcalt, An approach toward energy balance simulation over rugged terrain, *Geogr. Anal.*, 11, 65-85, 1979.
- Elassal, A. A. and V. M. Caruso, Digital elevation models, *Circ. 895-B*, U.S. Geol. Survey, Alexandria, VA, 1983.
- Hochstrasser, U. W., Orthogonal polynomials, in *Handbook of Mathematical Functions*, edited by M. Abramowitz and I. A. Stegun, pp. 771-802, Dover, New York, 1965.
- Kasten, F., A new table and approximation formula for the relative optical air mass, *Arch. Meteorol. Geophys. Bioklim.*, B-14, 206-233, 1966.
- Kneizys, F. X., E. P. Shettle, L. W. Abreu, J. H. Chetwynd, G. P. Anderson, W. O. Gallery, J. E. A. Selby, and S. A. Clough, Users Guide to LOWTRAN7, *Rep. AFGL-TR-88-0177*, Air Force Geophys. Lab., Bedford, MA, 1988.
- Male, D. H. and R. J. Granger, Snow surface energy exchange, *Water Resour. Res.*, 17, 609-627, 1981.
- Marks, D., Climate and energy exchange at the snow surface in Emerald Lake Basin, Sierra Nevada, Ph.D. Thesis, 159 pp., Dept. Geogr., Univ. Calif., Santa Barbara, 1988.
- Marks, D. and J. Dozier, A clear-sky longwave radiation model for remote alpine areas, *Arch. Meteorol. Geophys. Bioklim.*, B-27, 159-187, 1979.
- Marshall, S. E. and S. G. Warren, Parameterization of snow albedo for climate models, in *Large Scale Effects of Seasonal Snow Cover*, edited by B. E. Goodison, R. G. Barry, and J. Dozier, IAHS Publ. No. 166, pp. 43-50, Intl. Assoc. Hydrol. Sci., Wallingford, UK, 1987.

- Meador, W. E. and W. R. Weaver, Two-stream approximations to radiative transfer in planetary atmospheres: a unified description of existing methods and a new improvement, *J. Atmos. Sci.*, 37, 630-643, 1980.
- Nussenzveig, H. M. and W. J. Wiscombe, Efficiency factors in Mie scattering, *Phys. Rev. Lett.*, 45, 1490-1494, 1980.
- Olyphant, G. A., Insolation topoclimates and potential ablation in alpine snow accumulation basins: Front Range, Colorado, *Water Resour. Res.*, 20, 491-498, 1984.
- Olyphant, G. A., Longwave radiation in mountainous areas and its influence on the energy balance of alpine snowfields, *Water Resour. Res.*, 22, 62-66, 1986.
- Siegel, R. and J. R. Howell, *Thermal Radiation Heat Transfer, Second Edition*, McGraw-Hill, New York, 1981.
- van de Hulst, H. C., *Multiple Light Scattering*, 739 pp., Academic Press, New York, 1980.
- Warren, S. G., Optical properties of snow, *Rev. Geophys. Space Phys.*, 20, 67-89, 1982.
- Williams, L. D., R. G. Barry, and J. T. Andrews, Application of computed global radiation for areas of high relief, *J. Appl. Meteorol.*, 11, 526-533, 1972.

VIII. WET DEPOSITION AND IONIC LOADING

A. Introduction

In much of western North America and mountainous regions of Europe and Asia, deep snowpacks form through the late autumn, winter and early spring. The montane snowpack accumulates wet and dry atmospheric deposition, which is held in storage until release during a melt period. Although the concentration of solutes in montane snow is usually low, the large accumulation in the snowpack can produce considerable chemical loading [e.g. Laird et al., 1986].

The rugged and variable topography characteristic of alpine areas can cause significant spatial differences in the chemistry [Tranter et al., 1987] and snow water equivalence [Elder et al., 1989] of snow. Quantifying the solute storage in the snowpack of an alpine basin is therefore difficult, but important to investigations of the effect of snowmelt runoff on the hydrochemistry and aquatic biota of these basins. Moreover, water input from precipitation to alpine basins is known to vary 50% or more on an annual basis [California Cooperative Snow Surveys, 1930-1989]. Therefore multi-year sampling is necessary to successfully characterize the input of solutes to alpine basins from wet deposition.

Atmospheric deposition of solutes is important to alpine ecosystems, yet there exists little data on year-round and multi-year precipitation chemistry. The quality and quantity of wet deposition changes significantly with precipitation type and with seasons at lower elevations. For example, in eastern North America the ratio of NO_3^- to SO_4^{2-} is much higher in snowfall than in rainfall [Chan et al., 1987], which can have important consequences to the acidification of watersheds [Galloway et al., 1987]. Storm tracks have seasonal trends, which can shift the origin of ions in precipitation from regions with little anthropogenic influences to regions with high anthropogenic influences [Anlauf et al., 1986].

In the western United States, atmospheric deposition at high altitudes has received little attention, and several important questions are outstanding. The relative importance of sea salt, continental, and anthropogenic aerosols is unknown. The relative importance of the strong acid anions (NO_3^- , SO_4^{2-} , and Cl^-), the balancing cations H^+ and NH_4^+ , and organic anions, is also unknown. How these parameters vary on a seasonal basis, an annual basis, and by precipitation type, has not been investigated at high elevation in the Sierra Nevada.

In this chapter we quantify the precipitation chemistry over a three-year period to an alpine watershed in the Sierra Nevada. Sampling for wet deposition at the Emerald Lake watershed (ELW) spanned the three water years of 1985 through 1987, and includes winter snowfall in 1988. Water amounts in precipitation ranged from one of the wettest years on record (1986) to one of the driest (1987). We compare the volume-weighted mean chemistry and ionic loading of snowfall and rainfall, with particular emphasis on the relationships of NO_3^- , SO_4^{2-} and NH_4^+ . Source areas for ions in precipitation are evaluated. Particular emphasis is given to the chemistry of snow, as snow is the dominant precipitation input to the Sierra Nevada. We assess the storage of solutes in the snowpack, by comparing the solute loading from cumulative snowfalls to snowpits. For purposes of chemical mass

balance calculations and modeling efforts we investigate spatial variation in the chemistry of snowfall and the snowpack, to permit an accurate calculation of ionic loading, with estimates of standard error, to the watershed.

B. Methods

1. Precipitation Sampling

Sampling for wet deposition spanned three water years, 1985 through 1987, and included winter snowfall in 1988. Our water year begins on October 1 and runs through the following September 30, and is designated by the second calendar year. Winter snowfall is defined as accumulating snowfall, generally deposited during the months of November through April. Winter snowfall was sampled using two techniques. In water years 1985 and 1986 snow was sampled on an event basis at 1-4 sites (Figure 30); for water years 1987 and 1988 snow was sampled at six snowpits (Figure 30) during the period of maximum snow accumulation (week of April 2 in 1987, week of March 23 in 1988).

Integrated samples of the entire snowpack were obtained by digging pits to the ground and collecting duplicate, contiguous, vertical cores in increments of 40 cm. The snow samples were collected using PVC tubes (5-cm diameter, 50-cm long), which had been soaked in 10% HCl and then rinsed at least five times with deionized water. The snow cores were transferred into polyethylene bags, then placed into a second bag to avoid contamination or leakage from abrasion or melting during transport from the watershed. Snowfall events were collected on 1 m² snowboards. Collection of snow on snowboards followed the same protocol as snowpits. Duplicate profiles were sampled at each snowboard, there were two snowboards at each site, and 1-4 sites were sampled, depending on weather and avalanche conditions.

Volume-weighted concentrations for each ion in winter snowfall were calculated by the relation

$$\bar{C} = \frac{\sum P_i C_i}{\sum P_i}$$

Here \bar{C} is the volume-weighted mean of the ion, P_i is the snow water equivalence (SWE) for sample i , and C_i is the concentration of the ion in sample i . The ionic concentrations of each snowfall event were determined by calculating the volume-weighted means for each vertical profile, then a weighted average was calculated for each board, then for each site, and finally a volume-weighted mean concentration for the snow event was calculated by combining weighted means from all sites. A similar procedure was used to calculate the volume-weighted mean concentrations of solutes in the snowpack from snowpits.

Rain is precipitation that is 100% liquid water, or liquid water plus hail, at the collector. Rain generally fell in the months of May through October. Autumn snow is defined as wet snow, or a mixture of snow and rain, that was deposited in the months of September and October (which are in different water years), and where significant snowmelt occurred after deposition. Designation of precipitation type was made by field personnel during the storm. Solutes in rain and autumn snow were collected with a wet-only Aerochem Metrics model 301 sampler, located at the inlet.

Precipitation amount in a storm or the snowpack was sampled independently of the chemistry. The snow water equivalence (SWE) used to calculate areal solute loading from snowfall for water year 1985 is from cumulative measurements from snowboards at the inlet site. The SWE used to calculate areal solute loading for water years 1986 through 1988 is from snow surveys conducted during the period of maximum snow accumulation, and corrected for snowmelt and sublimation losses. Depth of the snowpack was measured at 86 to 354 points, each of which was the average of five depth measurements, and density was measured at multiple snow pits. Areal estimates of rain and autumn snow at the ELW used a combination of Belfort rain gages located at low (2800 m), medium (3000 m) and high (3200 m) elevation zones, along with 8 pairs of non-recording gages distributed throughout the watershed.

Ionic loading to the basin was calculated as the product of the volume-weighted mean chemistry of precipitation and the precipitation amount over the basin. Volume-weighted mean concentrations of solutes in the snowpack were calculated from cumulative event totals of winter snowfall in 1985 and 1986. The accumulated solutes from autumn snowfall were added to winter snowfall in 1986. For water years 1987 and 1988, the volume-weighted concentrations of solutes in the snowpack were the volume-weighted averages from six snowpits selected to represent the major elevational, slope and radiation classes of the basin (Figure 30). Precipitation chemistry of rainfall and autumn snowfall were from the collector at the inlet.

2. Sample Collection, Storage and Analysis

Careful cleaning, collection, storage, processing, and analysis are required to insure reliable chemical measurements of the very dilute snow that occurs in the Sierra Nevada. Only plasticware (usually PVC, polyethylene, or polycarbonate) containers were used. Prior to use the containers were soaked in 10% HCL and fastidiously rinsed at least five times with deionized water (conductance $0.2\text{--}0.5\ \mu\text{S cm}^{-1}$). If liquid samples were to be obtained, the containers were rinsed with the sample also. Bags used to collect snow samples were acid-washed as above in 1985 and 1986. Due to the possibility of contamination from the acid-washing procedure, in 1987 and 1988 bags were fastidiously rinsed five times with deionized water, soaked overnight in deionized water, and then rinsed five more times with deionized water.

All snow samples were kept frozen at -20°C until ready for analysis. In the laboratory individual samples were placed in a covered polyethylene bucket, and melted at room temperature ($\approx 20^{\circ}\text{C}$, 1985 and 1986), or at 4°C (1987 and 1988). As soon as the sample was melted, pH and conductivity were measured on unfiltered samples. Subsamples were filtered through pre-rinsed, 47 mm filters with ca. $1\ \mu\text{m}$ pore size (Gelman A/E glass fiber in 1985, 1986 and the first part of 1987; Nuclepore filters in the remainder of 1987 and in 1988). One set of subsamples was immediately analyzed for ammonium and phosphate in water years 1986 and 1987. A second set was stored in the dark at 4°C for subsequent cation and anion determinations. A third set in 1987 and 1988 was preserved with chloroform and stored in the dark at 4°C for organic anion analysis.

The pH measurements were made with combination electrodes suitable for use in dilute waters (Sargent Welch S-30072-15 or Ross 8104) and a Fisher Accumet 805 pH meter. For each series of measurements the electrode was calibrated with pH 7.00 and pH 4.00 reference buffers and washed twice for 3 minutes with stirred deionized water. The electrode was rinsed with an aliquot of sample, and the temperature compensated pH determination made on a fresh, quiescent sample after five minutes. Conductance was measured with a Yellow Springs Instruments Model 32 meter and glass electrode with a 0.1 cell constant. Simultaneous temperature measurements were made, and conductivity was standardized to 20°C using a coefficient of 2% per °C. The conductivity cell was calibrated with dilute solutions of KCl.

Ammonium and phosphate were determined spectrophotometrically by the indophenol-blue and molybdenum-blue methods [Strickland and Parsons, 1972]. Calcium, magnesium, sodium, and potassium were analyzed with a Varian AA6 atomic absorption spectrophotometer. An air-acetylene flame was used; addition of lanthanum chloride suppressed chemical and ionization interferences during calcium and magnesium determinations. Especially dilute samples were also analyzed with a graphite furnace and manual 20 μL injections. Chloride, nitrate, sulfate, acetate (CH_3COO^-) and formate (HCOO^-) were measured by ion chromatography (Dionex Model 2010i) employing chemical ion suppression and conductivity detection.

Our program for quality assurance and quality control incorporated the following features. A standard protocol was followed for sample collection, processing, and analysis. At least duplicate samples were obtained and analyzed in most cases. Care was taken to avoid touching any surface that was to contact the sample. Filter blanks were done with varying amounts of rinse water. Results were scrutinized for any evidence of contamination (*e.g.* high Na^+ and Cl^- in one sample of a duplicate set) and deleted if clearly in error. Freshly prepared calibration standards and reagent blanks were used in every array.

Precision of analytical results was assessed as percent relative standard deviation (RSD, the percent ratio of the standard deviation to the mean) of the means of duplicated samples to which known additions were made. Duplicate samples were separated by 10-15 samples in each run. Analytical precisions for Ca^{2+} , Mg^{2+} , Na^+ and K^+ were 3.1, 1.0, 3.3 and 6.2 RSD, respectively (Table 69). Analytical precisions for NO_3^- , SO_4^{2-} and Cl^- were 1.2, 2.7 and 13.4 RSD, respectively. Limits of detection for major ions were established in accord with the Scientific Apparatus Makers Association (SAMA) definition for detection limit: that concentration which yields an absorbance equal to twice the standard deviation of a series of measurements of a solution whose concentration is detectable above, but close to the blank absorbance. Detection limits of all solutes was less than 0.5 $\mu\text{eq L}^{-1}$, except for Ca^{2+} , which was 1.0 $\mu\text{eq L}^{-1}$.

Analytical accuracy was assessed as the degree of conformity of values obtained to an accepted true value. Certified controls were included in each analytical run. A synthetic charge balance control was incorporated into analytical runs of cations and anions. Overall agreement of measured values of cations and anions with NBS certified controls warranted no corrections. Our charge balance control demonstrated there was no bias in our analytical

performance.

Evaluation of ion leaching from filters indicated that there was no filter effect on ionic concentrations, except for Na^+ . Gelman A/E glass fiber filters that are pre-rinsed add, on average, $2.0 \mu\text{eq L}^{-1}$ of Na^+ to samples, while Nuclepore filters do not affect ionic concentrations of Na^+ in samples. Ninety out of 392 samples in 1987 were filtered with Gelman A/E glass fiber filters, before Nuclepore filters were employed. An average value of $2.0 \mu\text{eq L}^{-1}$ was subtracted from the measured Na^+ in these 90 samples, to correct for Na^+ contamination by the glass fiber filters. If the corrected Na^+ value was 0 or less, that sample was assigned a Na^+ concentration of $0.1 \mu\text{eq L}^{-1}$. All snow samples in 1985 and 1986 were filtered with Gelman A/E glass fiber filters. Sodium concentrations for these samples were corrected by deleting samples clearly in error.

Charge balance totals for the major inorganic ions in deposition for water years 1985 through 1987, and winter snowfall in 1988, were calculated to evaluate the quality of wet deposition data. Table 70 presents a summary of the charge balance calculations, where n is the number of samples, Σ^+ is the sum of positive ions, Σ^- is the sum of negative ions, Σ ions is the sum of all inorganic ions, and Σ^+ / Σ^- is the sum of positive ions divided by the sum of negative ions. Cation to anion ratios ranged from 1.27 to 1.91. There was no difference in the cation to anion ratio by precipitation type, with the exception of the high ratio (1.91) in winter snowfall in 1988. Ion percent differences ranged from 12% to 31%; IOD is the difference of cations minus anions divided by the sum of cations plus anions, times 100. For winter snowfall these IOD percentages are well within the chemical reanalysis criteria of $\pm 60\%$ set by the NADP quality assurance guidelines for charge totals less than $50 \mu\text{eq L}^{-1}$ [Peden, 1983]. Of the 834 individual snow samples, only 4 exceeded the IOD reanalysis criteria set by the NADP.

Several factors contribute to the bias of positive charge in snowpack samples. One is the leaching of sodium from glass fiber filters. A secondary contribution to the charge imbalance could be a slight overestimate of calcium, which is frequently near its detection limit. However, re-analysis of some of these samples with the graphite furnace made only slight improvements. Another contributor may be an unmeasured ion. Bicarbonate was not consistently measured, because at the pH of the samples it is below detection by the Gran titration method. Occasional analysis for bicarbonate always resulted in concentrations less than $1 \mu\text{eq L}^{-1}$. Dissolved organic carbon is known to occur in western snow at very low levels [Laird et al., 1986]. Our measurements of dissolved organic N and P in snow support the likelihood of dissolved organic carbon, and hence organic anions, in snow [Melack, unpublished]. Measurement of organic anions in 1988 improved the charge balance of the seasonal snowpack from a cation to anion ratio of 1.40 in 1986 to 1.22 in 1988.

Samples of rainfall and autumn snowfall were kept frozen and mailed within 24 hours to the analytical laboratory at the California Air Resources Board. Conductance and pH were measured immediately in the field as well as in the laboratory. Analytical techniques were the same as for winter snow. Laboratory quality control included daily calibration and reanalysis every tenth sample. The laboratory participates in semi-annual EPA performance surveys to determine the accuracies of ion analyses. Accuracy of Ca^{2+} was consistently

biased on the high side. No other ions showed bias in accuracy. Analytical precisions for Ca^{2+} , Mg^{2+} , Na^+ , K^+ , and NH_4^+ were 29.2, 6.8, 29.1, 12.7, and 9.2 RSD, respectively. Analytical precisions for NO_3^- , SO_4^{2-} , Cl^- , pH and conductance were 6.0, 3.6, 9.5, 1.6, and 1.4 RSD, respectively. Additional details on analytical techniques, accuracy and precision are reported by Blanchard et al. [1989].

C. Results

The volume-weighted mean concentrations of major ions in winter snowfall for water years 1985 through 1988 were very low (Table 71). Concentrations of individual ions were all less than $5 \mu\text{eq L}^{-1}$. Hydrogen had the highest concentration of the major ions ($4.6 \mu\text{eq L}^{-1}$); all other ions had concentrations less than $3 \mu\text{eq L}^{-1}$. Hydrogen concentration was similar from 1985 through 1987, about $4.6 \mu\text{eq L}^{-1}$ and a pH of about 5.34. Conductivity also had little variation among those years, with a range of 3.5 to $4.0 \mu\text{S cm}^{-1}$. Hydrogen concentration and conductivity were slightly lower in 1988: $3.8 \mu\text{eq L}^{-1}$ and $2.5 \mu\text{S cm}^{-1}$, respectively.

There was a difference in Cl^- , Na^+ , NO_3^- and NH_4^+ concentrations of winter snowfall between water years 1985-1986 and water years 1987-1988. Annual Cl^- concentrations in winter snowfall during the later two years were lower by about 50% ($3.1 \mu\text{eq L}^{-1}$ in 1986 compared to $1.5 \mu\text{eq L}^{-1}$ in 1987), as was Na^+ ($1.4 \mu\text{eq L}^{-1}$ in 1986 compared to $0.7 \mu\text{eq L}^{-1}$ in 1987). Nitrate concentrations were more than twice as high ($1.8 \mu\text{eq L}^{-1}$ in 1986 compared to $4.2 \mu\text{eq L}^{-1}$ in 1987), as were NH_4^+ concentrations ($1.4 \mu\text{eq L}^{-1}$ in 1986 compared to $3.8 \mu\text{eq L}^{-1}$ in 1987). A change from Gelman glass fiber filters in 1985 and 1986 to Nuclepore filters in 1987 and 1988 may contribute to the differences in Na^+ concentration.

Analysis for the organic anions, acetate and formate, began in water year 1987. These organic anions composed 9% and 21% of measured anions in 1987 and 1988. Methodological problems associated with analysis of organic anions in 1987, primarily degradation over time during storage, probably resulted in low values for 1987.

Relative ranking of ionic concentrations in winter snowfall indicate that H^+ was the dominant ion all four years (Table 72). The relative ranking of the other ions was markedly different between water years 1985-1986 and water years 1987-1988. Chloride changed in rank from position 2 in the first two water years to position 6 in the second two water years. Nitrate and NH_4^+ had the opposite pattern, ranking higher in the second two years than in the first two years. This shift in ion ranking parallels a change from normal or above normal snowfall in water years 1985 and 1986, to below normal snowfall in water years 1987 and 1988. Acetate in 1988 was ranked equal to NO_3^- , and was more abundant than Cl^- or SO_4^{2-} .

The ratio of NO_3^- to SO_4^{2-} in winter snow from water years 1985 through 1988 varied from 0.77 to 1.75, on an equivalent basis (Table 73). The NO_3^- to SO_4^{2-} ratio was lowest in years of normal and above normal snowfall, and greatest in years of below normal snowfall. The NH_4^+ to strong acid anion (Σ^-) ratio in winter snowfall ranged from 0.1 to 0.4 (Table 73). Neutralization of strong acid anions by NH_4^+ was least in years of normal and above normal snowfall, and most in years of below normal snowfall. Neutralization of

strong acid anions in winter snowfall by H^+ was greater than that of NH_4^+ in all years. Ammonium was strongly correlated with the sum of NO_3^- and SO_4^{2-} ; regression analysis for all winter snowfalls in water years 1985 and 1986 had an r^2 of 0.82, $n = 20$ (Figure 31).

Solute storage in the winter snowpack was investigated in water year 1986 by comparing the chemistry of cumulative snowfalls measured on snowboards with the chemistry of the snowpack at the same site. Hydrogen, SO_4^{2-} , and Cl^- had similar volume-weighted mean concentrations and loading (charge/unit area) in cumulative snowfalls and in the snowpack, as did SWE. Nitrate had a small but persistent decrease in snowpits compared to cumulative events. For example, on March 5 at the inlet, SWE and loading of H^+ , SO_4^{2-} , and Cl^- in the snowpit were all within 10% of cumulative event totals (Figure 32). Nitrate loading in the snowpack, on the same date and on January 18, was about 80% of cumulative deposition. After the onset of snowmelt in early April, anions left the snowpack at a much faster rate than water or H^+ . Basic cations and NH_4^+ concentrations were variable in cumulative event and snowpack concentrations. This variability may be an artifact of concentrations being close to detection limits.

If solutes from snowfall are stored in the snowpack, then dry deposition will result in the ionic loading in the snowpack being greater than the ionic loading from cumulative snowfalls. Solute loading in the snowpack was less than or equal to solute loading from cumulative snowfalls, for H^+ , SO_4^{2-} , NO_3^- , and Cl^- , in water year 1986. The equivalence between cumulative snowfall and snowpack loading indicates that dry deposition was not an important contributor of these ions to the solute loading in the winter snowpack.

For the three snowfalls in water year 1986 that were sampled at sufficient sites to test for spatial variability, there was no significant spatial variation in the chemistry of the strong acid anions. For example, 4 replicate snow cores were sampled at 4 sites within the watershed during a snowfall (171-mm SWE) on January 9. A one-way analysis of variance for the volume-weighted mean concentrations of NO_3^- and SO_4^{2-} yielded no significant differences among the tower, inlet, pond, and ridge sites.

Spatial variation in the volume-weighted mean chemistry of the snowpack was evaluated in water years 1987 and 1988. Table 74 presents the ionic volume-weighted mean concentrations (\bar{X}) at maximum snow accumulation, as well as arithmetic standard deviation (SD), Standard Error (SE), 95% Confidence Interval (CI), and relative standard deviation (RSD), from 6 sites. The maximum RSD for conductance, H^+ , NH_4^+ , Ca^{2+} , Mg^{2+} , NO_3^- and SO_4^{2-} was less than or equal to 30% for both water years; the mean RSD for these six ions was about 20%. The slightly larger RSD for Cl^- may in part be a result of the relatively high analytical error in measuring Cl^- . The standard error of the mean for these ions was within 5% to 10% of the mean. Sodium and K^+ concentrations were near their detection limits, which may explain their relatively high RSD. Similarly, methodological problems in measuring the organic anions in water year 1987 may be responsible for their large variances in that year.

The sum of the major inorganic ions stored in the basin's snowpack at maximum accumulation ranged from 87 eq ha^{-1} in 1988 to 370 eq ha^{-1} in 1986 (Table 75). Solute loading of individual ions in the snowpack at maximum snow accumulation for the four

water years ranged from 8 to 95 eq ha⁻¹ (Table 75). Ionic loading is not shown for Na⁺, K⁺, CH₃COO⁻ and HCOO⁻ because concentrations of these ions were all close to their detection limits.

The standard error of ionic loading to the basin from snowfall was calculated for water years 1987 and 1988 by propagating the standard error from measurements of the volume-weighted mean concentrations of solutes in the snowpack (from Table 74) and the SWE of the snowpack (Chapter III), using the procedure described in Bevington [1969]

$$SE = \left[(\bar{C}_i^2 \times SE_{SWE}^2) + (\overline{SWE}^2 \times SE_{C_i}^2) \right]^{1/2}$$

where \bar{C} is the volume-weighted mean concentration of an ion in the basin, SE_{C_i} is the standard error of the measured volume-weighted mean concentration of that ion, \overline{SWE} is the mean SWE of the basin, and SE_{SWE} is the standard error of the measurement of SWE. If there is a correlation in measurement error between the two parameters, then the covariance between parameters needs to be considered. Since the measurements of SWE and solute chemistry were independent, the covariance term can be ignored when propagating measurement error. Calculations of measurement error with and without the covariance terms showed little difference, indicating that there was no significant covariance between the two measurements. The covariance term for propagation of errors was therefore not used. The standard error of ionic loading during maximum snow accumulation in 1987 and 1988 was approximately 10% of the mean concentration for each ion (Table 75). The width of the 95% confidence interval was about 20% of the mean concentration for each ion.

The chemistry of wet deposition differed markedly with season and with precipitation type. A summary of the volume-weighted mean concentrations of ions in rainfall and autumn snowfall, for water years 1985 through 1987, is presented in Table 76. The pH of rainfall was about 4.9, compared to a pH of about 5.3 for winter snowfall. The conductance of rainfall was about 20 $\mu\text{S cm}^{-1}$, compared to about 3.5 $\mu\text{S cm}^{-1}$ for winter snowfall. In general, the volume-weighted mean concentrations of the major ions in rainfall were about 10 times greater than in winter snowfall. Autumn snowfall was generally intermediate in concentration between rainfall and winter snowfall. Ammonium, NO₃⁻, and SO₄²⁻, were the major ions in rainfall and autumn snowfall.

Solute concentrations in rainfall had an average cation to anion ratio of about 1.30, showing a positive bias similar to snowfall (Table 70). However with an ionic strength of about 200 $\mu\text{eq L}^{-1}$, the IOD values of 15% and 16% for solutes in seasonal rainfall equal or exceed the reanalysis criteria set by the NADP quality assurance guidelines [Peden, 1983]. There was no bias in our analytical performance. The IOD values thus indicate the presence of unmeasured ions. Autumn snowfall had the same positive bias in charge balance as rainfall. The positive bias in the charge balance of rainfall and autumn snowfall and our measurements of organic anions in snowfall, indicate that CH₃COO⁻ and HCOO⁻ probably comprise about 25%-30% of the anions in rain and autumn snow.

Nitrate concentrations were higher than SO₄²⁻ in volume-weighted mean concentrations of rainfall and autumn snowfall in all three water years (Table 73). Nitrate to sulfate ratios in rainfall ranged from 1.11 to 1.32, and in autumn snowfall ranged from 1.51 to 2.93. These ratios are in the middle range of the NO₃⁻ to SO₄²⁻ ratios found in winter snowfall,

with the exception of the 2.93 value in the fall of 1987. Ammonium to strong acid anion (Σ^-) ratios in rainfall ranged from 0.49 to 0.63 and in autumn snowfall from 0.55 to 1.14 (Table 73). The NH_4^+ to H^+ ratio in rainfall and autumn snowfall was always greater than one, in contrast to winter snowfall where the NH_4^+ to H^+ ratio was always less than one. Ammonium in rainfall in water year 1986 neutralized 11-fold more strong acid anions than H^+ in rainfall of that year. Ammonium was strongly correlated with the sum of NO_3^- and SO_4^{2-} ; regression analysis for all rain and autumn snowfalls in 1985 and 1986 had an r^2 of 0.88, $n = 20$ (Figure 31).

Seasonal and interannual variability in solute loading from wet deposition was pronounced. Solute flux from winter snowfall was about 300 eq ha^{-1} , from autumn snowfall about 100 eq ha^{-1} , and rain was about 35 eq ha^{-1} , in years of normal (1985) and above normal (1986) precipitation. On a percentage basis, winter snowfall for both years deposited about 91% of the annual water to the basin, and about 68% percent of the ion flux to the ELW (Table 77); autumn snow provided about 8% of the water flux and 20% of the ion flux to the basin. Annual snowfall (autumn and winter snowfall) for these two water years supplied about 99% of the water and 90% of the solute flux to the watershed. Rain provided about 1% of the water flux to the watershed, and about 10% of the ion flux, during the two water years

The below normal water year (1987) had very different fluxes of water and solutes, by precipitation type. Water flux from rainfall in 1987 was 159 mm, about five times the 32 mm deposited in 1986, and about ten times the 16 mm deposited in 1985. Rainfall in 1987 accounted for 17% of the water flux to the basin and 66% of the annual solute flux, while autumn snow only provided only 2% of the water and 4% of the solute flux, and winter snow supplied 81% of the water and 30% of the solutes. However 85% of the solute flux in rainfall in 1987 occurred during the time period of snowmelt runoff.

The volume-weighted mean concentrations of each of the major ions in the annual wet deposition to the watershed were less than or equal to $5.4 \mu\text{eq L}^{-1}$, for water years 1985 through 1987 (Table 78). The annual ionic content of all wet deposition for the three water years, from major inorganic ions, was $30 \mu\text{eq L}^{-1}$. No one ion dominated the annual flux of wet deposition to the ELW. Ammonium and H^+ each accounted for about 18% of the total ionic content of precipitation, followed closely by NO_3^- (17%), SO_4^{2-} (14%) and Cl^- (12%). The remaining 21% of ionic flux was divided among Ca^{2+} , Na^+ , K^+ and Mg^{2+} , in that order.

The average annual wet deposition to the watershed, for water years 1985 through 1987, was 472 eq ha^{-1} (Table 78). There was a two-fold difference in annual loading from wet deposition during water years 1985 through 1987. Somewhat surprisingly, solute loading in water years 1986 and 1987 was similar, even though 1986 was one of the largest water years on record and 1987 one of the lowest.

D. Discussion

1. Chemistry of Winter Snow

a. Acidity. Winter snowfall at the ELW was slightly acidic (Table 71). Pure water in equilibrium with atmospheric CO₂ should have a pH of about 5.6 [Barrett and Brodin, 1955], or a H⁺ concentration of 2.5 μeq L⁻¹. However only in the absence of naturally-occurring aerosols, such as NH₃, SO₂ and SO₄²⁻, is the pH of precipitation about 5.6 [Charlson and Rodhe, 1982]. The volume-weighted mean H⁺ concentration in winter snowfall from 1985 through 1988 at the ELW was 4.6 μeq L⁻¹; the acidity may be from either natural or anthropogenic sources.

Comparison of acidity values from the Emerald Lake watershed with precipitation from remote areas of the world helps assess the influence of anthropogenic emissions on the local precipitation chemistry. Measurements of the acidity of ice cores taken from the Agassiz ice cap and Mt. Oxford areas in the Canadian high Arctic, at an elevation of about 1600 m, permit such a comparison [Barrie et al., 1985]. Hydrogen concentration of the snowpack during the Arctic summer has remained relatively constant throughout this century, at approximately 5.8 μeq L⁻¹. However, the acidity of the wintertime snowpack at these remote sites has increased from a H⁺ concentration of 8 μeq L⁻¹ between 1925 and 1956, to 14 μeq L⁻¹ from 1957 to 1977. Barrie et al. [1985] attribute this increase in acidity during the Arctic winter to European emissions of SO₂ and NO_x. The annual hydrogen ion concentration of 4.6 μeq L⁻¹ in winter snow from water years 1985 through 1988 at the ELW is comparable to the background (summer) acidity of the Arctic, and less than the acidity of winter snowfall in the Canadian Arctic.

Analysis of sediment cores from Emerald Lake indicates that the current pH of the lake is within the historical range for the basin [Melack et al., 1987]. Since snowmelt runoff provides the majority of water input to Emerald Lake, by inference it appears that the present pH (about 5.34) of snowfall is similar to that of the pH from snowfall for the past 150 years. However geochemical reactions may have buffered any increase in the acidity of snowfall before snowmelt runoff reached Emerald Lake.

The pH of winter snowfall at the ELW is slightly lower (ca. 0.2 pH units) than values reported by other investigations on the quality of snowfall in the Sierra Nevada [Feth et al., 1964; Brown and Skau, 1975; Melack et al., 1982; and Laird et al., 1986]. Other solutes in the winter snowpack at ELW are similar to event and snowpack measurements reported in other high-altitude locations in the Sierra Nevada [Melack et al., 1982; Stoddard, 1987; Sickman and Melack, 1989].

Snowpack chemistry from other periods and sites on the west coast is in general agreement with our Emerald Lake results (Table 79). A transect of snowpack chemistry in the Cascade-Sierra Nevada from the U.S.-Canadian border to a point northeast of Bakersfield, California generated a median pH of 5.6 [Laird et al., 1986]. Snowpack chemistry from the Alpine Lakes Wilderness Area east of Seattle also had an average pH of 5.6 [Welch et al., 1984], though the pH of snow along the Pacific Coast of Canada was found by McBean and Nikleva [1986] to be 5.4. Michaels et al. [1987] report a pH of 5.3 in an

alpine snowpack in the Colorado Rockies, with the remaining ions about 5 to 6-fold more concentrated than at the ELW. Solutes in snowfall from eastern North America and northern Europe are at times much higher than snowfall at the ELW (Table 79). Snowfall in these areas can have a pH of 4.0, and other soluble ions can have concentrations 30-fold higher than the snowfall at the ELW.

b. Organic Anions. Measurement of organic anions with low molecular weight in the precipitation of remote areas of the world has received attention only recently. Keene et al. [1983] have found that formic and acetic acids contributed 25-59% of the volume-weighted free acidity in remote areas of the world, while Galloway and Gaudry [1984] report that CH_3COO^- and HCOO^- contributed 25% of the free acidity in precipitation to remote Amsterdam Island in the Indian Ocean. The concentration of organic acids found in central Virginia receiving a large amount of strong mineral acidity are similar to those found in remote central Australia, suggesting that organic acids may make a disproportionately greater contribution to the free acidity of precipitation in areas of North America which receive little mineral acidity from anthropogenic activity [Keene and Galloway, 1984].

Organic acids are an important constituent of wet deposition to the Sierra Nevada. Measurements of CH_3COO^- and HCOO^- in the snowpack at each of four high-altitude watersheds that Sickman and Melack [1989] studied in 1987 and 1988 indicate that the organic anions contributed 25-30% of the anions; this percentage is similar to our results (Table 71). They did not measure organic anions in rainfall, but report a positive bias of about 25% in the charge balance of rainfall chemistry; this bias indicates that organic anions were probably an important component of rainfall at their sites. Gunz [California Institute of Technology, personal communication, 1988] has found that 25-30% of the anions in the snowpack of Yosemite National Park in the Sierra Nevada are acetate and formate. Hoffmann et al. [1989] report that organic anions contributed significantly to the composition of cloudwater sampled at Sequoia National Park (elevation 1856 m), with the percentage of organic anions increasing as total ionic charge decreased. Furthermore Hoffmann et al. attribute a large percentage of acidity in cloudwater to organic anions. Interestingly, formate concentration was greater than acetate concentration in the cloudwater samples analyzed by Hoffmann et al. at a mid-elevation site in Sequoia National Park, while at the ELW acetate was always greater than formate in snow samples. Organic acids thus comprise about 25% to 30% of all anions in wet deposition flux to alpine basins in the Sierra Nevada. These measurements of acetate and formate in precipitation at the ELW are comparable in percentage to organic anions in remote areas of the world that receive little anthropogenic acidity.

Sources of organic anions are not well understood. Galloway and Gaudry [1984] list several proposed sources, oxidation of formaldehyde and oxidation of olefinic marine compounds, as well as biomass burning, biomass emissions and bacterial processes in clouds. Oxidation of isoprene, a natural hydrocarbon emitted from vegetation, may be an important source of formic acid [Jacob and Wofsy, 1988]. Automotive exhaust is an important anthropogenic source [Talbot et al., 1988]. The fate of organic anions once they enter the terrestrial and aquatic ecosystems of alpine basins is also unknown. Because organic anions are rapidly assimilated by the biota, many researchers assume that they are

unimportant to the acidification of the environment [e.g. Keene and Galloway, 1984]. However the relatively low biological activity and short hydrologic residence time characteristic of alpine watersheds could result in organic anions having a role in the water chemistry of these watersheds. For example, acidity in recently deglaciated, granitic headwater reaches of the clearwater Jamieson Creek in British Columbia was from organic anions [Driscoll et al., 1988].

c. *Solute Storage.* Storage of solutes in snowpacks that remain below freezing have been reported to be similar to those in cumulative snowfall [e.g. Cadle et al., 1984] and to show significant losses from the snowpack relative to cumulative snowfall [e.g. Jeffries and Snyder, 1981]. The agreement of H^+ , SO_4^{2-} and Cl^- loadings in the snowpack and in cumulative snowfall at the ELW (Figure 32) is similar to that reported by Cadle et al. [1984] for a northern Michigan snowpack. Cadle et al. [1984] also report a NO_3^- loss of 10% from the snowpack relative to cumulative snowfall, but attribute the loss in part to sampling and analytical problems. The 20% loss of NO_3^- from the snowpack at the ELW agrees with the findings of Jeffries and Snyder [1981], who report a similar loss of all major ions (except Cl^-) from the snowpack in central Ontario. They attribute this loss to migration through the snowpack to underlying soils, which occurred during periods of no significant melting. The mechanism of this solute migration from the snowpack downwards towards the ground was unknown. Barry and Price [1987] and Jones and Laberge [1988] report that NO_3^- can be lost from a snowpack under cold conditions ($<0^\circ C$) while SO_4^{2-} is not lost in the same snowpack. Movement of NO_3^- from the snowpack at the ELW to soils in 1986 is supported by the soil lysimeter data of Aaron Brown [University of California at Riverside, personal communication, 1989].

The variability in measurement of basic cation and NH_4^+ concentrations in snowfall and in snowpits in water year 1986 makes it difficult to assess their storage in the winter snowpack. Cadle et al. [1984] report that there was no significant difference in basic cations and NH_4^+ concentrations between cumulative snowfall and snowpits in northern Michigan. Since our results for SWE, H^+ , SO_4^{2-} , and NO_3^- are similar to those of Cadle et al. [1984], it may be a reasonable inference to assume that cations are stored in the snowpack at the ELW. The observed differences between precipitation chemistry and snowpack storage, with the exception of NO_3^- , are probably due in part to sampling and analytical problems. Therefore we conclude that solute losses from the snowpack are minimal as long as the snow temperature remains below freezing. Sampling of the snowpack in late winter, during the period of maximum snow accumulation, provides an estimate of atmospheric deposition of solutes during winter, if there is no significant snowmelt or rain on snow events prior to sample collection. For this reason our protocol for sampling the precipitation chemistry of winter snowfall was changed from event sampling in 1986 to snowpack sampling at the period of maximum accumulation in 1987 and 1988.

Dry deposition can be a major pathway of solute flux from the atmosphere to watersheds. In California, dry deposition has been shown to be an important source of solute flux. The rate of dry deposition is surface dependent and is a function of atmospheric turbulence, increasing with increasing turbulence and surface roughness [Whelpdale and Shaw, 1974]. The stable temperature gradients over snow surfaces and low surface roughness of snow

generally result in snow having low depositional velocities, averaging from about 0.05-1.6 cm s^{-1} for SO_4^{2-} [Whelpdale and Shaw, 1974; Dovland and Eliassen, 1976; Barrie and Walmsley, 1978; Granat and Johansson, 1983; Cadle et al., 1985; Bales et al., 1987].

Dry deposition does not appear to be an important contributor of H^+ , SO_4^{2-} , NO_3^- , or Cl^- to the chemical loading of the snowpack at the ELW during the snow accumulation season (Figure 32). However, particulates were excluded from the chemical analyses by filtering; therefore the contribution of particulates greater than 0.4 μm to dry deposition cannot be ascertained. The possibility that ionic losses from the snowpack were matched by dry deposition cannot be discounted, but is unlikely. The snowfall pattern at the ELW is one of large magnitude but infrequent storms, resulting in a snowpack surface that is generally composed of older, sintered snow grains. The infrequent storms also result in a relatively stable temperature gradient over the snowpack, minimizing atmospheric turbulence. Bales et al. [1989] have shown in laboratory studies that SO_4^{2-} depositional velocities are lowest for colder, dry snow that has undergone significant metamorphism (0.02 cm s^{-1}). Our field data corroborate the laboratory work of Bales et al. that dry deposition of SO_4^{2-} to well-sintered snow is low. It was not possible to evaluate the importance of the dry deposition of basic cations and NH_4^+ to the winter snowpack.

d. Spatial Variability of Snow Chemistry. The chemistry of the snowpack can be highly variable on the scale of a small watershed [Tranter et al., 1987] as well as on a regional scale [Barrie and Vet, 1984]. This variability in snow chemistry may be from spatial differences in the chemistry of snow during deposition, from redistribution of ions after deposition, or from a combination of the two. Estimating the areal loading of solutes stored in the snowpack is thus difficult. Variability in many of the physical properties of snowcover has been shown to affect the ionic concentration and chemical loading in alpine watersheds [Richards, 1973]. The rugged topography characteristic of the ELW and other alpine basins may result in spatial differences in snowpack chemistry due to localized snowmelt, sublimation or wind scouring after deposition in snowfall.

Spatial variation in the chemistry of snowfall at the scale of the ELW does not appear to be significant. The standard error of the volume-weighted mean concentrations of ions stored in the snowpack at maximum snow accumulation was low (5-10%) for the ions in sufficient concentration to provide good analytical precision (H^+ , NH_4^+ , Ca^{2+} , Mg^{2+} , NO_3^- , SO_4^{2-} and Cl^-) (Table 74). The chemistry of snow covered area in alpine areas of the Sierra Nevada can be effectively estimated from a limited number of sample sites. The location of sampling sites for snow chemistry in water years 1987 and 1988 were selected to represent the major elevational, slope and radiation classes of the watershed. To the extent that these sites do represent these terrain and flux classes, our procedure gives a better estimate of solute concentration in the snowpack than the error analysis indicates.

Calculations of chemical loading for mass balance and modeling efforts requires accurate measurements of chemical concentrations and precipitation volume. To reduce the standard error of our measurements of ionic loading in the basin's snowpack to 10% (Table 75), hundreds of depth measurements were necessary. Accurate calculations of the ionic loading from snowfall to watersheds requires many measurements of precipitation volume.

Our error analysis sets boundary conditions for chemical mass balance and modeling efforts of snowmelt runoff.

2. Chemistry of Rain and Autumn Snowfall

That rainfall contains about 10-fold higher concentrations of solutes than does winter snowfall (Table 76), may, in part, be due to physical differences between rain and snow in the atmosphere. Snow and rain transport solutes from the atmosphere to the earth's surface through two main processes, nucleation scavenging within the cloud (rainout or snowout) and below-cloud scavenging by attachment of particles to existing hydrometeors (washout) [Davidson and Honrath, 1987]. Hydrometeors in clouds begin as ice nuclei or condensation nuclei. Heterogeneous ice nucleation by atmospheric aerosols is template specific and consequently inefficient. These ice nuclei are generally composed of clay particles derived from the earth's crust [Mason, 1975]. Only about one in 10^9 aerosols are active as ice nuclei at -10°C [Schemenauer et al., 1981], whereas all hygroscopic particles in the atmosphere with diameters greater than $0.2\ \mu\text{m}$ make good condensation nuclei [Dennis, 1980]. The dissimilar nucleation processes between snow and rain can generate different ionic ratios between the two types of nuclei, *e.g.* anthropogenic sulfur-containing aerosols make poor ice nucleating agents, while many forms of particulate sulfate are active condensation nuclei [Davidson and Honrath, 1987].

Nucleated ice crystals grow by two methods: water vapor diffusion or by accretion of cloud droplets in warmer clouds. Cloud droplets grow by continued vapor diffusion and by coalescence with other liquid droplets. Droplets can interact with acidic precursor gases, such as SO_2 , to form acidic (*e.g.* H_2SO_4) droplets [Kumar, 1986]. Since the supersaturation of water vapor with respect to liquid water is always smaller than that with respect to ice, ice crystals often grow at the expense of cloud droplets. Growth of an ice crystal by diffusion is thus similar to a distillation process. Vapor diffusion concentrates the solutes in cloud drops and dilutes the solutes in ice crystals. Borys et al. [1983] found that in an alpine area of northwest Colorado, cloud water contains three times the acidity and four to five times the conductivity of unrimed snow crystals. Nucleation differences and subsequent growth differences between cloud droplets and ice crystals result in rainfall having more concentrated solutes than snowfall, even when rain and snow precipitate from the same air mass. Differences in state (liquid versus solid) may thus explain a large part of the higher concentration of solutes in rainfall versus snowfall.

Rainfall was acidic (Table 76). The volume-weighted mean concentration of H^+ in rainfall from water years 1985-1987 was about $13\ \mu\text{eq L}^{-1}$. Acidic rainfall has been reported also in the Los Angeles basin [Morgan and Liljestrang, 1980], the San Francisco Bay Area [McColl, 1980] and the San Joaquin Valley [Rowe and Chestnut, 1985], as well as the west [Stohlgren and Parsons, 1987] and east [Melack et al., 1982] sides of the Sierra Nevada. The strong acid contaminants most likely come from urban and agricultural sources within California [Lawson and Wendt, 1982]. Part of the acidity in rainfall at the ELW may be from these anthropogenic sources.

Riming of snow crystals may be an important contributor to the chemistry of autumn and spring snowfall. Solute in autumn snowfall were intermediate in concentration between

those of rainfall and winter snowfall (Table 76). Additionally spring snowfall in 1986 was similar in concentration to autumn snowfall. [Dozier et al., 1987]. Mitchell [in press] reports that direct surface riming on snow crystals may contribute substantially to the chemical input of high alpine ecosystems in the Sierra Nevada. On average, he found that ionic concentrations in rime ice were greater than those in snow by a factor of 7.5. The solute concentrations of autumn and spring snowfall to the ELW were consistent with the higher solute concentrations reported in rimed snow crystals. Seasonal differences in the origin of air masses may also contribute to the observed solute concentrations in autumn and spring snowfall.

Autumn snowfalls are important to alpine basins for several reasons. In water years 1985 and 1986 they supplied a large percentage of the annual ionic flux to the ELW from wet deposition, depositing about 30% of the annual NO_3^- and SO_4^{2-} flux and about 50% of the annual NH_4^+ flux. Overland flow from snowmelt runoff in the autumn also rinses dry deposition from rock and vegetation surfaces, deposited during the relatively dry summer period. Additionally snowmelt runoff from autumn snowfalls flushes the products of biological activity from soils. As a result of snowmelt runoff from autumn snowfalls, streams at the ELW had elevated concentrations of solutes during the months of October and November [Melack et al., 1987].

3. Nitrate, Sulfate and Ammonium in Wet Deposition

Nitrate in wet deposition to alpine areas of California is as important, or more important, than SO_4^{2-} as a potential acidifying agent. The NO_3^- to SO_4^{2-} ratio was 1.16 on an equivalent basis, for all wet deposition to the ELW for water years 1985 through 1987 (Table 73). The mean NO_3^- to SO_4^{2-} ratio for wet deposition during the three years agrees with the findings of Stohlgren and Parsons [1987] at Giant Forest in Sequoia National Park, McColl et al. [1982] in northern California, and Liljestrand and Morgan [1980] in southern California, all of whom report a NO_3^- to SO_4^{2-} ratio greater than one. This NO_3^- to SO_4^{2-} ratio is much different than that of annual precipitation in the eastern United States, where SO_4^{2-} concentrations are generally two to three times greater than NO_3^- concentrations [Munger and Eisenreich, 1982].

There is little difference in the ratio of NO_3^- to SO_4^{2-} associated with precipitation type at the ELW, in contrast to eastern North America, where there is a consistent pattern of a high NO_3^- to SO_4^{2-} ratio in snow and a low NO_3^- to SO_4^{2-} ratio in rain at the same locations [Galvin and Cline, 1978; Frantisak et al., 1980; Barrie et al., 1983; Topol, 1986; and Chan et al., 1987]. However the NO_3^- to SO_4^{2-} ratio in wet deposition at the ELW is similar to that of snowfall in eastern North America.

The preferential scavenging by snow of NO_3^- over SO_4^{2-} is well-established [Hubert et al., 1983; Chang, 1984; Chan and Chung, 1986], and has often been invoked to explain the higher NO_3^- to SO_4^{2-} ratios of snowfall in eastern North America. The concentration of NO_3^- in precipitation in eastern North America shows little variation with season. The seasonal variation in the NO_3^- to SO_4^{2-} ratio is predominately caused by higher SO_4^{2-} concentration in rain and decreasing SO_4^{2-} concentration in snow (e.g. Chan et al. [1987]). This observation possibly reflects the lower oxidation of SO_2 to SO_4^{2-} during the cold

temperatures of winter [Anlauf et al., 1986], the negligible scavenging of SO_2 by snow [Chan and Chung, 1986], and seasonal changes in storm paths [Anlauf et al., 1986]. In California NO_x emissions can be 3 times higher than SO_2 emissions [California Air Resources Board, 1979]. The relative constancy of the NO_3^- to SO_4^{2-} ratio in rain and snow at the ELW may partly be due to the relatively low SO_2 emissions and high NO_x emissions in California.

Ammonium significantly neutralized the strong acid anions in wet deposition to the ELW (Table 73). Hydrogen ion concentration in rainfall could be as much as 11-fold higher if NH_4^+ were not present in atmospheric aerosols. Neutralization of acid anions in precipitation has been reported elsewhere. Munger and Eisenreich [1982] report that neutralization from major cations (*e.g.* Ca^{2+} and Mg^{2+}) averages 2-3-fold higher than from NH_4^+ in the continental United States. Chan et al. [1987] report that in Ontario NH_4^+ neutralized 19% to 36% of nitric and sulfuric acids in wet deposition, with the higher value in summer precipitation and the lower value in winter precipitation. Our results show a similar seasonal trend, with increasing NH_4^+ neutralization in summer. However neutralization of strong acid anions in precipitation by NH_4^+ at the ELW was approximately twice that of precipitation in Ontario, and much higher than the national average. Hoffmann et al. [1989] report similar neutralization of acidity by NH_4^+ in cloudwater at Sequoia National Park. Our findings indicate that without the large pool of atmospheric NH_3 , rainfall and snowfall at the ELW could become much more acidic.

Ammonium nitrate appears to be the principal NO_3^- containing molecule in wet deposition to the ELW. Photochemically initiated reactions result in the oxidation of NO_x to HNO_3 . Nitric acid can then react with NH_3 to form NH_4NO_3 aerosols. Wolff [1984] reports that in areas such as southern California, where NO_x emissions exceed SO_2 emissions and where there are strong sources of NH_3 , the $\text{NO}_3^-/\text{HNO}_3$ equilibrium strongly favors the production of NH_4NO_3 . Examination of the relationship between NH_4^+ and NO_3^- in aerosols in the Central Valley of California by the California Air Resources Board show a very strong relationship between NH_4^+ and NO_3^- , with an r^2 of 0.95 [California Air Resources Board, 1988]. This statistical relationship between NH_4^+ and NO_3^- suggests that NH_4NO_3 is the principal NO_3^- containing molecule in wet deposition to the ELW.

Further evidence that NH_4NO_3 is the principal NO_3^- containing molecule, and that $(\text{NH}_4)_2\text{SO}_4$ may be an important SO_4^{2-} containing molecule, was that there was no increase in protons associated with the increase in NO_3^- and SO_4^{2-} in winter snowfall of 1987 and 1988. However NH_4^+ increased 270% from 1986 to 1987. The correspondence between increases in NO_3^- and SO_4^{2-} with the increase in NH_4^+ suggests that NH_4NO_3 and $(\text{NH}_4)_2\text{SO}_4$ are the principal molecules containing NO_3^- and SO_4^{2-} , respectively. Protons generated by the oxidation of reduced S and N in emissions appear to react with NH_3 to produce $(\text{NH}_4)_2\text{SO}_4$ and NH_4NO_3 .

4. Source of Ions in Wet Deposition

Cations and anions in precipitation originate from a variety of sources, including oceanic spray, terrestrial dust, gaseous pollutants and volcanic emissions [Likens et al.,

1977]. Solute load in precipitation is to a large extent determined by the origin and pathway of the air masses from which the precipitation falls [Galloway et al., 1984]. Air masses that form over oceans contain diagnostic aerosols that originate from sea salts [Henriksen, 1980]. There are no known sources of terrestrial Cl^- near the ELW. If we make the reasonable assumption that most Cl^- in precipitation originates from sea salt aerosols, then Cl^- can be used to indicate the origin of some ions contained in wet deposition flux to the ELW. Ammonium and NO_3^- aerosols have a terrestrial source, and can be used to infer air masses that originate over land or mix with such air masses.

The high percentage of Cl^- in snowfall relative to Cl^- in rainfall suggests that winter air masses generally originate over the Pacific Ocean. Precipitation from frontal systems that originate over the Pacific Ocean is not contaminated by strong acids. For example, Kennedy et al. [1979] report that precipitation in the sparsely populated coastal region of the Mattole River basin of northern California had an average pH of 5.3, and average concentrations of $1.6 \mu\text{eq L}^{-1}$ of NO_3^- and $2.7 \mu\text{eq L}^{-1}$ of SO_4^{2-} . These ionic concentrations are comparable to the ionic concentrations of winter snowfall in the ELW during years of normal and above normal precipitation. Consequently the ions in winter snowfall appear to originate predominately from marine sources. Moreover relatively low concentrations of NH_4^+ in winter snowfall indicate that the oceanic frontal systems undergo only limited mixing with terrestrial air masses before depositing snowfall in the ELW.

Snowfall in years with lower than normal precipitation (1987) appears to have a different source of ions than snowfall in years of normal and above normal snowfall (1985 and 1986). Snowfall in years with lower than normal precipitation had a low ranking of Cl^- and Na^+ and a high ranking of NO_3^- and NH_4^+ , relative to snowfall in winters of normal and above normal precipitation. However the change from Gelman A/E glass fiber filters to Nuclepore may be partially responsible for the change in Na^+ concentrations. The ranking of ions in snowfall in a year of below normal precipitation was closer to the ranking of ions in rainfall than to ions in snowfall in a year of normal precipitation. A major source of ions in winter snowfall in water year 1987 was probably from air masses that originated over land, either from convective sources or from mixing of weak frontal systems with the air over the Central Valley of California, or a combination of the two.

Low Cl^- and high NH_4^+ concentrations in rain suggest that localized convective systems are the main source of ions in rainfall. Afternoon upslope air flows, induced by heating of air along the mountain slopes, have been shown to transport air masses from the San Joaquin Valley to the upper reaches of Sequoia National Park on a daily basis in the summer months [Smith et al., 1981]. Aerosol and gas phase species from the San Joaquin Valley are likely to supply a large percentage of the ions in rainfall. The agreement between NH_4^+ and NO_3^- ratios in rainfall to the ELW and in aerosols over the Central Valley of California is further evidence that the origin of ions in rainfall has a large terrigenous component.

E. Summary and Conclusions

Wet deposition was monitored from October 1984 through March 1988, at the Emerald Lake watershed in the southern Sierra Nevada. Precipitation amounts ranged from one of

the wettest years (1986) on record to one of the driest years (1987). Hydrogen and NH_4^+ each accounted for about 18% of the total ionic charge of solutes in precipitation; followed closely by NO_3^- (17%), SO_4^{2-} (14%) and Cl^- (12%). The remaining portion of ionic flux is divided among Ca^{2+} , Na^+ , K^+ and Mg^{2+} , in that order. The organic anions CH_3COO^- and HCOO^- comprise 25% of the total anionic content of wet deposition. Solute concentrations in rainfall were about 10-fold higher than in snowfall, with the exception of H^+ , which was about 2½-fold more concentrated in rain than in snow.

Snowfall was the major source of ions to the watershed from wet deposition, in years of normal or above normal precipitation, due to the high percentage of precipitation that was deposited as snow. Most of the solute flux from snowfall was stored in the seasonal snowpack, to be released during spring runoff. Dry deposition was not an important contributor of solute loading to the winter snowpack. During the year of large solute flux from rainfall (1987), 85% of the solute flux from rain was deposited during the time period of snowmelt runoff. Therefore about 90% of the annual solute flux from wet deposition entered the aquatic component of the watershed during the time period of snowmelt runoff. Most of the chemical loading to aquatic ecosystems in alpine areas of the Sierra Nevada thus occurs during the period of snowmelt runoff. Any increase in the acidity of snowfall will be stored during the winter season, to be released to the watershed at this time.

Nitrate was as important, or more important, than SO_4^{2-} as a potential acidifying anion in wet deposition to the watershed. Ammonium balanced as much as 11-fold more strong acid anions in rainfall than did H^+ . Both rainfall and snowfall would be much more acidic without a large atmospheric reservoir of NH_3 to neutralize the strong acids present in wet deposition. Any decrease in the atmospheric reservoir of NH_3 , that is not accompanied by a corresponding decrease in the strong acid anions, will cause a corresponding decrease in the pH of precipitation to alpine basins of the Sierra Nevada.

Source-receptor relationships in precipitation quality are important to the wet deposition of high-altitude watersheds in the Sierra Nevada. Ammonium was highly correlated with the sum of NO_3^- and SO_4^{2-} , for all precipitation types, in wet deposition to the ELW. Source areas for NO_3^- , SO_4^{2-} , and NH_4^+ may therefore be the same in winter snowfall, autumn snowfall, and rainfall. Principal factor analysis, applied to cloudwater chemistry in Sequoia National Park by Hoffmann et al. [1989], indicates that these three ions in cloudwater are from a single dominant source, hypothesized to be the large emissions of NH_3 characteristic of the central and southern San Joaquin Valley. Changes in the air quality of the San Joaquin Valley may directly effect the quality of precipitation in poorly-buffered watersheds of the Sierra Nevada.

TABLE 69. Detection Limits and Precision of Chemical Methods

Constituent	Units	<i>n</i>	Standard†	SD	DL	RSD
Ammonium	μM	10	DIW	0.15	0.30	---
Silica	μM	7	DIW	0.20	0.40	---
Nitrate	μeq L ⁻¹	7	0.50	0.10	0.20	1.2
Chloride	μeq L ⁻¹	7	0.50	0.19	0.38	13.4
Sulfate	μeq L ⁻¹	7	0.75	0.22	0.44	2.7
Calcium	μeq L ⁻¹	4	2.50	0.50	1.00	3.1
Magnesium	μeq L ⁻¹	4	2.06	0.16	0.32	1.0
Sodium	μeq L ⁻¹	6	1.09	0.25	0.50	3.3
Potassium	μeq L ⁻¹	6	0.64	0.22	0.45	6.2
Acetate	μeq L ⁻¹	4	1.2	0.21	0.42	3.5
Formate	μeq L ⁻¹	4	1.1	0.33	0.66	5.4

† Standard is the replicate determinations (*n*) of deionized water (DIW) or analyst prepared standards. SD is the standard deviation.

DL is the detection limit (= two SD).

RSD is the percent relative standard deviation.

TABLE 70. Charge Balance Summary for Wet Deposition

Type	Year	<i>n</i>	Σ ⁺	Σ ⁻	Σ Ions	Σ ⁺ /Σ ⁻	%IOD
Rain	1985	4	122	88	210	1.38	16%
Rain	1986	6	62.0	46.2	108	1.34	15%
Rain	1987	13	127	100	227	1.27	12%
Autumn Snow	1985	6	37.5	27.3	64.8	1.37	16%
Autumn Snow	1986	5	41.7	29.0	70.7	1.44	18%
Autumn Snow	1987	1	54.7	38.7	93.4	1.41	17%
Winter Snow	1985	29	11.9	9.3	21.2	1.28	12%
Winter Snow	1986	85	9.1	6.5	15.6	1.40	17%
Winter Snow	1987	328	12.4	8.6	21.0	1.44	18%
Winter Snow	1988	392	9.0	4.7	13.7	1.91	31%

n is the number of individual samples analyzed.

Σ⁺ is the sum of the positive inorganic ions.

Σ⁻ is the sum of the negative inorganic ions.

Σ Ions is the sum of major inorganic ions.

Σ⁺/Σ⁻ is the ratio of cations to anions.

%IOD is $\frac{\Sigma^+ - \Sigma^-}{\Sigma^+ + \Sigma^-}$ times 100.

TABLE 71. Volume-weighted Mean Ionic Concentrations ($\mu\text{eq L}^{-1}$), pH and Conductance ($\mu\text{S cm}^{-1}$) in Winter Snowfall, Water Years 1985-1988

	1985	1986	1987	1988	Mean†
pH	5.29	5.34	5.34	5.42	5.34
$\mu\text{S cm}^{-1}$	4.0	3.3	3.5	2.5	3.3
H^+	5.3	4.6	4.6	3.8	4.6
NH_4^+	0.9	1.4	3.8	1.9	1.7
Na^+	1.9	1.4	0.7	1.0	1.3
K^+	0.9	0.8	0.4	0.3	0.7
Ca^{2+}	2.2	0.6	1.8	1.5	1.3
Mg^{2+}	0.7	0.3	1.1	0.5	0.6
NO_3^-	2.3	1.8	4.2	2.1	2.3
SO_4^{2-}	3.0	1.6	2.9	1.2	2.0
Cl^-	4.0	3.1	1.5	1.4	2.8
CH_3COO^-	---	---	0.5	2.1	1.3
HCOO^-	---	---	0.3	0.6	0.4

†Mean is the volume-weighted mean for all four years.

TABLE 72. Rank of Volume-Weighted Mean Ionic Concentrations in Winter Snowfall; Water Years 1985-1988

Rank	Year			
	1985	1986	1987	1988
1	H^+	H^+	H^+	H^+
2	Cl^-	Cl^-	NO_3^-	NO_3^-
3	SO_4^{2-}	NO_3^-	NH_4^+	CH_3COO^-
4	NO_3^-	SO_4^{2-}	SO_4^{2-}	NH_4^+
5	Ca^{2+}	Na^+	Ca^{2+}	Ca^{2+}
6	Na^+	NH_4^+	Cl^-	Cl^-
7	NH_4^+	K^+	Mg^{2+}	SO_4^{2-}
8	K^+	Ca^{2+}	Na^+	Na^+
9	Mg^{2+}	Mg^{2+}	CH_3COO^-	HCOO^-
10	---	---	K^+	Mg^{2+}
11	---	---	HCOO^-	K^+

TABLE 73. Ratios of $\text{NO}_3^-/\text{SO}_4^{2-}$, H^+/Σ^- , and NH_4^+/Σ^- in Wet Deposition, by Precipitation Type

Type	Year	$\text{NO}_3^-/\text{SO}_4^{2-}$	H^+/Σ^-	NH_4^+/Σ^-
Rain	85	1.32	0.19	0.49
	86	1.21	0.06	0.68
	87	1.11	0.13	0.63
Autumn Snow	85	1.51	0.31	0.55
	86	1.47	0.26	0.74
	87	2.93	0.16	1.14
Winter Snow	85	0.77	0.57	0.10
	86	1.12	0.71	0.21
	87	1.45	0.53	0.45
	88	1.75	0.81	0.40

Σ^- is the sum of NO_3^- , SO_4^{2-} and Cl^- .

TABLE 74. Spatial Variation in the Ionic Volume-Weighted Mean Concentrations ($\mu\text{eq L}^{-1}$) of the Snowpack at Maximum Snow Accumulation ($n = 6$), Water Years 1987 and 1988

	1987					1988				
	\bar{X}	SD	SE	CI	RSD	\bar{X}	SD	SE	CI	RSD
μS	3.5	0.4	0.2	0.4	11	2.5	0.3	0.1	0.3	12
H^+	4.6	1.0	0.4	1.0	20	3.8	0.2	0.1	0.2	6
NH_4^+	3.8	1.2	0.5	1.2	30	1.9	0.5	0.2	0.5	26
Ca^{2+}	1.8	0.4	0.2	0.4	21	1.5	0.3	0.1	0.3	20
Mg^{2+}	1.1	0.1	<0.1	0.1	7	0.5	0.1	<0.1	0.1	20
Na^+	0.7	0.4	0.1	0.4	51	1.0	0.4	0.2	0.4	40
K^+	0.4	0.1	0.1	0.1	34	0.3	0.2	0.1	0.2	67
NO_3^-	4.2	0.7	0.3	0.7	17	2.1	0.4	0.2	0.4	19
SO_4^{2-}	2.9	0.4	0.2	0.4	13	1.2	0.3	0.1	0.3	25
Cl^-	1.5	0.4	0.2	0.4	25	1.4	0.5	0.2	0.5	36
CH_3COO^-	0.5	0.7	0.3	0.7	133	2.1	0.4	0.2	0.4	19
HCOO^-	0.3	0.4	0.2	0.4	147	0.6	0.2	0.1	0.2	33

\bar{X} is the volume-weighted mean concentration.

SD is the arithmetic standard deviation.

SE is the standard error.

CI is the width of the 95% confidence interval.

RSD is the relative standard deviation.

TABLE 75. Ionic Loading (eq ha^{-1}) of the Basin's Snowpack at Maximum Snow Accumulation, Water Years 1985-1988

	H^+	NH_4^+	Ca^{2+}	NO_3^-	SO_4^{2-}	Cl^-
1985	53	9	23	23	31	41
1986	95	49	18	50	41	63
1987	31	25	11	28	19	10
SE	3	3	1	2	1	1
CI	5	6	2	4	2	2
1988	24	12	9	13	8	9
SE	1	1	1	1	1	1
CI	2	3	2	2	2	3

SE is the standard error.

CI is the width of the 95% confidence interval.

TABLE 76. Volume-Weighted Mean Ionic Concentrations ($\mu\text{eq L}^{-1}$), pH, and Conductance ($\mu\text{S cm}^{-1}$), in Rainfall and Autumn Snowfall, Water Years 1985-1987

	Rain				Autumn-Snow			
	1985	1986	1987	Mean†	1985	1986	1987	Mean
pH	4.93	4.87	4.88	4.88	5.07	5.11	5.21	5.10
$\mu\text{S cm}^{-1}$	19.1	13.0	19.3	18.3	6.8	8.0	9.1	7.7
H^+	16.7	10.7	13.1	13.0	8.3	7.4	6.2	8.0
NH_4^+	42.8	23.4	63.0	55.3	15.1	21.8	44.4	20.8
Na^+	18.1	5.0	17.2	15.4	5.5	3.0	1.3	3.7
K^+	5.6	2.0	3.7	3.8	1.2	1.4	0.5	1.5
Ca^{2+}	34.1	17.9	24.4	24.0	6.2	7.0	1.5	6.7
Mg^{2+}	4.7	3.1	5.3	4.8	1.3	1.1	0.8	1.2
NO_3^-	40.4	22.2	48.2	42.8	11.8	14.7	25.5	14.4
SO_4^{2-}	30.6	18.3	43.4	38.5	7.8	10.0	8.7	9.2
Cl^-	17.1	5.6	8.9	9.1	7.6	4.3	4.5	5.2
\sum Ions	210	108	227	206	64.8	70.7	93.4	70.6

† Volume-weighted mean for the three water years.

TABLE 77. Percent Flux of Ions and Water, by Precipitation Type, Water Years 1985-1987

	Rain			Autumn-Snow			Winter-Snow		
	1985	1986	1987	1985	1986	1987	1985	1986	1987
SWE	1	1	17	8	8	2	91	91	81
H ⁺	4	3	36	12	12	2	84	85	62
NH ₄ ⁺	24	9	72	46	53	6	30	38	21
Na ⁺	10	4	83	19	15	1	71	81	17
K ⁺	8	3	64	10	13	1	82	84	35
Ca ²⁺	16	17	73	17	43	1	67	41	27
Mg ²⁺	8	10	49	13	22	1	79	68	50
NO ₃ ⁻	15	9	67	27	38	4	58	53	29
SO ₄ ²⁻	11	9	74	17	33	2	72	58	24
Cl ⁻	5	2	53	14	11	3	81	87	44
Σ Ions	11	6	66	19	27	4	70	67	30

TABLE 78. Volume-Weighted Mean Concentrations and Average Loading of Ions in Annual Wet Deposition, Water Years 1985 through 1987

	Vol. Wt Mean (μeq L ⁻¹)				Loading (eq ha ⁻¹)			
	1985	1986	1987	Mean*	1985	1986	1987	Avg†
SWE (mm)	---	---	---	---	1157	2625	959	1580
pH	5.24	5.31	5.22	5.27	---	---	---	---
μS	4.4	3.8	6.2	4.5	---	---	---	---
H ⁺	5.8	4.9	6.0	5.3	67	128	58	84
NH ₄ ⁺	2.6	3.3	14.4	5.4	30	87	138	85
Ca ²⁺	2.9	1.3	5.6	2.6	34	35	54	41
Mg ²⁺	0.8	0.4	1.9	0.8	9	10	18	12
Na ⁺	2.4	1.6	3.5	2.2	28	41	34	34
K ⁺	1.0	0.9	1.0	0.9	11	23	10	15
NO ₃ ⁻	3.5	3.1	11.9	5.0	41	81	114	79
SO ₄ ²⁻	3.7	2.5	9.8	4.3	43	65	94	67
Cl ⁻	4.5	3.2	2.8	3.5	52	85	27	55
Σ Ions	27.2	21.1	56.9	30.0	315	555	547	472

* Volume-weighted mean ionic concentration; † arithmetic average ionic loading.

TABLE 79. Snow Chemistry of Emerald Lake Watershed ($\mu\text{eq L}^{-1}$) Compared to Other Locations

location	pH	Ca ²⁺	NO ₃ ⁻	SO ₄ ²⁻	Reference
EML	5.3	2.0	2.0	2.0	Vol-wt Mean, 1985-1988
Western North America					
Cascades	5.6	3.0	0.5	2.0	Laird et al., 1986
British Columbia	5.4	2.2	2.4	4.0	McBean and Nikleva, 1986
Colorado	5.3	14.0	10.0	10.0	Michaels et al., 1987
Eastern North America and Northern Europe					
Ontario	4.0	15	70	50	Schemenauer et al., 1985
Scotland	4.0	10	60	70	Brimblecombe et al., 1985
Norway	4.5	25	30	60	Johannessen and Henriksen, 1978

Figure 30. Wet Deposition Sampling Sites

Topographic map of the Emerald Lake watershed, and wet deposition sampling sites. Sampling sites are as follows: 1 tower, 2 inlet, 3 bench, 4 ridge, 5 ramp, 6 pond, 7 hole, 8 cirque.

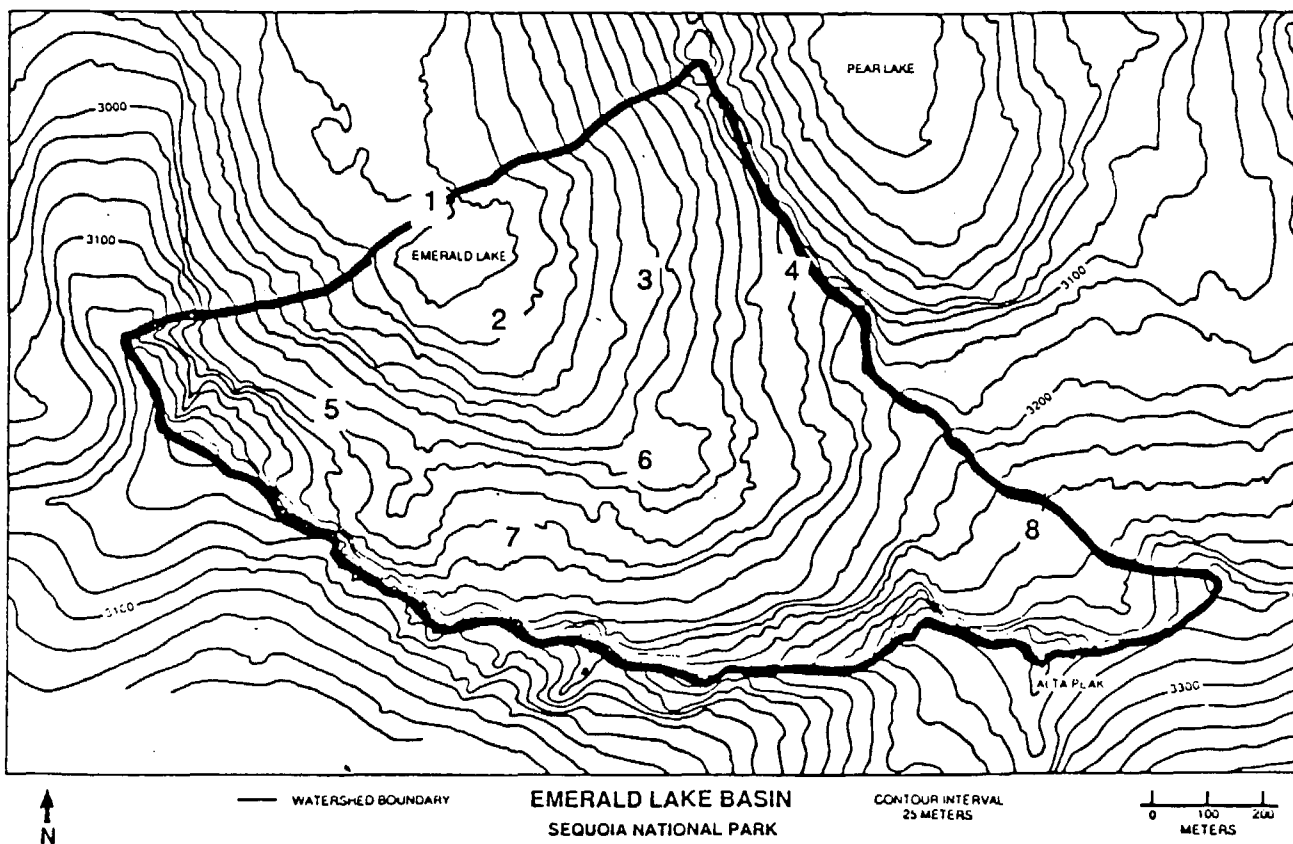
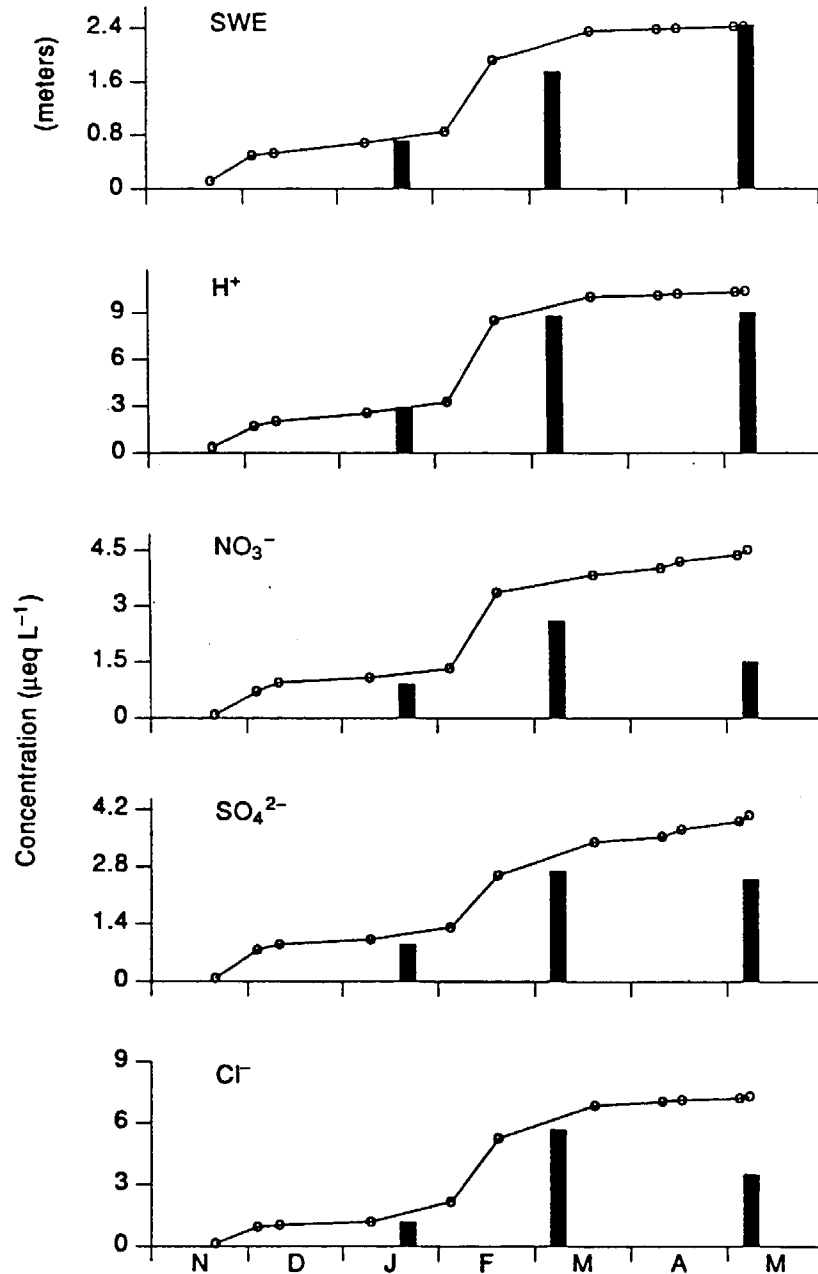


Figure 32. Comparison of Cumulative Snowfall Loading to Snowpack Loading

Comparison of cumulative snowfall loading (lines) to snowpack loading (bar graphs) in 1986 at the inlet, for SWE, H⁺ and the strong acid anions. Snow water equivalence, H⁺, SO₄²⁻, and Cl⁻ had good agreement between cumulative snowfall loading and snowpit loading, prior to the initiation of snowmelt runoff in April. Nitrate loading in the snowpack was about 20% lower than in snowfall.



F. References

- Anlauf, K. G., J. W. Bottenheim, K. A. Brice, and H. A. Wiebe, A comparison of summer and winter measurements of atmospheric nitrogen and sulfur compounds, *Water, Air Soil Poll.*, 30, 153-160, 1986.
- Bales, R. C. and R. E. Davis, and D. A. Stanley, Ion elution through shallow homogeneous snow, *Water Resour. Res.*, 25, 1869-1878, 1989.
- Bales, R. C., M. P. Valdez, G. A. Dawson, and D. A. Stanley, Physical and chemical factors controlling gaseous deposition of SO₂ to snow, in *Seasonal Snowcovers: Physics, Chemistry, Hydrology*, edited by H. G. Jones and W. J. Orville-Thomas, NATO ASI Ser. C: Vol 211, pp. 289-297, D. Reidel Publishing Company, Boston, 1987.
- Barrett, E. and G. Brodin, The acidity of Scandinavian precipitation, *Tellus*, 7, 251-257, 1955.
- Barrie, L. A., K. G. Anlauf, H. A. Wiebe, and P. Fellin, Acidic pollutants in air and precipitation at selected rural locations in Canada, *Proceedings of the American Chemical Society Symposium on Acid Rain, Las Vegas, NV*, Ann Arbor Science, Ann Arbor, MI, 1983.
- Barrie, L. A., D. Fisher, and R. M. Koerner, Twentieth century trends in Arctic air pollution revealed by conductivity and acidity observations in snow and ice in the Canadian High Arctic, *Atmos. Environ.*, 19, 2055-2063, 1985.
- Barrie, L. A. and R. J. Vet, The concentration and deposition of acidity, major ions and trace metals in the snowpack of the Eastern Canadian Shield during the winter of 1980-1981, *Atmos. Environ.*, 18, 1459-1469, 1984.
- Barrie, L. A. and J. L. Walmsley, A study of sulfur dioxide deposition velocities to snow in Northern Canada, *Atmos. Environ.*, 12, 2321-2332, 1978.
- Barry, P. J. and A. G. Price, Short-term changes in the fluxes of water and of dissolved solutes during snow-melt, in *Seasonal Snowcovers: Physics, Chemistry, Hydrology*, edited by H. G. Jones and W. J. Orville-Thomas, NATO ASI Ser. C: Vol 211, pp. 501-531, D. Reidel Publishing Company, Boston, 1987.
- Bevington, P. R., *Data Reduction and Error Analysis for the Physical Sciences*, McGraw-Hill, San Francisco, 1969.
- Blanchard, C., K. Tonnessen, and L. Ashbaugh, Acidic deposition in California forests: precipitation chemistry measurements from the California Acid Deposition Monitoring Program, *82nd Annual Air and Waste Management Association Meeting, Anaheim CA, June 19-23*, 1989.
- Borys, R. D., P. J. DeMott, E. E. Hindman, and D. Feng, The significance of snow crystal and mountain-surface riming to the removal of atmospheric trace constituents from cold clouds, in *Precipitation Scavenging, Dry Deposition, and Resuspension*, edited by H. R. Pruppacher, R. G. Semonin and W. G. N. Slinn, pp. 181-189, Elsevier Science Publishing

- Co., New York, 1983.
- Brimblecombe, P., M. Tranter, P. W. Abrahams, I. Blackwood, T. D. Davies, and C. E. Vincent, Relocation and preferential elution of acidic solute through the snowpack of a small, remote high-altitude Scottish catchment, *Ann. Glaciol.*, 7, 141-147, 1985.
- Brown, J. C. and C. M. Skau, Chemical composition of snow in the east central Sierra Nevada, *Cooperative Rep.*, University of Nevada, Natural Resources Division, Reno, 1975.
- Cadle, S. H., J. M. Dasch, and N. E. Grossnickle, Northern Michigan snowpack – a study of acid stability and release, *Atmos. Environ.*, 18, 807-816, 1984.
- Cadle, S. H., J. M. Dasch, and P. A. Mulawa, Atmospheric concentrations and the deposition velocity to snow of nitric acid, sulfur dioxide and various particulate species, *Atmos. Environ.*, 19, 1819-1827, 1985.
- California Air Resources Board, *Emission inventory-1979*, Calif. Air Resour. Board, Sacramento, CA, 1979.
- California Air Resources Board, Examination of the relationship between ammonium and nitrate ions from PM_{10} samplers in California, *Quarterly Air Quality Data Rep.*, 5 pp., Sacramento, 1988.
- California Cooperative Snow Surveys, *Bulletin 120 Series*, Calif. Dept. Water. Resour., Sacramento, 1930-1989.
- Chan, W. H. and D. H. S. Chung, Regional-scale precipitation scavenging of SO_2 , SO_4 , NO_3 , and HNO_3 , *Atmos. Environ.*, 20, 1397-1402, 1986.
- Chan, W. H., A. J. S. Tang, D. H. S. Chung, and N. W. Reid, An analysis of precipitation chemistry measurements in Ontario, *Environ. Sci. Technol.*, 21, 1219-1224, 1987.
- Chang, T. Y., Rain and snow scavenging of HNO_3 vapor in the atmosphere, *Atmos. Environ.*, 18, 191-197, 1984.
- Charlson, R. J. and H. Rodhe, Factors controlling the acidity of natural rainwater, *Nature*, 295, 683-685, 1982.
- Davidson, C. I., R. E. Honrath, J. B. Kadane, R. S. Tsay, P. A. Mayewski, W. B. Lyons, and N. Z. Heidam, The scavenging of atmospheric sulfate by Arctic snow, *Atmos. Environ.*, 21, 871-882, 1987.
- Dennis, A. S., *Weather Modification by Cloud Seeding*, Academic Press, New York, 1980.
- Dovland, H. and A. Eliassen, Dry deposition on a snow surface, *Atmos. Environ.*, 10, 783-785, 1976.
- Dozier, J., J. M. Melack, D. Marks, K. Elder, R. Kattelmann, and M. Williams, Snow deposition, melt, runoff and chemistry in a small alpine watershed, Emerald Lake Basin, Sequoia National Park, *Final Rep., Contr. A3-103-32*, Calif. Air Resour. Board, Sacramento, CA, 1987.

- Driscoll, C. T., N. M. Johnson, G. E. Likens, and M. C. Feller, Effects of acidic deposition on the chemistry of headwater streams: a comparison between Hubbard Brook, New Hampshire and Jamieson Creek, British Columbia, *Water Resour. Res.*, *24*, 195-200, 1988.
- Elder, K., J. Dozier, and J. Michaelsen, Spatial and temporal variation of net snow accumulation in a small alpine watershed, Emerald Lake basin, Sierra Nevada, California, U.S.A., *Ann. Glaciol.*, *13*, 56-63, 1989.
- Feth, J. H., S. M. Rogers, and G. E. Roberson, Chemical composition of snow in the northern Sierra Nevada and other areas, *Geological Survey Water-Supply Pap. 1535J*, U.S. Government Printing Office, Washington, DC, 1964.
- Frantisak, F., G. H. Pelletier, M. Bedard, and G. Castonguay, Precipitation quality in northwest Quebec, Canada, *73rd Annual Meeting, Air Pollution Control Association, APCA*, Pittsburgh, 1980.
- Galloway, J. N. and A. Gaudry, The composition of precipitation on Amsterdam Island, Indian Ocean, *Atmos. Environ.*, *18*, 2649-2656, 1984.
- Galloway, J. N., G. R. Hendrey, C. L. Schofield, N. E. Peters, and A. H. Johannes, Processes and causes of lake acidification during spring snowmelt in the west-central Adirondack Mountains, New York, *Can. J. Fish. Aquat. Sci.*, *44*, 1595-1602, 1987.
- Galloway, J. N., G. E. Likens, and M. E. Hawley, Acid precipitation: Natural versus anthropogenic components, *Science*, *226*, 829-831, 1984.
- Galvin, P. J. and J. A. Cline, Measurement of anions in the snowcover of the Adirondack Mountains, *Atmos. Environ.*, *12*, 1163-1167, 1978. Galvin, P. J. and J. A. Cline, Measurement of anions in the snowcover of the Adirondack Mountains, *Atmos. Environ.*, *17*, 191-192, 1983.
- Henriksen, A., Acidification of fresh waters-a large scale titration, in *Proceedings of the International Conference on Ecological Impact of Acid Precipitation*, edited by D. Drablos and A. Tollan, SNSF project, pp. 68-74, 1980.
- Hoffmann, M. R., J. L. Collett, Jr., and B. C. Daube, Jr., Characterization of cloud chemistry and frequency of canopy exposure to clouds in the Sierra Nevada mountains, *Final Rep., Contr. A6-185-32*, 319 pp., Calif. Air Resour. Board, Sacramento, 1989.
- Huebert, B. J., F. C. Fehsenfeld, R. B. Norton, and D. Albritton, The scavenging of nitric acid vapor by snow, in *Precipitation Scavenging, Dry Deposition, and Resuspension*, edited by H. R. Pruppacher, R. G. Semonin and W. G. N. Slinn, vol. 1, Elsevier Science Publishing Co., New York, 1983.
- Jacob, D. J. and S. C. Wofsy, Photochemical production of carboxylic acids in a clean continental atmosphere, in *Acid Deposition at High Elevation Sites*, edited by M. H. Unsworth and D. Fowler, NATO ASI Ser. C: Vol 252, pp. 73-92, Kluwer Academic Publications, Dordrecht, 1988.

- Jeffries, D. S. and W. R. Snyder, Variations in the chemical composition of the snowpack and associated waters in central Ontario, in *Proceedings of the 38th Eastern Snow Conference*, edited by B. E. Goodwin, pp. 11-22, 1981.
- Johannessen, M. and A. Henriksen, Chemistry of snow meltwater: changes in concentration during melting, *Water Resour. Res.*, 14, 615-619, 1978.
- Jones, H. G. and C. Laberge, Nitrate losses from snow strata in snowpacks under cold (<0°C) conditions, *Eos Transactions AGU*, 69, 1202, 1988.
- Keene, W. C. and J. N. Galloway, Organic acidity in precipitation of North America, *Atmos. Environ.*, 18, 2491-2497, 1984.
- Keene, W. C., J. N. Galloway, and J. D. Holden, Jr., Measurement of weak organic acidity in precipitation from remote areas of the world, *J. Geophys. Res.*, 88, 5122-5130, 1983.
- Kennedy, V. C., G. W. Zellweger, and R. J. Avanzino, Variation of rain chemistry during storms at two sites in northern California, *Water Resour. Res.*, 15, 687-702, 1979.
- Kumar, S., Reactive scavenging of pollutants by rain: a modeling approach, *Atmos. Environ.*, 20, 1015-1024, 1986.
- Laird, L. B., H. E. Taylor, and V. C. Kennedy, Snow chemistry of the Cascade-Sierra Nevada Mountains, *Environ. Sci. Technol.*, 20, 275-290, 1986.
- Lawson, D. R. and J. G. Wendt, Acid deposition in California, *SAE Tech. Pap. 821246*, 1981.
- Likens, G.E., F.H. Bormann, R.S. Pierce, J.S. Eaton, and N.M. Johnson, *Biogeochemistry of a Forested Ecosystem*, Springer-Verlag, New York, 1977.
- Liljestrand, H. M. and J. J. Morgan, Chemical source, equilibrium and kinetic models of acid precipitation in southern California, in *Energy and Environmental Chemistry: Acid Rain*, edited by L. H. Keith, pp. 103-122, Ann Arbor Science Publishers, Ann Arbor, Michigan, 1980.
- Mason, B. J., *Clouds, Rain and Rainmaking, Second Edition*, Cambridge University Press, New York, 1975.
- McBean, G. A. and S. Nikleva, Composition of snow in Pacific coastal mountains, *Atmos. Environ.*, 20, 1161-1164, 1986.
- McCull, J. G., A survey of acid precipitation in northern California, *Agricultural Experiment Station Rep. CA-B-SPN-3364-H*, Univ. Calif., Berkeley, CA, 1980.
- McCull, J. G., L. K. Monette, and D. S. Bush, Chemical characteristics of wet and dry atmospheric fallout in northern California, *J. Envir. Quality*, 11, 585-590, 1982.
- Melack, J. M., S. D. Cooper, R. W. Holmes, J. O. Sickman, K. Kratz, P. Hopkins, H. Hardenbergh, M. Thieme, and L. Meeker, Chemical and biological survey of lakes and streams located in the Emerald Lake watershed, Sequoia National Park, *Final Rep., Contr. A3-096-32*, Calif. Air Resour. Board, Sacramento, 1987.

- Melack, J. M., J. L. Stoddard, and D. R. Dawson, Acid precipitation and buffer capacity of lakes in the Sierra Nevada, California, in *Proceedings of the International Symposium on Hydrometeorology*, edited by A. I. Johnson and R. A. Clarke, pp. 465-471, Amer. Water Resour. Assoc., Bethesda, MD, 1982.
- Michaels, H. A., A. Bradman, C. L. Blanchard, and J. Harte, Investigation of snow pack chemistry on the western slope of the Colorado Rockies, *Rep. No. ERG-87-1*, Energy and Resources Group, University of California, Berkeley, 1987.
- Mitchell, D. L., The dependence of chemical deposition in the central Sierra on cloud droplet removal during snow storms, in *Mountain Watersheds*, edited by Poppoff, L., L. Leopold, C. Goldman and S. Loeb, Univ. Calif. Press, Berkeley, in press.
- Morgan, J. J. and N. M. Liljestrang, Measurement and interpretation of acid rainfall in the Los Angeles basin, *Final Rep.*, Calif. Air Resour. Board, Sacramento, 1980.
- Munger, J. W. and S. J. Eisenreich, Continental-scale variations in precipitation chemistry, *Environ. Sci. Technol.*, 17, 32A-42A, 1982.
- Peden, M. E., Sampling, analytical, and quality assurance protocols for the National Atmospheric Deposition Program, in *Sampling and Analysis of Rain*, edited by S. A. Campbell, pp. 72-83, ASTM, 1916 Race Str., Philadelphia, PA, 1983.
- Richards, T. L., Physics and chemistry of snowfall and snow distribution, in *The Role of Snow and Ice in Hydrology*, edited by J. C. Rodda, IAHS-AIHS Publ. No. 107, pp. 1-13, Intl. Assoc. Hydrol. Sci., Wallingford, UK, 1973.
- Rowe, R. D. and L. G. Chestnut, Economic assessment of the effects of air pollution on agricultural crops in the San Joaquin Valley, *J. Air Pollut. Control Ass.*, 35, 728-734, 1985.
- Schemenauer, R. S., M. O. Berry, and J. B. Maxwell, Snowfall formation, in *Handbook of Snow*, edited by D. M. Gray and D. H. Male, pp. 129-151, Pergamon Press, New York, 1981.
- Schemenauer, R. S., P. W. Summers, H. A. Wiebe, and K. G. Anlauf, Spatial and temporal variability of surface snowfall and snowpack chemistry in central Ontario, *Ann. Glaciol.*, 7, 185-190, 1985.
- Sickman, J. O. and J. M. Melack, Characterization of year-round sensitivity of California's montane lakes to acidic deposition, *Final Rep., Contr. A5-203-32*, Calif. Air Resour. Board, Sacramento, 1989.
- Smith, T. B., D. E. Lehrman, D. D. Reible, and F. H. Shair, The origin and fate of airborne pollutants within the San Joaquin Valley, *Final Rep.*, Calif. Air Resour. Board, Sacramento, 1981.
- Stoddard, J. L., Alkalinity dynamics in an unacidified alpine lake, Sierra Nevada, California, *Limnol. Oceanogr.*, 32, 825-839, 1987.

- Stohlgren, T. J. and D. J. Parsons, Variation of wet deposition chemistry in Sequoia National Park, California, *Atmos. Environ.*, *21*, 1369-1374, 1987.
- Strickland, J. D. and T. R. Parsons, A practical handbook of seawater analysis, *Bulletin of Fisheries Research Board Canada*, *167*, 83, 1972.
- Talbot, R. W., K. M. Beecher, R. C. Harriss, and W. R. Cofer, III, Atmospheric geochemistry of formic and acetic acids at a mid-latitude temperate site, *J. Geophys. Res.*, *93*, 1638-1652, 1988.
- Topol, L. E., Differences in ionic composition and behavior in winter rain and snow, *Atmos. Environ.*, *20*, 347-355, 1986.
- Tranter, M., T. D. Davies, P. W. Abrahams, I. Blackwood, P. Brimblecombe, and C. E. Vincent, Spatial variability in the chemical composition of snowcover in a small, remote, Scottish catchment, *Atmos. Environ.*, *21*, 853-862, 1987.
- Welch, E. B., W. H. Chamberlain, and D. E. Spyidak, Chemical content of snow and effect of melting on Cascade mountain lakes, *Northwest Science*, *58*, 85-93, 1984.
- Whelpdale, D. M. and R. W. Shaw, Sulfur dioxide removal by turbulent transfer over grass, snow and water surfaces, *Tellus*, *26*, 196-204, 1974.
- Wolff, G. T., On the nature of nitrate in coarse continental aerosols, *Atmos. Environ.*, *18*, 977-981, 1984.

IX. SOLUTE CHEMISTRY OF SNOWMELT AND RUNOFF

A. Introduction

The understanding of snowpack contributions to the chemistry of surface waters in alpine basins is complicated by the rugged and variable terrain. Large topographic differences over short distances result in spatial and temporal variation in the amount of snow and the onset of snowmelt within a given watershed [Williams and Melack, 1989]. The onset and rate of snowmelt at a particular location in the basin is a function of the interactions of aspect, elevation, slope and meteorological parameters [Elder et al., 1989]. Spatial and temporal differences in the onset of melt within a basin produce a snowpack with variable chemistry.

Numerous field and laboratory experiments have demonstrated that initial stages of melt often have ionic concentrations many times higher than averages for the whole snowpack [Johannessen and Henriksen, 1978; Colbeck, 1981; Suzuki, 1982; Cadle et al., 1984; Stein et al., 1986; Rascher et al., 1987]. As a result of snow metamorphism, ionic concentrations in the initial melt are often 6-12 times higher than the average concentration of the snowpack. Meltwater that is ionically more concentrated than bulk snowpack concentrations for a short period of time is generally termed an ionic pulse. Acidification of lake and stream waters during spring snowmelt has been reported in the United States (*e.g.* in New York by Galloway et al., [1987] and in Michigan by Cadle et al. [1984]), in Canada [Jeffries et al., 1979], in Norway [Skartveit and Gjessing, 1979], and in Sweden [Dickson, 1980]. The differential release of ionic solutes in the first fractions of snowmelt runoff is often attributed to be the main cause of the acidification.

Lakes in the Sierra Nevada have the lowest ionic concentrations in the United States [Landers et al., 1987], and watersheds in the Sierra Nevada have a limited capacity to neutralize acids [Melack et al., 1985; Sickman and Melack, 1989]. Snowfall in the Sierra Nevada is characterized by very low solute concentrations, generally less than $5 \mu\text{eq L}^{-1}$ for each ion [Laird et al., 1986; Chapter VIII]. An outstanding question is the effect of snowmelt runoff, from the dilute snowpack, on the hydrochemistry of high-altitude stream and lake waters in the Sierra Nevada.

In this chapter we report snowpack runoff contributions to the hydrochemistry of a headwater alpine watershed in the Sierra Nevada, in 1986 and 1987. The major inorganic ions, conductance, acid neutralizing capacity, and silica were measured in the snowpack and in melt water at three sites, and in all streams, at approximately weekly intervals through the snowmelt season in 1987. Less frequent sampling occurred in 1986. We determine if the chemically dilute snowpack in the Emerald Lake watershed (ELW) of the southern Sierra Nevada produces an ionic pulse, and quantify what effect snowmelt runoff has on the chemistry of surface waters. Spatial and temporal variations in the chemistry of snowmelt runoff, and their effect on surface water chemistry, is also investigated. Analysis of melt water and stream water chemistry allows us to evaluate the role of geochemical interactions in modifying the chemistry of snowmelt runoff in this alpine watershed, and also provides the opportunity to assess the susceptibility of this basin to present and future acidic deposition.

B. Methods

1. Sample Collection

Integrated samples of the entire snowpack were obtained by digging pits to the ground and collecting duplicate, contiguous, vertical cores in increments of about 40 cm. The snow five to ten cm above the ground was not sampled to eliminate the possibility of contamination from soils or overland flow. The snow cores were transferred into polyethylene bags, and kept frozen while in transit to our laboratory. Snow water equivalence (SWE) measurements were made using a 1 L stainless steel cutter [Chapter III]. Temperature of the snowpack was measured every 10 cm with Keithley digital thermometers, calibrated to $\pm 0.2^\circ\text{C}$. Snowpits in 1986 were located at the inlet and ridge; snowpits in 1987 were located at the bench, cirque, hole, inlet, pond and ramp (Figure 33). Snowpit locations in 1987 were selected to represent the major elevational, slope and radiation classes of the watershed, using the selection criteria described in Chapter III.

The enhancement of ionic concentrations in melt water were assessed using two different techniques. The ratio of the ionic concentration of melt water to the snowpack was calculated indirectly in 1986 from losses of the ionic loads and SWE in snow cover during snowmelt. Meltwater draining from the snowpack in 1987 was collected in lysimeters before contact with the ground. Locations of melt water sites in 1987 were the same as snowpit sites: the bench, cirque, hole, inlet, pond and ramp.

We collected melt water samples in an open, acid-washed, polyethylene container with dimensions of 10×10×50-cm, a surface area of 0.05 m and a volume of 5 liters. The lysimeter was placed in a 20-cm tall snowcave excavated at the bottom of the snowpack, on a thin (usually less than 5-cm thick) ice crust. Sample containers were situated so as to prevent surface runoff from flowing into the containers. The top of the snowcave was carved so as to direct melt water draining from the snowpack into the container. The snowcave and then the snowpit was refilled with snow; each snowcave was then reexcavated to collect samples, and refilled after sample collection. The sampling interval was approximately weekly; on occasion samples were collected more frequently. We attempted to begin melt water collection at the initiation of melt water runoff in each site, and continue collecting melt water until snow no longer remained at the site. Meltwater samples were collected continuously from the initiation of snowmelt through the melt season at only three sites, the inlet, bench, and cirque.

Solutes in rain were collected with a wet-only Aerochem Metrics model 301 sampler, located at the inlet. Sampling sites for water chemistry were located immediately above the lake for all inflows, and immediately below the lake for the outflow (Figure 33). Water samples were collected at about weekly intervals during snowmelt runoff and at intervals of four to six weeks from November through March, in acid-washed, linear polyethylene bottles that were copiously rinsed with deionized water, and then rinsed again with sample water.

2. Sample Storage and Analysis

Snow samples were stored frozen (-20°C) for three to nine months until analysis. Snow samples were placed in covered polyethylene buckets and melted at room temperature in

1986 and at 4°C in 1987. Subsamples were filtered through pre-rinsed, 47 mm filters with ca. 1 µm pore size (Gelman A/E glass fiber in 1985, 1986 and the first part of 1987; Nuclepore filters in the remainder of 1987). Conductance and pH were immediately measured on unfiltered samples, and NH_4^+ and PO_4^{3-} on filtered samples. Filtered samples were stored in the dark at 4°C for subsequent cation and anion analyses. Meltwater and stream water samples were subsampled in the field into unfiltered and filtered (Gelman A/E glass fiber, pre-rinsed with a minimum of 300 mls, 47 mm, 1.0 µm pore size) aliquots. Conductance and pH were analyzed on unfiltered samples, NH_4^+ and PO_4^{3-} were analyzed on filtered samples, all within 24-hours to seven days; additionally acid neutralizing capacity (ANC) was analyzed on unfiltered stream water samples using the Gran titration method. Filtered samples were then stored in the dark at 4°C for subsequent cation, anion and silica analyses.

The pH measurements were made with combination electrodes suitable for use in dilute waters (Sargent Welch S-30072-15 or Ross 8104) and a Fisher Acumet 805 pH meter. For each series of measurements the electrode was calibrated with pH 7.00 and pH 4.00 reference buffers and washed twice for 3 minutes with stirred deionized water. The electrode was rinsed with an aliquot of sample, and the temperature compensated pH determination made on a fresh, quiescent sample after five minutes. Conductance was measured with a Yellow Springs Instruments Model 32 meter and glass electrode with a 0.1 cell constant. Simultaneous temperature measurements were made, and conductivity was standardized to 25°C using a coefficient of 2% per °C. The conductivity cell was calibrated with dilute solutions of KCl.

Ammonium and phosphate were determined spectrophotometrically by the indophenol-blue and molybdenum-blue methods [Strickland and Parsons, 1972]. Calcium, magnesium, sodium, and potassium were analyzed with a Varian AA6 atomic absorption spectrophotometer. An air-acetylene flame was used; addition of lanthanum chloride suppressed chemical and ionization interferences during calcium and magnesium determinations. Especially dilute samples were also analyzed with a graphite furnace and manual 20 µL injections. Chloride, nitrate, and sulfate were measured by ion chromatography (Dionex Model 2010i) employing chemical ion suppression and conductivity detection.

Our program for quality assurance and quality control incorporated the following features. A standard protocol was followed for sample collection, processing, and analysis. At least duplicate samples were obtained and analyzed in most cases. Care was taken to avoid touching any surface that was to contact the sample. Filter blanks were done with varying amounts of rinse water. Results were scrutinized for any evidence of contamination (e.g. high Na^+ and Cl^- in one sample of a duplicate set) and deleted if clearly in error. Freshly prepared calibration standards and reagent blanks were used in every array.

Precision of analytical results was assessed as percent relative standard deviation (RSD, the percent ratio of the standard deviation to the mean) of the means of duplicated samples to which known additions were made. Duplicate samples were separated by 10-15 samples in each run. Analytical precisions generally had RSD less than 3%, with the exception of

K^+ (6.2%) and Cl^- (13.4%) in snow and melt water, and H^+ (9.8%) and NH_4^+ (15.0%) in stream water. Detection limits of all solutes was less than $0.5 \mu eq L^{-1}$, except for Ca^{2+} , which was $1.0 \mu eq L^{-1}$.

Analytical accuracy was assessed as the degree of conformity of values obtained to an accepted true value. Certified controls were included in each analytical run. A synthetic charge balance control was incorporated into analytical runs of cations and anions. Overall agreement of measured values of cations and anions with NBS certified controls warranted no corrections. Our charge balance control demonstrated there was no bias in our analytical performance.

C. Results

Water year 1986 and 1987 differed in several important ways. The peak accumulation of snow for the 1986 water year was 2000 mm SWE, about twice the 50-year mean, and peak accumulation for 1987 was 670 mm, about half the 50-year mean [Chapter III]. Mean depth of snow over the basin at maximum accumulation was 384 cm in 1986 and 140 cm in 1987. The snow covered area of the watershed was about 95% on May 15 1986, and 55% on the same date in 1987. Snow deposition in the two water years effectively bracketed the snow conditions in the Sierra Nevada over the last fifty years. The volume-weighted mean ionic concentrations of each ion, for all snowpits on all dates, never exceeded $5.0 \mu eq L^{-1}$. The 1986 winter was relatively mild, with snow temperatures generally above $-5^\circ C$; the ground and soils did not freeze. The winter of 1987 was relatively cold, with snow temperatures often below $-5^\circ C$, and extensive freezing of the ground and soils. Sheets of anchor ice in streams were common in 1987. Ice cover on Emerald Lake was about 6 m in 1986, and persisted into late July. Ice cover was only 1 meter thick in 1987, and was gone by early May.

1. Snowpack Meltwater

Anions were concentrated in melt water at the ridge in 1986. Snowpits sampled on April 14 and May 23 indicate a 4-fold increase in NO_3^- , a 2½-fold increase in SO_4^{2-} , and a 3.4-fold increase of Cl^- in snowpack melt water. There was no enhanced loss of H^+ . These numbers are the average enhancement of these ions in melt water over a 6-week period. Meltwater at shorter time periods may have had larger ionic concentrations. The inlet showed a slight enhancement in melt water of NO_3^- (1.7-fold) and SO_4^{2-} (2.3-fold), and no enhancement of H^+ and Cl^- . However samples were collected at the inlet from May 5 to May 23, several weeks after snowmelt runoff had started. Wet deposition during the period of snowmelt runoff in 1986 added less than 1% of the amount of ions and water stored in the snowpack.

All the major inorganic ions were concentrated in melt water relative to bulk snowpack concentrations in 1987, with the notable exception of H^+ . Ionic concentrations in melt water were generally highest on the first or second sampling date, and then decreased with time. This is illustrated in Figures 34, 35, and 36, which are a time series of ionic concentrations in the snowpack and melt water at the bench, inlet and cirque. Ionic concentrations in melt water increased noticeably after rainfalls, which began on April 27, 1987. Silica and PO_4^{3-} concentrations in melt water were generally near detection limits,

and always less than $1 \mu\text{M}$ and $1 \mu\text{eq L}^{-1}$, respectively.

Of the three sites sampled for melt water at the initiation of runoff, the bench had the lowest concentrations of ions in the first fraction of melt water. Nitrate concentration in melt water was $9.2 \mu\text{eq L}^{-1}$, SO_4^{2-} was $6.2 \mu\text{eq L}^{-1}$, Cl^- was $2.5 \mu\text{eq L}^{-1}$, and Ca^{2+} was $7.4 \mu\text{eq L}^{-1}$ (Figure 34). Ionic concentrations in melt water decreased with time. Bulk snowpack concentrations of ions were about half the melt water concentrations at the initiation of snowmelt, with the exception of H^+ which was higher in the snowpack. Ionic concentrations in the snowpack decreased as the time period of snowmelt increased. Melt occurred rapidly at the bench, with SWE decreasing from 55.6 cm on April 2 to 25.9 cm on April 23. The bench is an exposed site that receives much more radiation than the other sites.

Ionic concentrations in the first fraction of melt water at the inlet were generally two to three-fold higher than at the bench, with the exception of H^+ , which was similar (Figure 35). Nitrate concentration in melt water was about $20 \mu\text{eq L}^{-1}$, SO_4^{2-} was about $15 \mu\text{eq L}^{-1}$, Cl^- about $6 \mu\text{eq L}^{-1}$, and Ca^{2+} about $22 \mu\text{eq L}^{-1}$, compared to $5.0 \mu\text{eq L}^{-1}$, $2.8 \mu\text{eq L}^{-1}$, $2.5 \mu\text{eq L}^{-1}$, and $1.6 \mu\text{eq L}^{-1}$, respectively, in the snowpack. Again, H^+ alone was not enhanced in melt water. After several melt-freeze cycles, from April 20 to the 23, Ca^{2+} showed a five-fold increase in melt water concentration. Other ions, with the exception of H^+ , showed a slight increase in concentration on April 23. Hydrogen concentration in melt water on April 23 decreased about five-fold. Bulk snowpack concentrations were similar to those at the bench. The volume-weighted mean ionic concentrations of the snowpack decreased with time, except for a slight increase on April 17. Snowmelt at the inlet was initiated on about the same date as the bench, but melt occurred at a slower rate at the inlet, with SWE decreasing from 63.9 cm on April 2 to 43.7 cm on April 23.

Snowmelt started at the cirque on April 17, about 2 weeks later than at the bench or the inlet. The rate of snowmelt was also slower than at the other two sites, with the cirque's SWE decreasing from 86.3 cm on April 17 to 78.8 cm on April 23 (Figure 36). Ionic concentrations in the first fraction of melt water at the cirque were comparable to those of the inlet. All ionic concentrations in melt water at the cirque increased 50% to 100% on April 23 after several melt-freeze cycles, with the notable exception of H^+ . The volume-weighted mean ionic concentrations of the snowpack decreased with time, except for a small increase of NO_3^- and Cl^- from April 17 to April 23. The volume-weighted mean ionic concentrations of the snowpack at the cirque were similar to those at the bench and inlet.

The enhancement of ionic concentration in melt water (C_m) relative to bulk snow concentration (C_p), at the initiation of snowmelt in 1987, is summarized in Table 80 for NO_3^- , SO_4^{2-} , and Cl^- . The percentage of snowmelt is also shown in this table. The faster the increase in the amount of snowmelt, the lower the maximum C_m/C_p . For example, after eight days of melt at the cirque, SWE was reduced about 10.7% and C_m/C_p was about 3-4. At the inlet after nine days of melt, SWE was reduced 31% and C_m/C_p was 2 or less. Sulfate had a greater enrichment in the initial fraction of melt water at the inlet and cirque sites than did NO_3^- or Cl^- . The NO_3^- and SO_4^{2-} values of C_m/C_p decreased to 1 or lower

after the first 30% of melt at the inlet and bench sites, while Cl^- values remained greater than 1 after 30% of melt. Chloride enhancement in the first fraction of snowmelt was lower than NO_3^- or SO_4^{2-} , except in the first fraction of melt water at the inlet.

A time series of NO_3^- and SO_4^{2-} concentrations in the snowpack at the cirque, just prior to and at the initiation of snowmelt, is illustrated in Figure 37. Prior to the initiation of snowmelt runoff on April 17, NO_3^- and SO_4^{2-} in the upper portion of the snowpack decreased, while the lower portion of the snowpack increased in concentration. Snowpack temperatures on March 31 were about -3°C from the top of the snowpack to 80 cm above the ground, increasing to -0.6°C at the snow-ground interface. On April 9 the top 40 cm of the snowpack was at 0°C , with the temperature decreasing to -3°C at 130 cm, then increasing again from 80 cm to the bottom of the snowpack. The snowpack was isothermal at 0°C on April 17. Apparently NO_3^- and SO_4^{2-} moved from the top of the snowpack towards the bottom of the snowpack, as the snowpack temperature increased towards 0°C . After the initiation of snowmelt runoff, the upper portion of the snowpack continued to lose NO_3^- and SO_4^{2-} , as did the lowest layer of the snowpack. However the concentrations of NO_3^- and SO_4^{2-} increased in the layer from 90 cm to 40 cm, on April 23.

Mass balance calculations consistently show less depletion of solutes from the snowpack than solutes in snowmelt runoff during the same time period, at the same location. Solute loss from the snowpack was calculated by subtracting the ionic load (SWE times the volume-weighted mean concentration) at the end of the time period in question from the beginning of the time period. For example, SO_4^{2-} loading in the snowpack at the cirque decreased $520 \mu\text{eq m}^{-2}$ from April 17 to April 23. Solute loading in snowmelt runoff over the same time period was calculated by multiplying the solute concentration in melt water by the decrease in SWE of the snowpack. The calculated ionic loading from snowmelt runoff, at the same time period, was $2300 \mu\text{eq m}^{-2}$, about 4-fold more than the observed loss from the snowpack.

The chemistry of snowpack melt water at a given time varied spatially over the watershed. For example on April 23, SO_4^{2-} concentrations at the cirque ($29 \mu\text{eq L}^{-1}$) were more than ten-fold higher than at the bench ($1.1 \mu\text{eq L}^{-1}$). This spatial variation in the solute concentration of snowpack melt water was a function of the timing and magnitude of snowmelt at a particular site. In turn, the spatial variation in the chemistry of melt water caused spatial variation in ionic loading from snowmelt runoff to soil and rock surfaces. For example, from April 17 to April 23, NO_3^- loading from snowmelt runoff was $330 \mu\text{eq m}^{-2}$ at the bench, $3.5 \mu\text{eq m}^{-2}$ at the inlet, and $1,540 \mu\text{eq m}^{-2}$ at the cirque. Again, all other ions except H^+ demonstrated this pattern.

Water and ionic loading from wet deposition during the period of snowmelt runoff in 1987 were important inputs to the hydrology and chemistry of snowmelt runoff (Table 81). For example, rainfall during spring runoff deposited about 2.2×10^3 equivalents (eq) of H^+ to the 1.6×10^3 eq of H^+ stored in the snowpack on April 27. The combination of high ionic concentrations and large amount of water resulted in more ionic loading from spring rainfall than winter snowfall for NO_3^- , SO_4^{2-} , NH_4^+ , Na^+ and Mg^{2+} , in water year 1987. The chemistry of snowmelt runoff in 1987, after April 27, was therefore a combination of

snowpack melt water and spring rains.

The snowpack retained little to none of the solute input from rainfall. For example, the volume-weighted concentration of SO_4^{2-} in the snowpack at the inlet site decreased from $1.6 \mu\text{eq L}^{-1}$ on April 29 to $0.8 \mu\text{eq L}^{-1}$ on May 7, after a 32 mm rain event with a SO_4^{2-} concentration of $47.7 \mu\text{eq L}^{-1}$. The rain event supplied $1500 \mu\text{eq m}^{-2}$ of SO_4^{2-} to the snowpack, yet SO_4^{2-} load in the snowpack decreased from $490 \mu\text{eq m}^{-2}$ on April 29 to $120 \mu\text{eq m}^{-2}$ on May 7. The other major ions, including H^+ , exhibited a similar lack of retention by the snowpack from rainfall inputs. Snowpack melt water samples and concurrent snowpit samples provide an additional method of determining snowpack-rainwater interactions. Figure 38 illustrates this snowpack-rainwater interaction for H^+ , Ca^{2+} and SO_4^{2-} at the inlet site after two rain events. Snowpack melt water collected after the rain events had a solute content intermediate in concentration between the relatively high concentration of rainfall and the low concentration in the snowpack, the result of concentrated rainwater mixing with dilute melt water.

2. Chemistry of Stream Water

Temporal and spatial variation in the NO_3^- and SO_4^{2-} concentrations of streams flowing into Emerald Lake, and the lake's outflow, in 1986, is presented in Figure 39. Snowmelt started in a south-east facing (east joint) basin then progressed temporally to more north-facing basins [Williams and Melack, 1989]. The initiation of snowmelt in the subbasins of the ELW spanned about 20 days, from April 14 at the east joint and inflow 1, to May 5 at inflow 4. Nitrate and SO_4^{2-} concentrations in streams were highest at the initiation of snowmelt in each subbasin, then decreased as the amount of snowmelt increased. As a consequence of temporal differences in the initiation of snowmelt within the ELW, there was a spatial difference in the NO_3^- and SO_4^{2-} concentration of inflowing streams to Emerald Lake. For example, on May 18, NO_3^- concentrations in the southeast gully, inflow 1, inflow 2, inflow 4, and the outflow were $0 \mu\text{eq L}^{-1}$, $6.1 \mu\text{eq L}^{-1}$, $10.3 \mu\text{eq L}^{-1}$, $18.0 \mu\text{eq L}^{-1}$, and $10.3 \mu\text{eq L}^{-1}$, respectively. Nitrate and SO_4^{2-} concentrations in the outflow remained elevated for a longer time period than any of the inflows to the lake.

Analysis of temporal variation in the NO_3^- and SO_4^{2-} concentrations of stream flowing into Emerald Lake in 1987 was confounded by inputs from spring rainfall. However the pattern of NO_3^- and SO_4^{2-} concentrations in inflowing streams and the outflow was similar to that in 1986, until the advent of rains on April 27.

The discharge of the Emerald Lake outflow during the period of snowmelt runoff, for water years 1986 and 1987, is presented in Figure 40. Snowmelt runoff in 1986 began in mid April, peaked in early May followed by a decrease due to a cold spell, and remained large through the months of June and July. The increases in discharge in February and March, 1986 are due to avalanche and snowfall activity pushing water out of the lake. Snowmelt runoff in 1987 started in early April, with discharge generally increasing until a cold spell at the end of May, except for slight decreases due to cold temperatures around April 20 and May 1. Discharge then increased after rainstorms in early June, and by the end of June decreased to near pre-snowmelt amounts. Discharge during snowmelt runoff in 1986 was three-fold greater than in 1987, and snowmelt runoff lasted about two months longer in

1986 than in 1987.

Silica concentration in the outflow in 1986 decreased steadily from a winter concentration of 59 μM to minimum of 21 μM towards the end of snowmelt runoff (Figure 40). In 1987 silica concentration increased from a winter concentration of 26 μM to 40 μM at the beginning of runoff, then decreased to 21 μM near maximum discharge on the first of June. Inflowing concentration of silica to Emerald Lake for both water years was about 60 μM . Differences in the thickness and type of ice-cover on Emerald Lake between the two years may be partly responsible for the difference in silica concentration. Ice on Emerald Lake is a mixture of snow, lake slush, and black ice. Black ice is a good transmitter of light in the visible wavelengths (37% transmittance of incoming light at 20 m by pure ice), while snow absorbs visible light readily due to scattering by the snow grains (ca. 100% attenuation at 1 m). In 1986 the ice thickness was 6 m and composed primarily of snow and slush, while in 1987 ice thickness was 1 m, and composed primarily of black ice. Photosynthetically active radiation (PAR) can limit plant growth under ice cover. Higher levels of PAR in 1987, and consequent biological utilization of silica, may explain why the winter concentrations of silica were lower in the outflow in 1987 than in 1986. The increase of silica concentration in the outflow with the initiation of snowmelt runoff in 1987 may be due in part to the lower residence time of water in the lake as discharge increased, decreasing organic uptake of silica. Additional evidence of biological utilization of silica in Emerald Lake is that mass balance calculations of lake inputs and outputs, during the summers of 1987 and 1988, showed the only significant changes were decreases in silica and NO_3^- , which were similar [Melack et al., 1989].

Minimum ANC concentrations occurred at maximum discharge, with ANC decreasing from a winter concentration of about 40 $\mu\text{eq L}^{-1}$ to 12 $\mu\text{eq L}^{-1}$ in 1986 and to 16 $\mu\text{eq L}^{-1}$ in 1987, decreases of 70% and 60%, respectively (Figure 40). ANC concentrations were inversely correlated with the period of increasing discharge in 1986 ($r^2 = 0.90$, $n = 9$), but not in 1987 ($r^2 = 0.17$, $n = 11$). At the same time period ANC was also correlated with silica in 1986 ($r^2 = 0.97$, $n = 9$), but again only weakly in 1987 ($r^2 = 0.40$, $n = 10$). After maximum discharge, ANC concentration increased steadily towards pre-snowmelt runoff concentration.

During the initiation of snowmelt runoff, H^+ concentration decreased slightly in 1986 and remained relatively constant in 1987 (Figure 40). Hydrogen ion concentration in both water years peaked near the time of maximum discharge. Maximum concentration of H^+ in the outflow for both water years was about 2 $\mu\text{eq L}^{-1}$, an increase of 170% over the winter concentration of 0.70 $\mu\text{eq L}^{-1}$.

The strong acid anions (NO_3^- , SO_4^{2-} , and Cl^-) increased in concentration during the first thirty days of snowmelt runoff in 1986, then decreased in concentration to below winter levels at maximum discharge (Figures 40). In 1987 the strong acid anions also increased in concentration during the first thirty days of snowmelt runoff. However in contrast to 1986, concentrations remained elevated through the period of maximum discharge, which coincided with the period of spring rainfall in 1987. Maximum concentrations of NO_3^- (11 $\mu\text{eq L}^{-1}$) and SO_4^{2-} (8 $\mu\text{eq L}^{-1}$) were similar in the two years, and the maximum

concentration of Cl^- was higher in 1986 ($7.7 \mu\text{eq L}^{-1}$) than in 1987 ($5.1 \mu\text{eq L}^{-1}$). Nitrate concentration prior to snowmelt runoff in 1986 ($5.9 \mu\text{eq L}^{-1}$) was much higher than in 1987 ($1.7 \mu\text{eq L}^{-1}$). The lower concentration in 1987 may be due to biological utilization, as a result of the higher levels of PAR in the lake during the winter of 1987, compared to 1986.

Nitrate and Cl^- had larger amplitude increases and decreases in concentration during snowmelt runoff than did SO_4^{2-} . Figure 41 shows the variation of NO_3^- , SO_4^{2-} , and Cl^- concentrations from winter values, during snowmelt runoff, as a percentage. Nitrate and Cl^- had similar patterns in 1986, with maximum and minimum concentrations about 100% greater and 50% lower than winter concentrations. However Cl^- increases peaked before NO_3^- in 1986, so that the correlation between the two ions was weak ($r^2 = 0.42$, $n = 9$). Chloride was strongly correlated with NO_3^- in 1987 ($r^2 = 0.83$, $n = 7$). The 500% increase in NO_3^- concentration during snowmelt runoff in 1987 indicates that NO_3^- changed from a relatively immobile anion in winter to a mobile anion in the spring. There was an inverse relationship between NO_3^- and silica concentration during the period of rising NO_3^- concentration with $r^2 = -0.77$, $n = 8$, in 1986, and again in 1987. Sulfate maxima and minima were 30% greater and 30% lower than the winter concentration, in both years.

The sum of basic cations ($C_b = \text{Ca}^{2+}$, Mg^{2+} , Na^+ , and K^+) remained near winter values ($56 \mu\text{eq L}^{-1}$) during the first 30 days of snowmelt runoff in 1986, then decreased consistently during the remainder of snowmelt runoff to a minima of $23 \mu\text{eq L}^{-1}$ (Figure 41). In 1987 C_b increased from $45 \mu\text{eq L}^{-1}$ to $59 \mu\text{eq L}^{-1}$ during the first 30 days of snowmelt runoff, and then decreased to slightly below winter concentrations the remainder of snowmelt runoff.

Ammonium concentrations were generally at or below detection limit in stream waters, and never exceeded $2 \mu\text{eq L}^{-1}$. Ammonium was a highly ranked ion in winter snow and spring rains in 1987. And NH_4^+ concentrations were enhanced several-fold in snowpack melt water. The low concentrations of NH_4^+ in stream waters indicates basin retention of the ion.

3. Mass Balance Calculations

Geochemical interactions between the basin's terrestrial components and snowmelt runoff can be partially determined by comparing the loading of ions stored in the snowpack to that in streams flowing into Emerald Lake. Streams flowing into the lake, rather than the lake outflow, were used for the loading calculations so as not to confound mass balance calculations with sources or sinks within the lake. This mass balance calculation is shown in Table 82 for H^+ , NO_3^- , SO_4^{2-} , and Cl^- . Ionic storage in the snowpack was calculated as the ionic volume-weighted mean concentration of snow covered area times snow water equivalent [Chapter VIII], and includes wet deposition from spring rainfall in 1987. Stream loading was calculated as discharge (measured every 15 minutes, Chapter V) times concentration (sampled about weekly) during the period of snowmelt runoff (April 1 through July 30, 1986 and April 1 through June 30, 1987).

Hydrogen showed a consistent pattern both years, with more H^+ released from the snowpack than reaching Emerald Lake. Seventy-seven percent of the H^+ released from the snowpack was consumed before it reached the lake in 1986, and 91% was consumed in

1987. More NO_3^- was in stream water than in the snowpack in 1986, while much more NO_3^- was deposited to the basin than reached the lake in 1987. The basin was therefore a source of about 20% of the NO_3^- in stream waters in 1987, and a large sink (75%) for NO_3^- in wet deposition in 1987. Sulfate showed the same pattern, with much more SO_4^{2-} in stream water than stored in the snowpack in 1986 and SO_4^{2-} retention in the basin in 1987. Chloride in 1987 acted conservatively during the time period of snowmelt runoff. The small amount of Cl^- retention (12%) indicated by mass balance calculations is within the error bars of analytical precision for Cl^- (13.4%).

D. Discussion

1. Chemistry of Snowpack Meltwater

The ionically dilute snowpack of the ELW produced a C_m/C_p ratio similar in magnitude to snowpacks with much higher concentrations [Johannessen and Henriksen, 1978; Colbeck, 1981; Cadle et al., 1984; Tranter et al., 1986; Rascher et al., 1987]. Bales et al. [1989] report that in laboratory studies larger initial peaks occurred in the solute concentration of melt water in snow subjected to melt-freeze cycles, when compared with replicates not subject to melt-freeze action. They attribute the enhancement of ionic concentrations in melt water by melt-freeze cycles to the ionic enrichment of residual liquid in grain clusters as the grain bond areas grow during freezing. Colbeck [1981] has also reported that in laboratory experiments multiple melt-freeze actions enrich the first fraction of melt water.

At the ELW, areas with rapid melt had the lowest maximum concentrations of solutes in melt water (bench); areas with lower rates of snowmelt had higher maximum concentrations of solutes in melt water (cirque). Furthermore after a series of melt-freeze cycles, from April 17 to April 22, the ionic concentration in melt water increased at both the inlet and cirque. Our research in a natural snowpack thus supports the laboratory experiments of Bales et al. [1989] and Colbeck [1981] that melt-freeze cycles enhance the concentrations of solutes in snowpack melt water. The number of melt-freeze cycles that a snowpack undergoes may be more important than the concentration of solutes in the snowpack in determining the enhancement of solutes in melt water.

Lateral flow within the snowpack may also contribute to the observed melt water concentrations at the ELW. Natural snowpacks are rarely ideal systems with vertical Darcian-type flow in an unsaturated porous medium. Structural anomalies in the snowpack can change melt water flow patterns [Marsh and Woo, 1984], which in turn have a direct influence on the chemistry of melt water. Ice lenses or other discontinuities in the snowpack can cause lateral flow, increasing the concentration effect as longer flow paths result in greater snow-melt water contact [Bales et al, personal communication, University of Arizona, 1989]. Vertical macropores can short-circuit melt water to the ground [Kattelmann, 1985], which can lead to a decrease in the concentration effect at macropore exits [Jones and Sochanska, 1985].

Replenishment of solutes in the snowpack by lateral flow may explain why mass balance calculations do not balance between snowpack loss of solutes over time and solutes in snowmelt runoff. Bales et al. [personal communication] also found that snowpack losses of solutes were less than solutes collected in lysimeters in a Wyoming snowpack. The increase

of NO_3^- and SO_4^{2-} concentration near the bottom of the snowpack at the cirque, on April 22, may have been from lateral flow of water in the snowpack. Similarly, much of the increase in bulk solute concentrations of the snowpack at the inlet on April 17 occurred at depth. The steep gradient of the basin and well-developed ice lenses (up to 2-cm thickness) may have contributed to lateral water flow within the snowpack at the ELW. Dry deposition is another possible source of ionic input to the snowpack during snowmelt runoff. However snowpack profiles showed no increase in solute concentration at the top of the snowpack. Dry deposition is therefore not likely to be the cause of the imbalance.

Preferential release of one ionic species over another, from the snowpack to melt water, has been reported by several researchers [Davies et al., 1982; Tsiouris et al., 1985; Tranter et al., 1986; Tranter et al., 1987]. The ionic sequences generally have SO_4^{2-} and NO_3^- eluted before Cl^- [Brimblecombe et al., 1985]. Physicochemical reasons for this phenomenon are unknown. Preferential elution of ions may be the result of many factors: ionic species have different solubilities in ice; solutes are inhomogeneously distributed within snow grains; ionic solubility depends on the rate of freezing; chromatographic separation may occur during melt water percolation through the ice matrix [Tranter et al., 1986]. Different distributions of ionic species on the scale of individual crystals have been hypothesized to be the main cause of preferential elution, with condensation nuclei (e.g. Cl^- in sea-salt aerosols) being retained within the crystal and species scavenged during snowfall (e.g. SO_4^{2-} and NO_3^-) being eluted first [Tsiouris et al., 1985; Tranter et al., 1986].

Our melt water samples indicate that preferential elution occurs among the strong acid anions at the ELW, with SO_4^{2-} eluted before NO_3^- , and Cl^- eluted last. A major source of Cl^- in snowfall at the ELW is sea-salt aerosols [Chapter VIII]. Differences in the atmospheric history of snowfall may partially explain the elution sequence of ions in snowmelt at the ELW.

That H^+ did not produce a consistent ionic pulse in snowpack melt water of the ELW, and that H^+ concentration in melt water was at times lower than snowpack concentrations, indicates that H^+ was consumed in melt water or the snowpack before contact with the ground. This decrease of H^+ in melt water relative to the other major inorganic ions is similar to that reported by Hornbeck et al. [1977], Jones and Sochanska [1985], and Cadle et al [1987]. Contamination from soilwater is a potential source of H^+ buffering, but silica measurements indicate that there was little or no soilwater in the lysimeters. A possible mechanism for the buffering of free hydrogen in the snowpack or melt water is organic acids. Jones and Hornbeck et al. attribute the relative decrease of H^+ in melt water to interactions with organic detritus. Organic acids compose about 25-30% of the anions in the snowpack at the ELW [Chapter VIII]. Their pK's ($\text{CH}_3\text{COO}^- = 4.76$, $\text{HCOO}^- = 3.75$) are such that at the pH levels in snowpack melt water the organic acids will be dissociated and available to buffer free acidity.

Clay and dust particulates in the snowpack are another potential source of H^+ buffering. Calcium and magnesium particulates can react with atmospheric CO_2 to form HCO_3^- and Ca^{2+} or Mg^{2+} in melt water (or free water in the snowpack). This would result in increased Ca^{2+} and Mg^{2+} concentrations and decreased H^+ concentration in melt water. This

hypothesis is supported by the five-fold increase in concentration of Ca^{2+} and five-fold decrease in H^+ concentration in melt water at the inlet site on April 23, 1987. Results from a leaching experiment performed in 1989, where particulates were filtered from snow collected in the central Sierra Nevada and then leached in melt water for seven days at 5°C , showed significant increases in the alkalinity of melt water compared to controls (Alice Murphy, personal communication, University of California at Santa Barbara, 1989). Particulates in the snowpack may be an important source of H^+ buffering.

Hydrogen buffering may also occur as an artifact of our sampling protocol. If particulates occur in the snowpack, they may collect in the sample container. Our protocol of weekly sampling may allow sufficient time for weathering reactions between clay and dust particulates and melt water to consume H^+ . However the indirect method used in 1986 also showed no enhancement of H^+ in melt water, indicating that container effects contribute at most a small role in H^+ buffering of melt water.

2. Chemistry of Stream Water

Nitrate is the dominant strong acid anion in surface waters of the ELW during the time period of spring runoff. Nitrate is only weakly adsorbed on soil surfaces and is readily leached from watersheds [Reuss and Johnson, 1986]. However biological uptake can maintain NO_3^- at very low levels, such that the concentration of NO_3^- is generally not an important factor in determining the acidification of fresh waters. Algal uptake and other biological processes do result in NO_3^- becoming an immobile ion during the summer months at the ELW [Melack et al., 1989]. But during snowmelt runoff NO_3^- becomes a mobile anion, presumably as the result of decreases in biological activity. Sickman and Melack [1989] report a similar pattern, with elevated NO_3^- concentrations in stream water at the initiation of snowmelt runoff followed by decreases to near detection limits, at each of four high-altitude watersheds they have studied in the Sierra Nevada.

The source of the elevated NO_3^- concentrations in stream water during the initial increase in discharge may be from (1) the high NO_3^- concentrations in the ionic pulse of snowmelt runoff, (2) nitrification processes in soils and subsequent transport by melt water percolating through the soils or (3) a combination of 1 and 2. The negative correlation between silica and NO_3^- concentrations indicates that NO_3^- concentrations in stream water increased as the contribution of soilwater and groundwater to stream water decreased. ANC, the product of chemical weathering reactions, also decreased in stream waters as NO_3^- concentrations increased. Furthermore NO_3^- concentrations in soilwater were less than or equal to the bulk NO_3^- concentrations in the snowpack. [A. Brown, personal communication, University of California at Riverside, 1989]. Therefore mineralization of organic nitrogen and subsequent nitrification in the soils of the ELW is unlikely to be the major source of the elevated NO_3^- concentrations in stream water.

If the measured NO_3^- pulse in stream waters was from snowpack runoff, the amount of NO_3^- released from the snowpack should be equal to the amount of NO_3^- that entered Emerald Lake from its inflowing streams. The stream to snowpack ratio in 1986 of 1.21 indicates that there was an additional source of NO_3^- in stream water. About 20% of the NO_3^- in snowfall was not stored in the snowpack in 1986, and apparently moved from the

snowpack to soil reservoirs [Chapter VIII]. If we add the amount of NO_3^- apparently lost to soil water in 1986 to that stored in the snowpack, the ratio of NO_3^- in streams to that in snow was 0.98. The lack of NO_3^- retention by the basin in 1986 may be the result of low biological activity due to the deep snowpack (mean depth of 384 cm) and large percentage of snow covered area (95% on May 15). The retention of NO_3^- by the basin during spring runoff in 1987 (75%) may be the result of biological utilization, due to a thin snowpack (140 cm) and reduced amount of snow covered area (55% on May 15). Our mass balance calculations clearly show that the NO_3^- in snowfall (1986), or snowpack plus rain (1987), can account for the NO_3^- in stream waters during the period of snowmelt runoff.

Acidification models for fresh waters have generally neglected nitrogen transformations because of biological uptake [e.g. Nikolaidis et al., 1988]. The net acidification potential of nitrogen to an ecosystem is expressed as the moles of NO_3^- exported from the watershed, and is virtually independent of the form in which nitrogen enters the ecosystem [Reuss and Johnson, 1986]. Nitrate is more prevalent in wet deposition to the ELW than is SO_4^{2-} [Chapter VIII]. The increased concentration of NO_3^- in stream waters of the ELW during spring runoff therefore increases the potential for acidification, even when NO_3^- is not associated with protons during deposition. In the Sierra Nevada, NO_3^- must be considered when assessing the susceptibility of lake and stream waters to acidification.

The retention of NH_4^+ in the basin can also increase the susceptibility of the ELW to acidification. Oxidation of NH_4^+ to NO_3^- releases 2 H^+ for each mole of NO_3^- formed. If NO_3^- is then taken up by plants, OH^- is released, resulting in a net production of 1 mole of H^+ [Reuss and Johnson, 1986]. Nitrification of NH_4^+ is known to produce HNO_3 [van Breemen et al., 1982]. Other vegetation effects of nitrogen excess from NH_4^+ include a decrease in frost hardiness and increased susceptibility to attacks by insects, fungi, bacteria and viruses, as well as a distorted mineral balance which can lead to deficiencies in magnesium, potassium, phosphorus, boron and other minerals [Nihlgard, 1985].

Maximum concentrations of Cl^- in stream water were similar to maximum concentrations of SO_4^{2-} , which is different than eastern North America; which generally has very low concentrations of Cl^- relative to SO_4^{2-} , with little variation in the Cl^- concentration of stream water. Chloride concentration in surface waters is often omitted in acidification studies of this area, by subtracting an equal amount of basic cations [e.g. Galloway et al., 1987]. Chloride must be considered when assessing the susceptibility of alpine watersheds in the Sierra Nevada to acidification. An interesting and unexplainable aspect of Cl^- in streams was that Cl^- showed the same magnitude increase in concentration as NO_3^- at the start of snowmelt runoff, but increased sooner than did NO_3^- in both years.

Sulfate concentrations in stream water increased during the first thirty days of snowmelt runoff, but the increase was less than half that of NO_3^- and Cl^- . The attenuation of SO_4^{2-} concentrations in stream water with respect to the higher concentrations in melt water at the initiation of snowmelt and the lower concentrations in melt water towards the end of snowmelt runoff was surprising. This attenuation was unexpected since developed soils comprise only 20% of the surface area of the watershed. Furthermore hydraulic residence time during snowmelt runoff at the ELW is on the order of hours to days, with a large

component of snowmelt runoff occurring as overland flow [Kattelman, 1989].

Adsorption-desorption by the clay minerals of the basin is a possible source of this SO_4^{2-} attenuation. Sulfate adsorption on soil surfaces is concentration-dependent, with the capacity of soils to adsorb SO_4^{2-} increasing with increasing SO_4^{2-} concentration in the soil solution [Reuss and Johnson, 1986]. As SO_4^{2-} inputs increase, from snowmelt runoff or rainfall, new adsorption sites are activated on soil sesquioxide surfaces, causing a net SO_4^{2-} retention in the soil. During desorption, output exceeds input, and SO_4^{2-} previously retained during adsorption is leached from the soil. The kinetics of SO_4^{2-} sorption are on the order of seconds to hours.

Mass balance calculations between SO_4^{2-} released from the snowpack and SO_4^{2-} in stream water during the period of snowmelt runoff provide additional evidence of SO_4^{2-} sorption in the Emerald Lake basin. Water year 1986 was a large snow year with low SO_4^{2-} concentration in snowfall [Chapter VIII]. More SO_4^{2-} entered stream water in 1986 than entered the basin from wet deposition, indicating that the basin supplied about 46% of the SO_4^{2-} in stream water. The SO_4^{2-} source in the basin could be dry deposition or weathering reactions of source materials. However no evidence exists for dry deposition of SO_4^{2-} during the winter [Chapter VIII], nor for the weathering of SO_4^{2-} -bearing minerals in sufficient quantity to produce the amount of SO_4^{2-} measured in stream waters [Clow, 1987]. That SO_4^{2-} desorption from the basin's soils was a source of SO_4^{2-} in the outflow in 1986 is indicated by concentrations that remained relatively constant at around $4 \mu\text{eq L}^{-1}$ towards the end of snowmelt runoff, compared to bulk snowpack concentrations that were less than $1 \mu\text{eq L}^{-1}$ at this time [Dozier et al., 1987]. Fifty percent of SO_4^{2-} in wet deposition was retained by the basin in 1987, the opposite of water year 1986. Sulfate adsorption in soils is indicated by the constancy of SO_4^{2-} concentration in the outflow at about $7 \mu\text{eq L}^{-1}$, during both periods of high SO_4^{2-} input from rainfall and after discharge had returned to pre-snowmelt runoff levels.

The low H^+ ion concentration in stream water during snowmelt runoff indicates interactions between runoff and geochemical processes within the watershed. Eighty percent of the H^+ stored in the snowpack in 1986 was consumed before reaching Emerald Lake; 90% was consumed before reaching the lake in 1987. The magnitude of H^+ buffering is surprising, given the short residence time of snowmelt runoff in groundwater and soil reservoirs or in contact with bedrock during overland flow.

Ion exchange, weathering, adsorption, titration of HCO_3^- , and protonation of anions of weak organic acids are all possible sources of H^+ buffering during snowmelt runoff. Chemical weathering and ion exchange both consume H^+ and release cations. They differ in that the kinetics of ion exchange are rapid (seconds to hours) relative to those of chemical weathering (days to weeks). The generation of silicic acid in watersheds is one measure of aluminosilicate weathering that is distinct from ion exchange [Schnoor and Stumm, 1986]. The relatively slow kinetics of chemical weathering and the consistent decrease in silica concentration in the outflow in 1986, indicates that chemical weathering was probably not responsible for the majority of H^+ buffering, prior to maximum H^+ concentrations.

Several different types of ion exchange may have contributed to the observed H^+ buffering. Sulfate adsorption is often accompanied by a rise in pH, apparently resulting from the replacement of OH^- groups on the mineral surface by SO_4^{2-} . That the concentration of basic cations in the outflow did not decrease during the initial period of snowmelt runoff in 1986, while silica concentration decreased, indicates that cation exchange for H^+ may have occurred in the basin. However, the maintenance (1986) or increase (1987) of C_b during the first thirty days of snowmelt runoff may be partly from an ionic pulse of basic cations in snowmelt runoff.

Aluminium exchange with H^+ might be an important source of pH buffering. The process of mineral weathering of aluminosilicates common in the ELW provides an abundant source of aluminium [Johnson, 1984]. Small increases in the aluminium concentration of stream waters in the ELW could have large effects on aquatic organisms. Toxicity effects to organic organisms by mobile aluminium concentrations as low as $7.5 \mu M$ have been documented [Driscoll et al., 1980; Baker and Schofield, 1982]. Increased mobility of aluminium in the surface waters of a Massachusetts catchment as a result of the ion exchange of aluminium for the H^+ in episodic rain events has been shown by McAvoy [1989]. And Liu [1988] reports that aluminium was mobilized during experimental acidification of soils from the ELW. More research on the role of aluminium in buffering H^+ is needed, in the Sierra Nevada.

There is an abundant source of weak organic acids to the ELW, with about 25% of all anions in wet deposition composed of CH_3COO^- and $HCOO^-$ [Chapter VIII]. The role that protonation of these organic acids has in buffering H^+ is unknown, but could be important. Buffering of H^+ by titration of HCO_3^- may be locally important within the watershed, but does not appear to buffer a significant amount of the H^+ in snowmelt runoff. The close correlation between decreases in silica and ANC, and between decreasing ANC and increasing discharge, indicate that dilution, not titration, was the main reason for the decrease in ANC observed during snowmelt runoff in 1986. However the weak correlation in 1987 between ANC and discharge, and between ANC and silica, indicates that processes other than dilution may be involved in the decrease in ANC in that year.

The large quantity of H^+ buffering that occurs in snowmelt runoff at present deposition levels has important implications for the susceptibility to acidification of alpine watersheds. High-altitude basins in the Sierra Nevada may not be as sensitive to acid deposition as indicated by the characteristically low concentrations of ANC in surface waters. Alternatively the geochemical processes that are presently buffering H^+ inputs from wet deposition may be nearly saturated, and small increases in H^+ flux may cause large increases in the acidification of alpine basins. Knowledge of the mechanism of H^+ buffering is needed to effectively assess the susceptibility of this alpine watershed to potential increases in acid deposition.

Galloway et al. [1987] define "spring acidification" as the loss of alkalinity (ALK) in excess of that observed at other times of the year. Acidification results from decreases in alkalinity whose component parts are C_b and C_a (the sum of strong acid anions). The relationship between C_a , C_b and alkalinity can be expressed as

$$\text{ALK} = C_b - C_a = [\text{HCO}_3^-] + [\text{CO}_3^{2-}] + [\text{OH}^-] - [\text{H}^+]$$

where

$$C_b = [\text{Ca}^{2+}] + [\text{Mg}^{2+}] + [\text{Na}^+] + [\text{K}^+]$$

and

$$C_a = [\text{NO}_3^-] + [\text{SO}_4^{2-}] + [\text{Cl}^-]$$

(all concentrations are expressed as $\mu\text{eq L}^{-1}$).

Decreases in alkalinity during spring snowmelt can be caused by decreases in C_b or increases in C_a , or a combination of the two.

Changes in the alkalinity of surface waters of the ELW during snowmelt runoff in 1986 are illustrated in Figure 42. A representative sample of water collected before snowmelt is compared to samples collected during elevated anion concentration and during the dilution period of snowmelt runoff. The main inflow (inflow 2) in 1986 was chosen as the sampling site, rather than the lake outflow, to prevent confounding of changes in the alkalinity of stream water caused by snowmelt runoff with those that might be caused by lake processes. However the same analysis performed on the outflow produced similar results. Dilution by snowmelt runoff decreased ALK by $4 \mu\text{eq L}^{-1}$ on May 1, while increases in the strong acid anions decreased ALK by another $10 \mu\text{eq L}^{-1}$. ALK at this time, calculated as $C_b - C_a$, was $17 \mu\text{eq L}^{-1}$, compared to $38 \mu\text{eq L}^{-1}$ on January 7. On June 10 all solutes exhibited considerable dilution. The C_b was lowered to $24 \mu\text{eq L}^{-1}$, a $30 \mu\text{eq L}^{-1}$ loss compared to premelt concentrations, while C_a decreased only $6 \mu\text{eq L}^{-1}$ compared to premelt concentrations. The ALK of inflow 2 at maximum dilution in 1987, calculated as $C_b - C_a$, was $13 \mu\text{eq L}^{-1}$. The sensitivity of surface waters to acidification during the period of snowmelt runoff, measured as $C_b - C_a$, was almost as great near the start of runoff as at maximum dilution.

The period of time that the outflow and Emerald Lake are susceptible to acidification was increased by spatial and temporal variations in the timing and magnitude of snowmelt [Williams and Melack, 1989]. Solute loading to the ELW from snowpack runoff varied spatially for a given time and varied temporally for a given location. When snowmelt was initiated within a subbasin of the ELW, rock and soils of that subbasin received concentrated solutes from snowpack runoff. As a stream draining one subbasin became more dilute in solute concentration, solutes in a stream draining another subbasin where melt had started became more concentrated. The net effect of spatial and temporal changes in the timing of snowmelt was a sequential generation of an ionic pulse through the watershed. The Emerald Lake basin therefore experienced an ionic pulse in snowpack runoff for a longer time period than the two to ten days that had been measured at a single location, and caused concentrations of the strong acid anions to remain elevated for a longer time period in the outflow than any individual inflowing stream.

3. Rain on Snow Events

Alpine ecosystems are potentially most vulnerable to acidification during the period of snowmelt runoff. Calcium-bicarbonate weathering reactions in the basin are the source of ANC (acid neutralizing capacity), primarily HCO_3^- , in lake and stream waters of the ELW. Snowmelt runoff in the ELW dilutes soil and groundwater contributions of basic cations and HCO_3^- to lake and stream waters. The maximum potential for ecosystem effects from

acidic deposition may thus occur during the time period of snowmelt runoff, when the buffering capacity of lake and stream waters are at their annual minima. Acidic rainfall during the snowmelt season in water year 1987 provided a natural experiment to test the hypothesis that lake and stream waters are more sensitive to acidic deposition during the period of snowmelt runoff.

Prior to the rain events, pH in the outflow was similar to that of the normal water year in 1985, and much higher than that in the large water year of 1986 (Figure 43). Immediately after the rain events pH declined abruptly, followed by a rapid recovery to near pH levels in 1985. Acidic rain events during snowmelt runoff in the low snow year of 1987 caused pH (5.68) in the outflow to decrease to the minimum pH (5.70) measured in the large snow year of 1986. The increase in strong acid anion concentration, the result of an ionic pulse in snowmelt runoff and high concentrations in rainfall, further increased the acidification of surface waters during snowmelt runoff.

It is apparent that alpine basins are more sensitive to acidic deposition during the period of snowmelt runoff. The observed pH depression in surface waters may be from (1) different hydrologic pathways during the rain event, (2) acidic input from the rain exceeding the buffering capacity of the current hydrologic pathways, or (3) a combination of 1 and 2. This depression in pH as a result of rain events during snowmelt runoff underscores the need for more research on the role of geochemical interactions in modifying snowmelt runoff.

E. Summary and Conclusions

Solutes in the initial fraction of snowpack melt water (C_m) were enhanced relative to the initial bulk concentrations of the snowpack (C_p), with the C_m/C_p ratio varying from 5-12. The C_m/C_p ratio is comparable to that from snowpacks where the initial bulk concentrations were as much as 30-fold higher than at the ELW. This relationship suggests that the C_m/C_p ratio may be independent of the bulk ionic concentration of the snowpack.

Solute concentrations in melt water were higher when the rate of snowmelt decreased. A series of melt-freeze cycles, which occurred after the initiation of snowmelt runoff, increased the concentration of solutes in melt water relative to concentrations in melt water prior to the melt-freeze cycles. Melt-freeze cycles in a natural snowpack enrich the solute concentration of snowpack melt water. The rate of snowmelt and number of melt-freeze cycles that a snowpack undergoes may be more important in determining the concentration of solutes in melt water than the initial concentration of solutes in the snowpack.

Sulfate and NO_3^- concentrations in melt water decreased below the initial bulk concentrations after about 30% of the snowpack had melted; while Cl^- concentrations remained elevated above bulk snowpack concentrations after 30% of the snowpack had melted. At two of the three sites SO_4^{2-} and NO_3^- enhancement was greater than Cl^- . Sulfate enhancement was greater than NO_3^- at two of three sites. Our results indicate that anions are preferentially eluted from the snowpack, in the order $\text{SO}_4^{2-} > \text{NO}_3^- > \text{Cl}^-$.

The time span of the ionic pulse in melt water, at a point, decreased as the rate of snowmelt increased. At a site with a relatively rapid rate of snowmelt, the ionic pulse lasted about two days; at a site with a relatively slow rate of snowmelt the ionic pulse lasted about

ten days. The initiation of snowmelt runoff varied temporally throughout the basin. As a consequence of spatial and temporal variation in the initiation and magnitude of snowmelt, solute concentrations in the basin's melt water, at a point in time, varied spatially by a factor of 10 or more.

Snowmelt runoff had a dramatic effect on the hydrochemistry of the ELW. The ionic pulse in melt water was associated with a corresponding increase in the concentration of strong acid anions in stream waters of the basin. Nitrate was the dominant anion in stream waters; maximum SO_4^{2-} and Cl^- concentrations were similar to each other. The increase in anions was followed by a decrease below winter concentrations.

Alkalinity decreases were almost as great during the initiation of snowmelt runoff, as a result of the increase in concentration of anions, as during the dilution period of snowmelt runoff. The time period that alkalinity remained near its minima was approximately doubled as result of the ionic pulse in snowpack runoff. The chemistry of snowfall at present deposition levels, and consequent concentration of the strong acid anions in melt water as a result of snow metamorphism processes within the snowpack, does increase the susceptibility of the ELW to acidification. However regression analyses among the various ions, silica, and discharge indicate that the large decreases in acid neutralizing capacity (ca. 65%) during snowmelt runoff were due primarily to dilution.

Spatial and temporal differences in the chemistry of snowmelt runoff affected the hydrochemistry of the basin. The duration of the ionic pulse in snowpack runoff, throughout the watershed, was increased by these differences. In turn, the duration of elevated concentrations of strong acid anions in the basin's lake, and its outflow, was increased. Snowmelt models used to produce a watershed estimate of the solute concentration entering a stream or lake over time, based on point estimates of solute flux from the snowpack, need to incorporate the spatial and temporal variation in the solute concentration of melt water.

Mass balance calculations of snowpack release and stream water loading showed that the NO_3^- pulse in stream water was from snowpack release of NO_3^- , that sorption processes may have regulated SO_4^{2-} levels in stream water, and that 80-90% of the H^+ stored in the snowpack was consumed before it reached Emerald Lake. The buffering of H^+ and homeostasis of SO_4^{2-} concentrations in stream water indicate that geochemical interactions in modifying snowmelt runoff are important to the hydrochemistry of alpine basins. The small amount of developed soils, and high percentage of bedrock outcrops and undeveloped sand and gravel deposits, indicate that geochemical reactions that occur on bedrock and in unconsolidated deposits may control the hydrochemistry of alpine watersheds. More research on the the geochemical dynamics of unconsolidate deposits and bedrock is needed to accurately predict susceptibility of alpine watersheds to potential increases in acidic deposition.

Interactions among the solutes released from the snowpack, energy flux throughout the basin, and hydrologic pathways were all important to the hydrochemistry of the ELW during snowmelt runoff. Any increase in the strong acid anion concentration of snowfall will be magnified several-fold in surface waters, as a result of snow metamorphism. The variable topography of the Emerald Lake watershed resulted in a highly variable energy flux in time

and space, which in turn generated spatial and temporal variations in the initiation and rate of snowmelt in the basin. Apparently contact time on the order of hours to days between snowmelt runoff and the terrestrial part of the watershed is enough to consume H^+ and remove or add SO_4^{2-} to snowmelt runoff.

TABLE 80. Ratio of Meltwater Concentration (C_m) to Initial Bulk Snowpack Concentration (C_p), and Percent Snowmelt, 1987

Site	Ion	April				
		8	10	17	23	25
Bench	NO ₃ ⁻	2.6	---	1.0	0.8	---
	SO ₄ ²⁻	2.4	---	0.8	0.4	---
	Cl ⁻	1.8	---	1.4	1.4	---
	% melt	---	9.5	33.0	53.0	---
Inlet	NO ₃ ⁻	4.2	2.7	0.7	0.8	---
	SO ₄ ²⁻	5.5	2.9	0.7	1.1	---
	Cl ⁻	6.4	6.2	2.1	2.6	---
	% melt	---	7.6	31.0	32.0	---
Cirque	NO ₃ ⁻	---	---	4.6	6.6	3.1
	SO ₄ ²⁻	---	---	7.3	10.9	3.4
	Cl ⁻	---	---	3.3	5.0	4.2
	% melt	---	---	---	8.7	10.7

TABLE 81. Rainfall Chemistry during Spring Runoff, 1987

	April	May				June	
	27	5	12	19	26	6	8
Water (mm)	8	32	27	17	29	12	14
pH	4.48	4.94	4.87	5.13	5.04	5.06	4.55
μS cm ⁻¹	25.0	16.7	12.5	13.4	29.7	13.2	19.2
H ⁺	33.1	11.5	13.5	7.4	9.1	8.7	28.2
NH ₄ ⁺	24.4	48.2	32.2	45.5	133.1	30.9	44.8
Ca ²⁺	28.4	43.9	14.5	19.5	23.5	6.4	8.7
Mg ²⁺	4.9	5.8	3.3	4.9	9.1	1.4	2.6
Na ⁺	6.1	10.0	2.2	4.4	27.0	53.3	38.1
K ⁺	3.3	2.8	3.8	6.9	3.6	1.4	1.4
NO ₃ ⁻	43.1	45.2	21.9	39.2	95.5	14.9	41.1
SO ₄ ²⁻	38.9	47.7	31.2	29.4	74.1	16.9	33.1
Cl ⁻	5.6	6.5	4.8	4.5	18.9	5.2	3.9

TABLE 82. Ion Loading (10^3 eq) in the Snowpack and Stream Inflows to Emerald Lake, Spring Runoff 1986 and 1987

Ion	Snowpack		Streams		Fraction*	
	1986	1987	1986	1987	1986	1987
H ⁺	11.4	10.8	2.6	0.5	0.23	0.09
NO ₃ ⁻	6.0	11.2	7.3	6.4	1.21	0.57
SO ₄ ²⁻	4.9	9.5	9.1	4.6	1.87	0.49
Cl ⁻	---	2.5	4.4	2.2	---	0.87

*Fraction is the ratio of loading in streams to loading in the snowpack

Figure 33. Subbasins of the Emerald Lake Basin

Topographic map of the Emerald Lake watershed. Subbasins are as follows: A east joint, B southeast gully, C inflow 1, C+D inflows 1 & 2, D inflow 2, E inflow 3, F inflow 4, G west joint. Sampling sites are as follows: 1 tower, 2 inlet, 3 bench, 4 ridge, 5 ramp, 6 pond, 7 hole, 8 cirque.

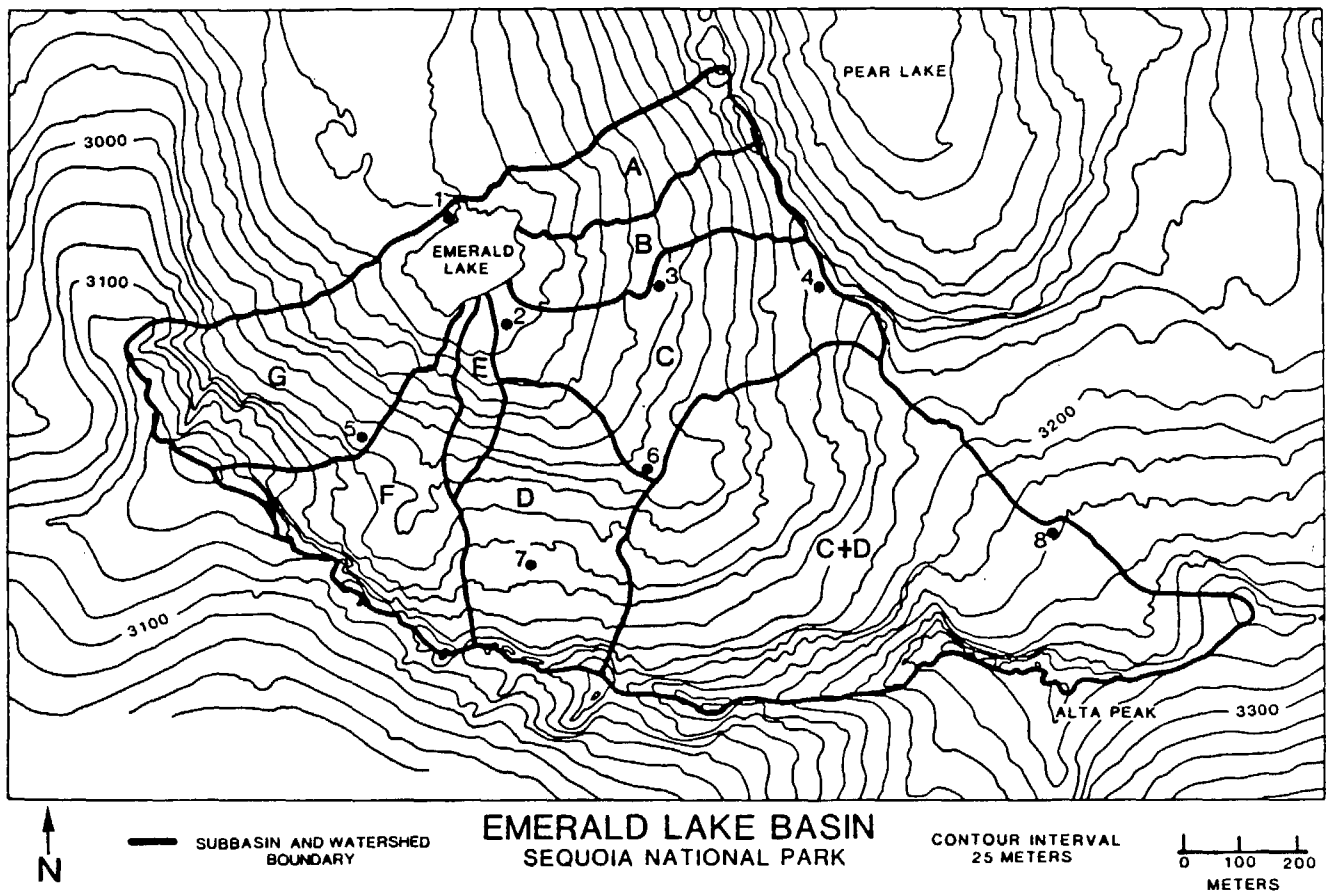


Figure 34. Concentrations of Major Ions in the Snowpack and Meltwater, Bench Site SWE and the concentration of major ions in the snowpack (clear boxes) and in snowpack meltwater (black boxes) at the bench, in 1987. Solutes in the initial fraction of meltwater were higher than in the snowpack, then decreased with time. The increase in meltwater concentrations on April 29 was due to rainfall.

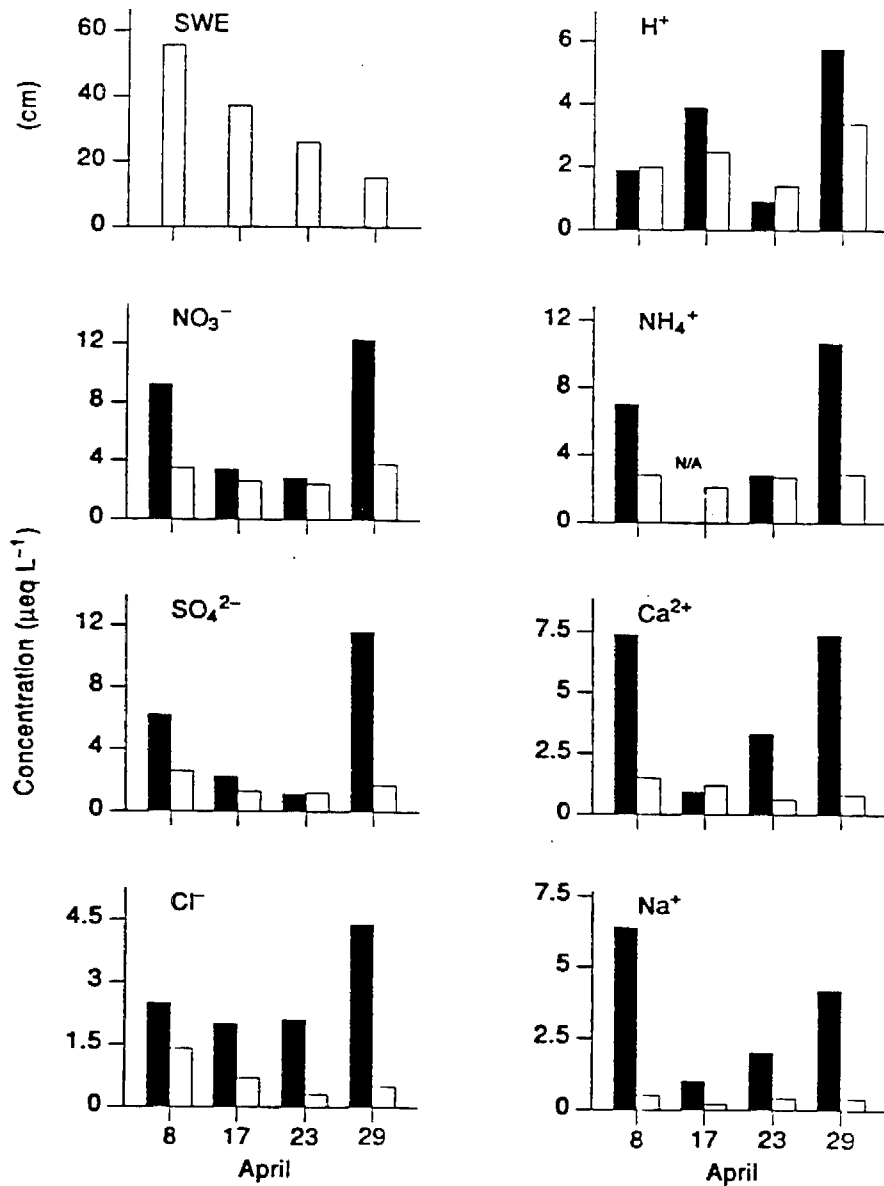


Figure 35. Concentrations of Major Ions in the Snowpack and Meltwater, Inlet Site SWE and the concentration of major ions in the snowpack (clear boxes) and in snowpack meltwater (black boxes) at the inlet, in 1987. Solutes in the initial fraction of meltwater were higher than in the snowpack, then decreased with time. The increase in meltwater concentrations on April 29 was due to rainfall.

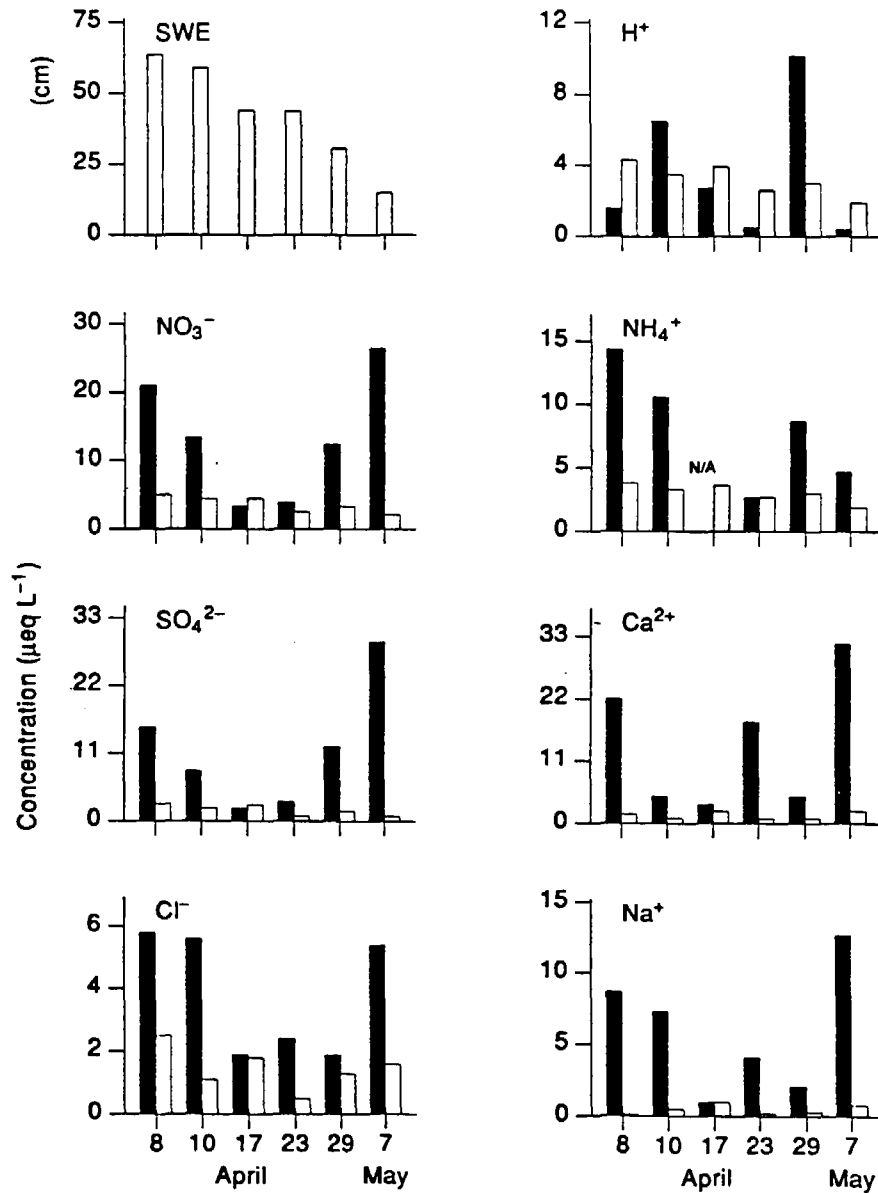


Figure 36. Concentrations of Major Ions in the Snowpack and Meltwater, Cirque Site SWE and the concentration of major ions in the snowpack (clear boxes) and in snowpack meltwater (black boxes) at the cirque, in 1987. Solutes in the initial fraction of meltwater were higher than in the snowpack. Solute concentrations in meltwater increased on April 23, after a series of melt-freeze events. The increase in meltwater concentrations on April 29 was due to rainfall.

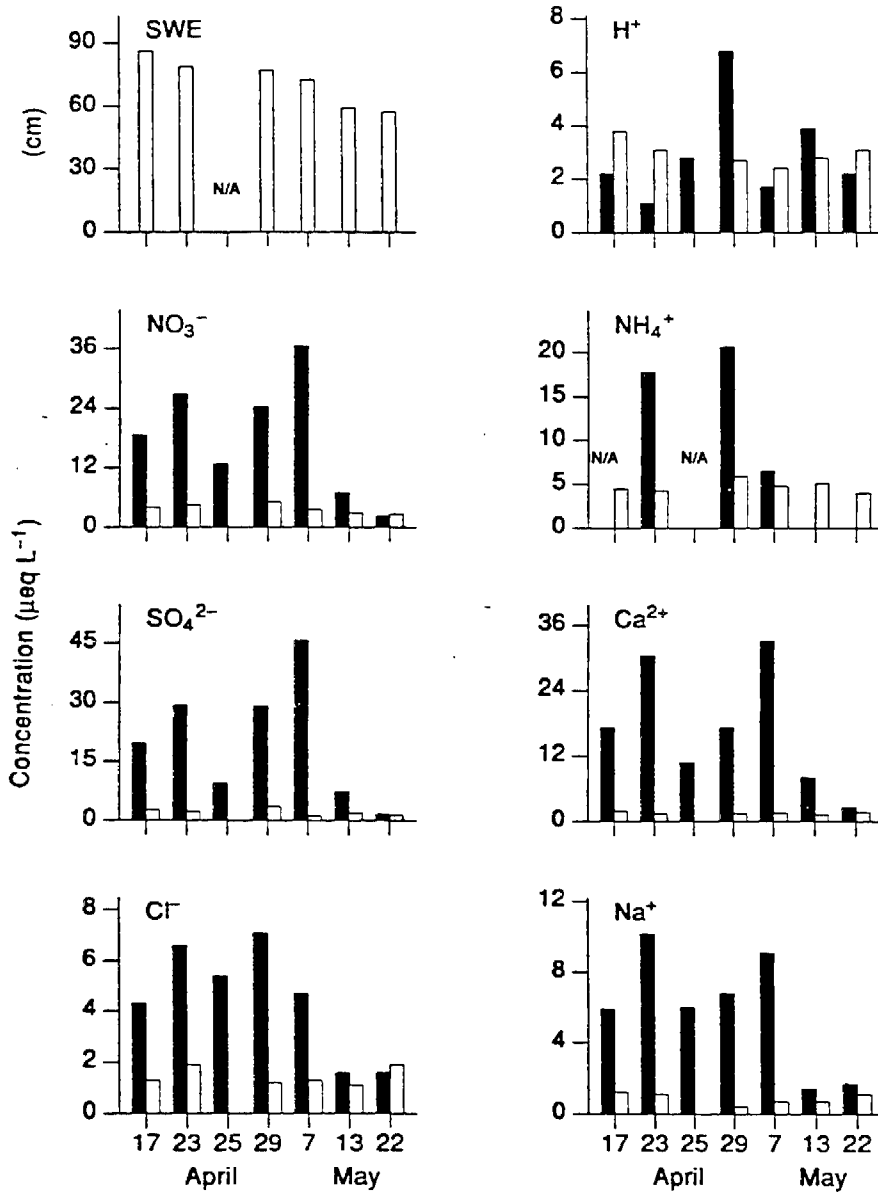


Figure 37. A Time Series of NO_3^- and SO_4^{2-} Concentrations in the Cirque Snowpack
 A time series of NO_3^- and SO_4^{2-} concentrations in the snowpack at the cirque, in 1987, prior to (March 31 and April 9) and after (April 23) the initiation of snowmelt runoff on April 17. The depth of the snowpack decreases with time. Solute concentrations near the top of the snowpack decreased with time. Solute concentrations near the bottom of the snowpack increased with time, prior to the initiation of snowmelt runoff.

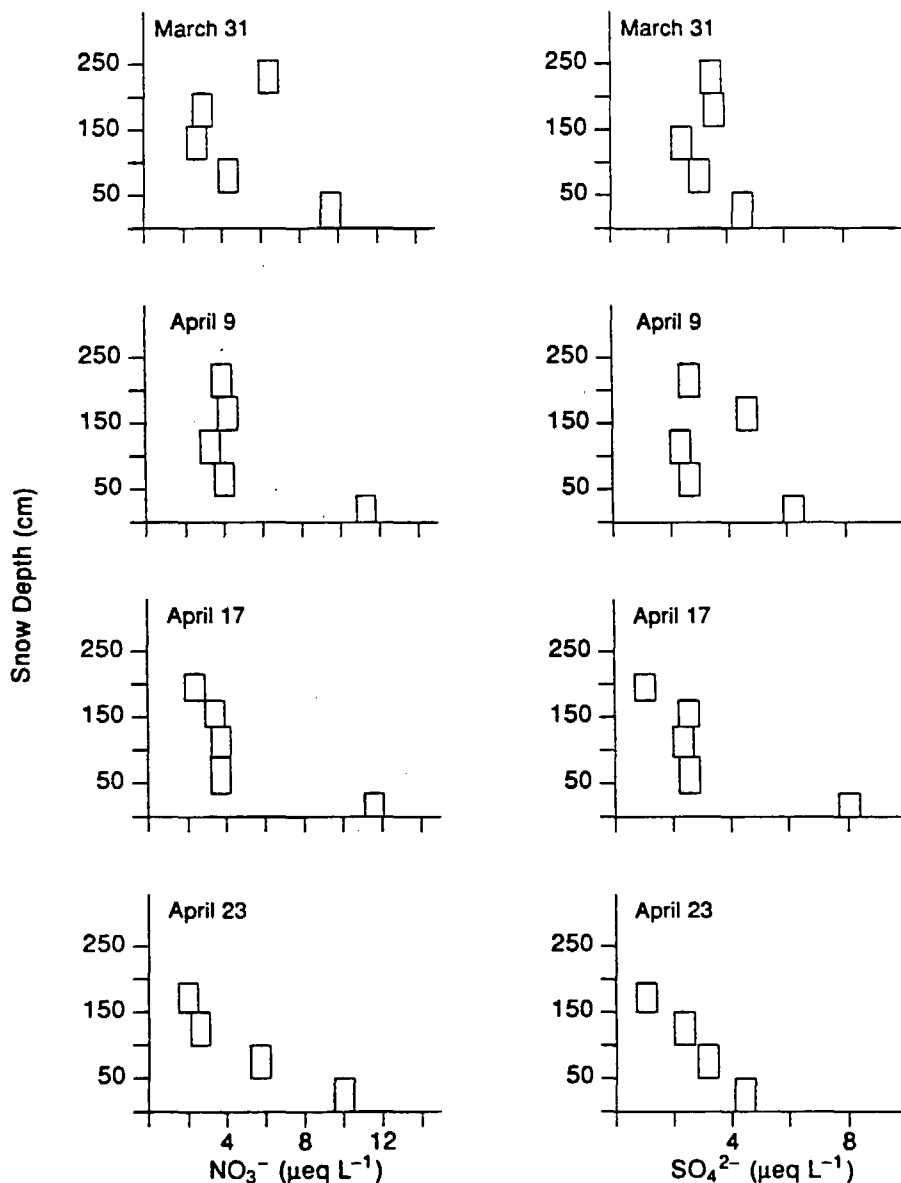


Figure 38. Comparison of H^+ , SO_4^{2-} , and Ca^{2+} in Rainfall, Meltwater, and the Snowpack Concentrations of H^+ , SO_4^{2-} , and Ca^{2+} in rainfall, meltwater, and the snowpack at the cirque in 1987. Meltwater concentrations are a mixture of concentrated rainfall and dilute snowpack runoff.

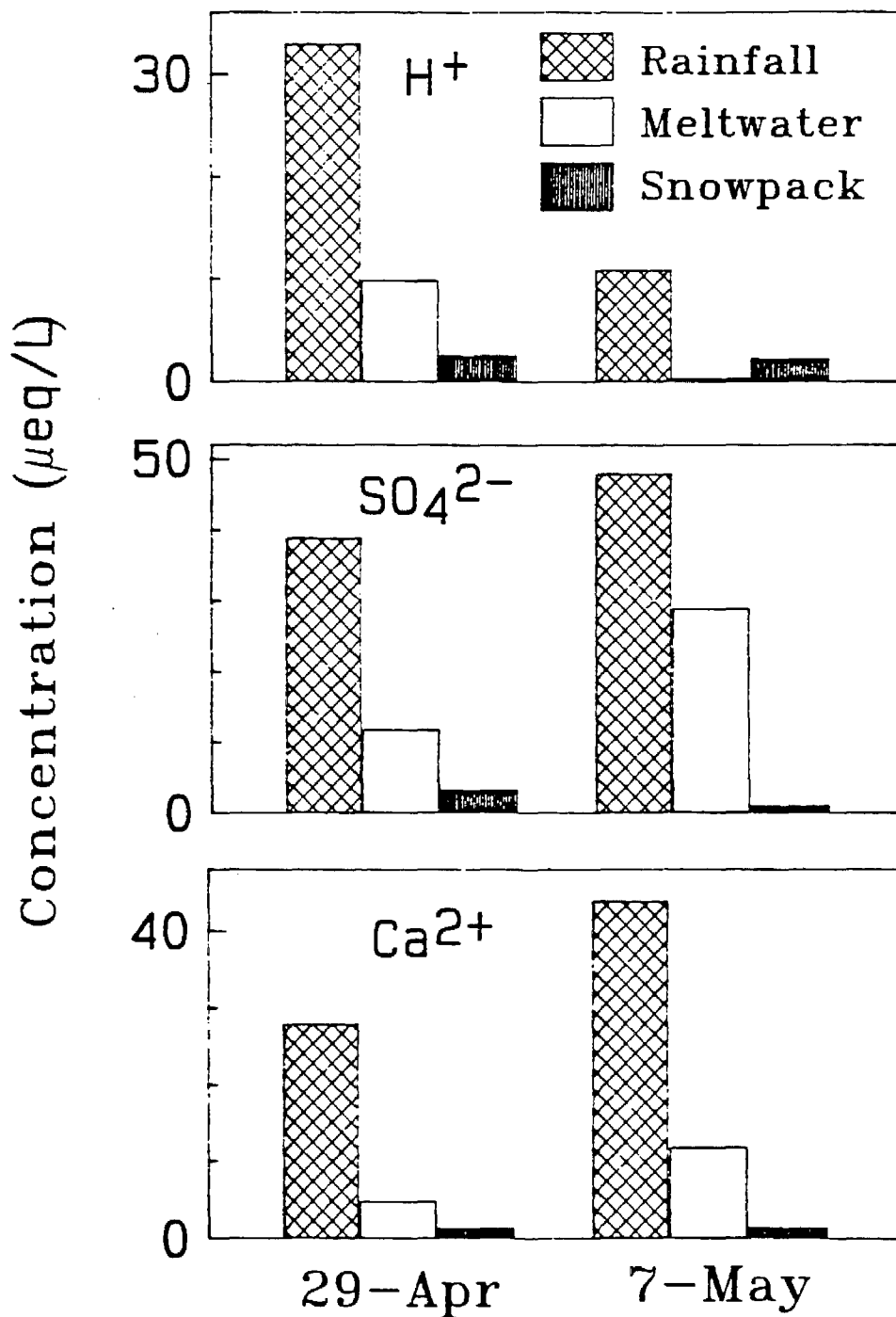


Figure 39. Nitrate and SO_4^{2-} of Inflowing Streams Compared to Snowmelt
 Nitrate and SO_4^{2-} concentrations of inflowing streams to Emerald Lake, and its outflow, compared to the percentage of snowmelt in their respective subbasins, during snowmelt runoff in 1986. Concentrations in inflowing streams were highest at the initiation of snowmelt, then decreased with time. As a consequence of the spatial and temporal variation in the chemistry of its inflowing streams, NO_3^- and SO_4^{2-} concentrations in the lake's outflow remain elevated for a longer period of time than individual inflowing streams (adapted from [Williams and Melack, 1989]).

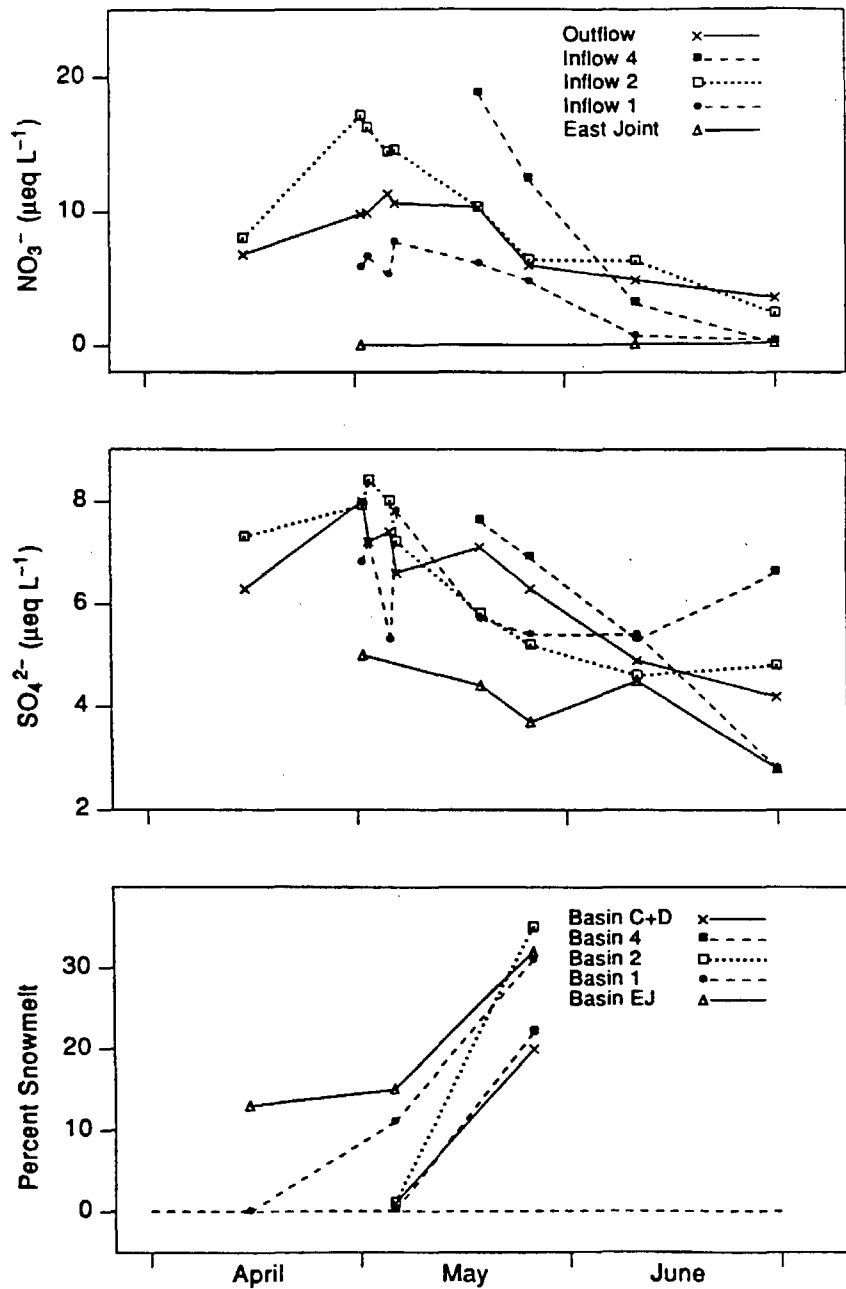


Figure 40. Concentrations of Major Ions in the Outflow
 Discharge, NO_3^- , SO_4^{2-} , Cl^- , silica, ANC, H^+ , and C_b in the outflow, during the time period of snowmelt runoff in 1986 and 1987.

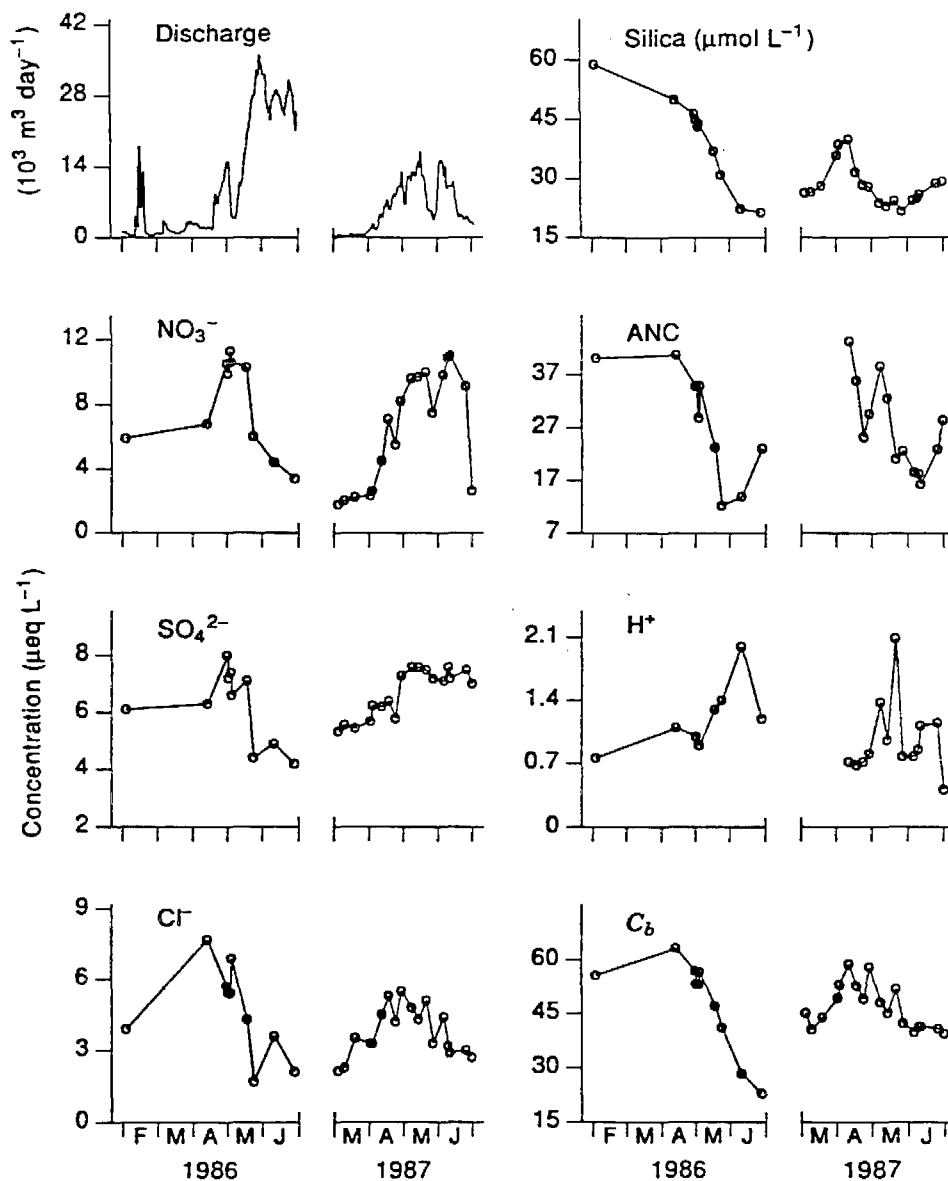


Figure 41. Percent Change of Anions in the Outflow
 Change in the concentrations of NO_3^- , SO_4^{2-} , and Cl^- in the outflow during snowmelt runoff, as a percentage of winter concentrations, in 1986 and 1987. The large increase in NO_3^- concentration indicates that NO_3^- became a mobile anion. Sulfate concentrations showed much less variation than NO_3^- or Cl^- . Note that the Y-axis scales are different for the two years.

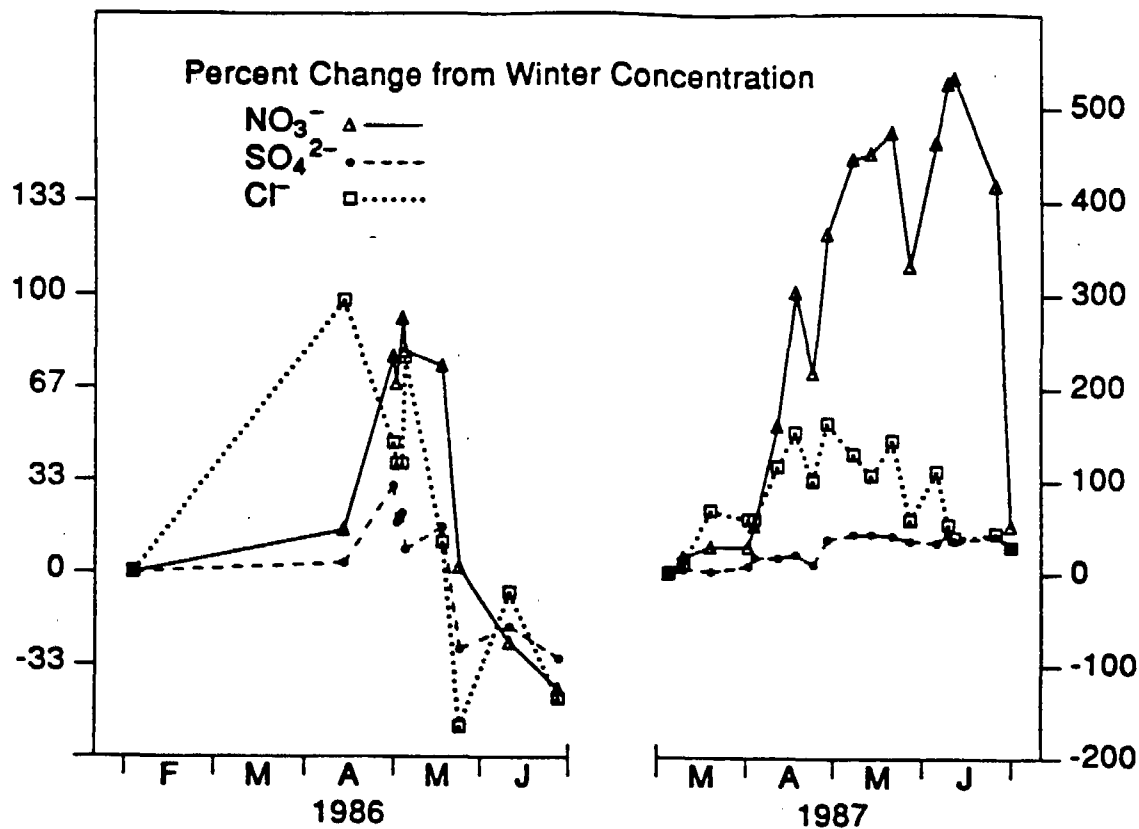


Figure 42. Changes in Alkalinity During Snowmelt Runoff

Alkalinity (measured as $C_b - C_a$) in inflow 2 during 1986, prior to snowmelt runoff (Jan 7), at the initiation of runoff (May 1), and at the period of maximum dilution (June 10). The decrease in alkalinity was almost as great at the start of runoff, due to the increase in strong acid anions, as at the period of maximum dilution.

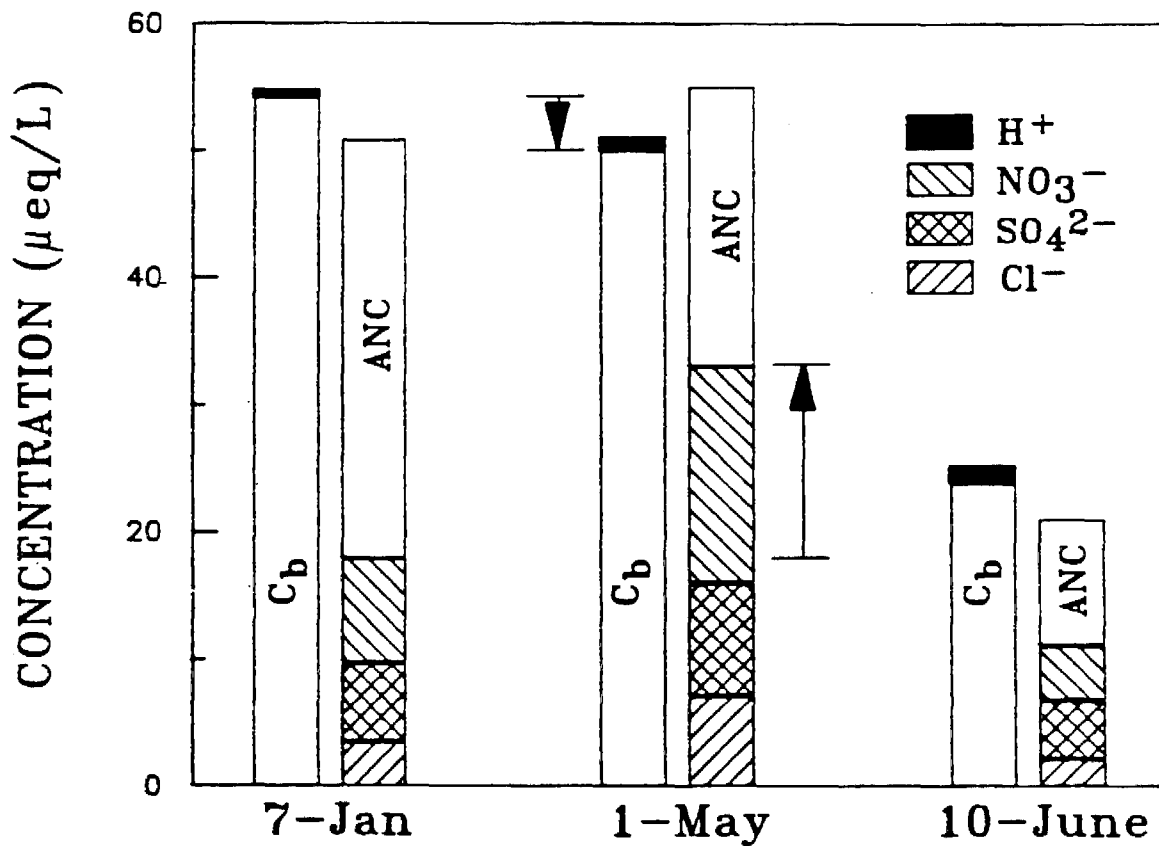
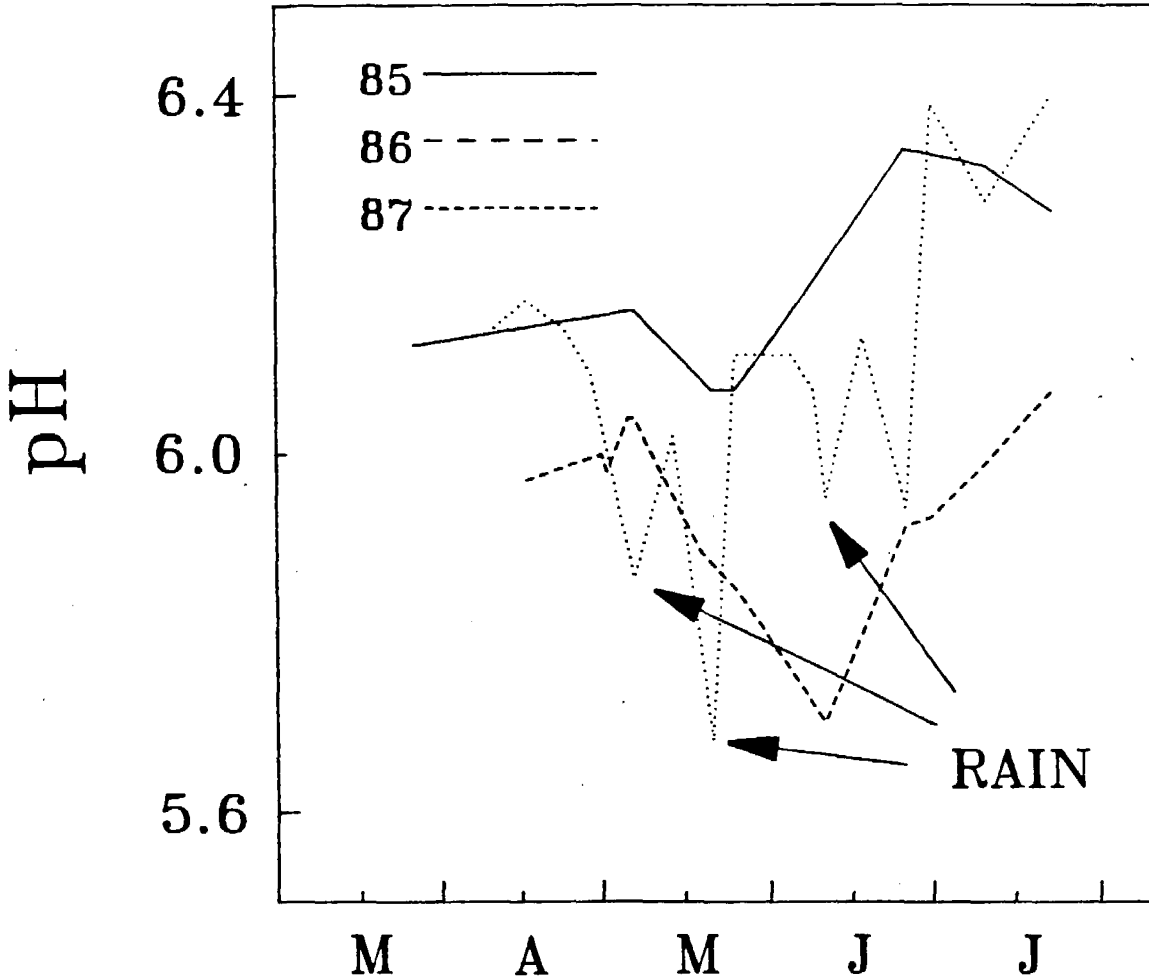


Figure 43. pH in the Emerald Lake Outflow During Snowmelt, 1985-1987
 Comparison of pH in the Emerald Lake outflow during snowmelt runoff in 1985, 1986 and 1987. Rain events during the low snow year of 1987 caused a depression in pH similar to the large snow year of 1986.



F. References

- Baker, J. P. and C. L. Schofield, Aluminium toxicity to fish in acidified water, *Water, Air Soil Poll.*, 18, 289-309, 1982.
- Bales, R. C. and R. E. Davis, and D. A. Stanley, Ion elution through shallow homogeneous snow, *Water Resour. Res.*, 25, 1869-1878, 1989.
- Brimblecombe, P., M. Tranter, P. W. Abrahams, I. Blackwood, T. D. Davies, and C. E. Vincent, Relocation and preferential elution of acidic solute through the snowpack of a small, remote high-altitude Scottish catchment, *Ann. Glaciol.*, 7, 141-147, 1985.
- Cadle, S. H. and J. M. Dasch, Composition of snowmelt and runoff in northern Michigan, *Atmos. Environ.*, 21, 295, 1987.
- Cadle, S. H., J. M. Dasch, and N. E. Grossnickle, Retention and release of chemical species by a Northern Michigan snowpack, *Water, Air Soil Poll.*, 22, 303-319, 1984.
- Clow, D., Geologic controls on the neutralization of acid deposition and on the chemical evolution of surface and ground waters in the Emerald Lake watershed, Sequoia National Park, California, M. S. Thesis, Department of Geology, California State University, Fresno, CA, 1987.
- Colbeck, S. C., A simulation of the enrichment of atmospheric pollutants in snow cover runoff, *Water Resour. Res.*, 17, 1383-1388, 1981.
- Davies, T. D., C. E. Vincent, and P. Brimblecombe, Preferential elution of strong acids from a Norwegian ice cap, *Nature*, 300, 161-163, 1982.
- Dickson, W., Properties of acidified waters, in *Proceedings of the International Conference on Ecological Impact of Acid Precipitation*, edited by D. Drablos and A. Tollan, SNSF project, pp. 75-83, 1980.
- Dozier, J., J. M. Melack, D. Marks, K. Elder, R. Kattelman, and M. Williams, Snow deposition, melt, runoff and chemistry in a small alpine watershed, Emerald Lake Basin, Sequoia National Park, *Final Rep., Contr. A3-103-32*, Calif. Air Resour. Board, Sacramento, CA, 1987.
- Driscoll, C. T., J. P. Baker, J. J. Bisogni, and C. L. Schofield, Effects of aluminium speciation on fish in dilute acidified waters, *Nature*, 284, 161-164, 1980.
- Elder, K., J. Dozier, and J. Michaelsen, Spatial and temporal variation of net snow accumulation in a small alpine watershed, Emerald Lake basin, Sierra Nevada, California, U.S.A., *Ann. Glaciol.*, 13, 56-63, 1989.
- Galloway, J. N., G. R. Hendrey, C. L. Schofield, N. E. Peters, and A. H. Johannes, Processes and causes of lake acidification during spring snowmelt in the west-central Adirondack Mountains, New York, *Can. J. Fish. Aquat. Sci.*, 44, 1595-1602, 1987.
- Hornbeck, J. W., G. E. Likens, and J. S. Eaton, Seasonal patterns in acidity of precipitation and their implications for forest stream ecosystems, *Water, Air Soil Poll.*, 7, 355-365,

1977.

- Jeffries, D. S., C. M. Cox, and P. J. Dillon, Depression of pH in lakes and streams in central Ontario during snowmelt, *J. Fish. Res. Bd. Canada*, 36, 640-646, 1979.
- Johannessen, M. and A. Henriksen, Chemistry of snow meltwater: changes in concentration during melting, *Water Resour. Res.*, 14, 615-619, 1978.
- Johnson, N. M., Acid rain neutralization by geologic material, in *Geological Aspects of Acid Deposition*, edited by O. P. Bricker, Acid Precipitation Ser., vol. 7, Butterworth, Stoneham, Mass., 1984.
- Jones, H. G. and W. Sochanska, The chemical characteristics of snow cover in a northern boreal forest during the spring runoff period, *Ann. Glaciol.*, 7, 167-174, 1985.
- Kattelmann, R., Groundwater contributions in an alpine basin in the Sierra Nevada, *Proceedings of the Headwaters Hydrology Symposium*, 361-369, Amer. Water Resour. Assoc., Bethesda, MD, 1989.
- Kattelmann, R. C., Macropores in snowpacks of Sierra Nevada, *Ann. Glaciol.*, 6, 1985.
- Laird, L. B., H. E. Taylor, and V. C. Kennedy, Snow chemistry of the Cascade-Sierra Nevada Mountains, *Environ. Sci. Technol.*, 20, 275-290, 1986.
- Landers, D. H. and others, Characteristics of lakes in the Western United States, *EPA/600/3-86/054a*, U. S. EPA, Washington, D.C., 1987.
- Liu, W. C., The sensitivity of selected soils from the Sierra Nevada to acidic deposition, Ph.D. Thesis, 102 pp., Univ. Calif. at Riverside, Riverside, CA., 1988.
- Marsh, P. and M.-k. Woo, Wetting front advance and freezing of meltwater within a snow cover, 1, Observations in the Canadian Arctic, *Water Resour. Res.*, 20, 1853-1864, 1984.
- McAvoy, D. C., Episodic response of aluminum chemistry in an acid-sensitive Massachusetts catchment, *Water Resour. Res.*, 25, 233-240, 1989.
- Melack, J. M., J. L. Stoddard, and C. A. Ochs, Major ion chemistry and sensitivity to acid precipitation of Sierra Nevada lakes, *Water Resour. Res.*, 21, 27-32, 1985.
- Nihlgard, B., The ammonium hypothesis-an additional explanation to the forest dieback in Europe, *Ambio*, 14, 2-8, 1985.
- Nikolaidis, N. P., H. Rajaram, J. L. Schnoor, and K. P. Georgakakos, A generalized soft water acidification model, *Water Resour. Res.*, 24, 1983-1996, 1988.
- Rascher, C. M., C. T. Driscoll, and N. E. Peters, Concentration and flux of solutes from snow and forest floor during snowmelt in the West-central Adirondack region of New York, *Biogeochemistry*, 3, 209-224, 1987.
- Reuss, J. O. and D. W. Johnson, *Acid Deposition and the Acidification of Soils and Waters*, 119 pp., Springer and Verlag, New York, 1986.

- Schnoor, J. L. and W. Stumm, The role of chemical weathering in the neutralization of acidic deposition, *Schweiz. Z. Hydrol.*, **48**, 171-195, 1986.
- Sickman, J. O. and J. M. Melack, Characterization of year-round sensitivity of California's montane lakes to acidic deposition, *Final Rep., Contr. A5-203-32*, Calif. Air Resour. Board, Sacramento, 1989.
- Skartveit, A. and K. T. Gjessing, Chemical budgets and chemical quality of snow and runoff during spring snowmelt, *Nordic Hydrol.*, **10**, 141-154, 1979.
- Stein, J., H. G. Jones, J. Roberge, and W. Sochanska, The prediction of both runoff quality and quantity by use of an integrated snowmelt model, in *Modelling Snowmelt-Induced Processes*, edited by E. M. Morris, IAHS Publ. No. 155, pp. 111-120, Intl. Assoc. Hydrol. Sci., Wallingford, UK, 1986.
- Strickland, J. D. and T. R. Parsons, A practical handbook of seawater analysis, *Bulletin of Fisheries Research Board Canada*, **167**, 83, 1972.
- Suzuki, K., Chemical changes of snow cover by melting, *Jap. J. Limnol.*, **43**, 102-112, 1982.
- Tranter, M., P. Brimblecombe, T. D. Davies, C. E. Vincent, P. W. Abrahams, and I. Blackwood, The composition of snowfall, snowpack, and meltwater in the Scottish Highlands - evidence for preferential elution, *Atmos. Environ.*, **20**, 517-525, 1986.
- Tranter, M., T. D. Davies, P. W. Abrahams, I. Blackwood, P. Brimblecombe, and C. E. Vincent, Spatial variability in the chemical composition of snowcover in a small, remote, Scottish catchment, *Atmos. Environ.*, **21**, 853-862, 1987.
- Tsiouris, S., C. E. Vincent, T. D. Davies, and P. Brimblecombe, The elution of ions through field and laboratory snowpacks, *Ann. Glaciol.*, **7**, 196-201, 1985.
- van Breemen, N., P. A. Burrough, E. J. Velthorst, H. F. van Dobben, T. de Wit, T. B. Ridder, and H. F. R. Reijnders, Soil acidification from atmospheric ammonium sulphate in forest canopy throughfall, *Nature*, **299**, 548-550, 1982.
- Williams, M. W. and J. M. Melack, Effects of spatial and temporal variation in snow melt on nitrate and sulfate pulses in melt waters within an alpine basin, *Ann. Glaciol.*, **13**, 285-289, 1989.

00001676



ASSET